ENZYMATIC AND ACTIN-BINDING PROPERTIES OF MICAL-1

by
Olivier Simon

A dissertation submitted to Johns Hopkins University in conformity with the requirements for the degree of Doctor of Philosophy

Baltimore, Maryland
May, 2014

Abstract.

MICAL is a large multi-domain monooxygenase with orthologues in flies and humans. MICAL is known to play an important role in axon guidance through semaphorin signaling and, in particular, it has recently been found to influence actin polymerization, with certain constructs capable of disassembling F-actin through methionine oxidation. MICAL also can produce hydrogen peroxide, a potential signaling molecule. In the following, I expressed and purified several proteins, including the MICAL-1 C-terminus, the cytoplasmic portion of the semaphorin receptor Plexin-A1, and the small GTP-binding protein Rnd1, combined these with MICAL constructs of varying length, and used kinetics, co-sedimentation, peroxide quantitation, HPLC, and size exclusion in an effort to characterize the factors necessary to activate MICAL's peroxide-producing and actin-disassembly functions.

Advisor and first reader: L.M. Amzel, Ph.D.

Reader: M.A. Bianchet, Ph.D.

Acknowledgments.

No list of acknowledgments can ever be quite complete; life is an endless web of acquaintances and influences, and so the list of people who in some subtle but vital way contributed to this several years' work, perhaps from a few degrees of separation, would likely run into the hundreds. Alas—most of it must go unwritten.

Still, any attempt at such a list has to begin with my mother, Liz Simon. The difficulties of a single woman in raising an absentminded, awkward and science-obsessed youngster are beyond my imagining, and yet through the years she has managed to guide and support my interests and keep a nice roof over both our heads in the process. Her style and substance are unusual. Unlike many parents today who seem bent on creating the most hyper-scheduled and careerist youth the world has ever seen, my mother saw the importance of leaving time free to dream, wander, and explore--by my own lights, as it were. Also, whether in politics, religion, society, or science, she stressed the importance of questioning conformity, of looking beneath the surface of things–even if what you find may not be what you originally hoped or imagined. Our long conversations and her regular advice and loving support, not least from having been a professor herself, were incredibly helpful through the years. Love you, Ma!

My PI, Dr. L. Mario Amzel. Throughout this long and inevitably frustrating process, no matter what seeming disaster had reared its head in my latest results, I could count on Dr. Amzel to project a wider perspective and a constant reassuring calm, informed by his vast knowledge, insight, achievements and experience. Especially towards the end, as I began preparing my thesis and a manuscript for publication, I am

well aware that I probably subjected Dr. Amzel to a flurry of visits, questions, rough drafts and revision requests that could have snowed under many an otherwise patient and resourceful man. But the revisions and comments were always ready like clockwork in a few days, and his door stayed open. Through the years, in a world of turmoil and constant funding and organizational intrigue, Dr. Amzel has also kept the lab as a place of stability and calm, where science reigns but with a gracious touch—no small feat.

Dr. Mario Bianchet is a mild and soft-spoken man in person but meticulous and tenacious in all matters of science. Like a lapidary who for some reason chose protein crystals over carbon ones, he guards and polishes every possible facet of the work–be it a crystal structure, an experimental control or a chance to teach–with tender, almost fatherly dedication. He is always around, always interested, always available to offer the benefit of his decades of experience. However frustrating a result or mistake may be—and he has dealt with some fine ones from us over the years–he always comes through at the end with a wry joke or a playful tease. His gallows humor is legendary to the lab: the most approving answer of Dr. Bianchet to a well-conducted or interesting experiment, or a well-written manuscript, is, "this gives me *hope!*" May we all continue to give him hope.

Since coming to the lab a couple of years ago, Dr. Anita Ghosh has been a constant calming presence, a fount of Eastern wisdom of her own unique stamp. As well as actually seeming to enjoy my madcap and even surreal humor, she has been a wealth of knowledge and encouragement in experimental matters and a valuable source of advice of all kinds. I wish her and her husband Deepak the best with their child on the way.

Dr. Saif Alqassim has been as upstanding a colleague as one could ask for. Since his joining the lab in my second year I have enjoyed our discussion and collaboration on the mysteries of MICAL. I also will not forget Saif's hospitality and spirit of fun, whether grilling up salmon steaks at his apartment for an evening of MarioCart, organizing group dinners at his beloved Lebanese Taverna, or gently field-testing a 350-hp Camaro on the JFX. I wish him all success as he returns to Dubai, and in his future career in Al Ain.

Dr. Mauricio Urquiza's constant optimism and puckish mirth would be enough to endear him but he has also been a fine colleague and friend. His kinetics work with MICAL and also the CTD meant we often worked closely through the years and he has always been fantastically helpful.

Dr. Srinivas Aripirala has recently graduated from the lab, but I remember him both for his friendship and his help and useful suggestions in the lab. As well as being a highly capable researcher, Srinivas is an avid amateur philosopher, fascinated with principles of wisdom, tranquility, good living and conduct, and we discussed these matters many times.

The irrepressible Dr. Sandra Gabelli, while I did not work under her directly, was always available for advice when the Marios were not available. She has the gift of appearing out of nowhere when no one else is around and a heavy silence has descended, dispelling it with a quick piece of joking advice and a wink, and then disappearing again. I have very good memories of her cooking and hospitality, whether making crème brulée or bringing her famous empanadas to lab meeting.

Besides Dr. Amzel, I would also like to thank my other thesis committee members, Drs. Alex Kolodkin, Dan Leahy, and Douglas Robinson, whose good-natured

suggestions, guidance and patience over the years made our meetings refreshing rather than an ordeal.

Tammy Watson, Kathleen Kolish, and all the office staff were constantly helpful, and do a remarkable job of keeping practical and worldly matters rolling while surrounded by nerds of every kind. To them, my thanks also.

I also should mention William Hong for his steadfast friendship and support during some of the most difficult times in the lab. Even without having decided on Ph.D work, the mighty "King Hong" has been apt to take on the work habits of the most ambitious graduate student. And so I would find him nights, likelier than not, slaving over an HPLC run or some GST beads until the last bus left. I thank him for mostly utterly un-scientific but highly engaging conversations and occasional games of Pylos, which helped take both our minds off the stress.

My gratitude to all the rest of the lab members past and present, in no particular order, who have all provided interesting discussion, good laughs or useful advice: Dr. Tzu-Lan Yeh, Andres Hernandez, Dr. Kasia Rudska, Dr. Danielle Chaves, Dr. Bora Erdemlii, Dr. Krisna Duong-Ly, Dr. Chizu Shimokawa, Dr. Simon Messing, Dr. Agedi Boto, Dr. Akunna Iheanacho, and the original Iowa crooner, Jesse Yoder.

Finally, I would like to acknowledge Professor Peyton W. Manning, whose expertise in another kind of kinetics was both inspirational and educative during a dark and snowy winter which often saw me working into the wee hours trying to get the last few experiments to work cleanly--those long last yards to graduation.

Table of Contents.

List of Tables.

List of Figures.

Chapter 1: Introduction.

1.1 Introduction to neurodevelopment and axon guidance.

Nervous systems, ranging from those of invertebrates to those of humans, show a remarkable degree of organization and structural intricacy. Even with a comparatively rudimentary nervous system and a brain consisting of a mere few hundred thousand cells, a normal fruit fly exhibits distinct nerve tracts that interconnect central ganglia with the motor and sensory organs in highly specific and predictable ways (1, 2). In insects, these patterns first begin to appear within hours of embryonic development with the appearance of a rudimentary neural tube, and within 16-20 hours are established and clearly recognizable by distinctive patterns of axon bundling, de-fasciculation and growth at critical choice-points (3).

In the far more complex mammalian nervous system, this challenge of organization is all the more daunting: not thousands, but billions of neurons must grow, differentiate and, crucially, extend axonal and dendritic projections in the correct directions to form many trillions of precise synaptic connections with neighboring neurons, muscle cells, or glands. Even slight perturbations in this development from the norm can lead to severe or lethal phenotypes (4-7).

The seemingly spontaneous development of such structures naturally raises questions regarding their underlying mechanisms. Beginning with the closure of the neural tube, it is thought that a carefully orchestrated succession of gene expression events establishes morphogen gradient patterns of increasing complexity, and constitutes an implicit "program" of nervous system development (4).

This program has been gradually (but far from completely) elucidated in recent

years by the identification of a plethora of morphogens and guidance molecules which are expressed in a developmental- and location-specific way, and direct the formation of specific neurological structures and cell types. These molecules include such well-known neural-patterning factors as Shh, Wnt, bone morphogenetic protein (BMP), and neurotrophins (1, 8). However, the program is far from being understood in its full intricacy, with many seemingly simple questions left unanswered. Moreover, the exact intracellular systems that transduce and affect the signals conveyed by these developmental factors are still, in many cases, poorly understood.

Of the many aspects of neural structure and differentiation, one of the most vital and promising areas of study in this regard has been axonal guidance. The pattern of axon path-finding, beginning with early neurite outgrowth and differentiation and ending in eventual innervation of their targets, constitutes an implicit "wiring diagram" of the nervous system. Within the brain, distinct sub-classes of neurons must extend axonal projections from highly specific regions of the cortex to equally precise areas of the thalamus, pons, tectum, or cortex itself (9), while motor and sensory axons must often grow tens of thousands of cell lengths before innervating their intended targets, with some exceeding a meter in length and showing extensive ramification into hundreds of synapses at their ends (2, 9).

1.2 Growth cone dynamics, guidance cues and receptors.

It is now known that the feat of axon guidance owes largely to the establishment of gradients of both secreted and cell-surface cues, which are produced during neural development and also after nerve injury (10-12). These cues are detected, either by direct contact or over a range of hundreds of micrometers, by a highly specialized, dynamic and

motile structure at the tip of the elongating axon known as the growth cone.

First observed by Cajal (3, 13), the growth cone is roughly fan-shaped and extends finger-like projections into the surroundings, called filopodia. Filopodia contain primarily F-actin fibers, which exhibit retrograde transport under the action of non-muscle myosin. In addition, in a process called "treadmilling" G-actin monomers assemble at the leading edge of the filopodia, travel proximally (i.e. back towards the base or "central domain" of the growth cone), and then are disassembled, releasing G-actin monomers for fresh polymerization (1, 8, 14).

Around the bases of the filopodia, webbing-like regions consisting primarily of an F-actin meshwork (as opposed to unidirectional fibers) form the lamellipodia, a kind of scaffolding region around the base of the filopodia, which accommodates organelles and also shows highly dynamic actin behavior. Still more proximally, in the central domain, the actin meshwork gives way to a more rigid zone of microtubules (Fig. 1.1), which also provide the structural integrity of the main shaft of the axon along its length (2, 8).

Control of the rate of actin fiber motion by myosin, or of the rates of polymerization at the leading edge and depolymerization within the cone, as well as of rigidity and bundling of actin fibers, allows for modulation of the cone's growth behavior with remarkable precision. In particular, though the exact mechanisms are still not fully understood, they allow precise control of the direction of the cone's growth by guidance cue gradients in the surroundings by differential rates of actin polymerization or disassembly on alternate sides of the growth cone (1, 8, 13).

Of these secreted cues, four main families, the so-called "canonical cues" have

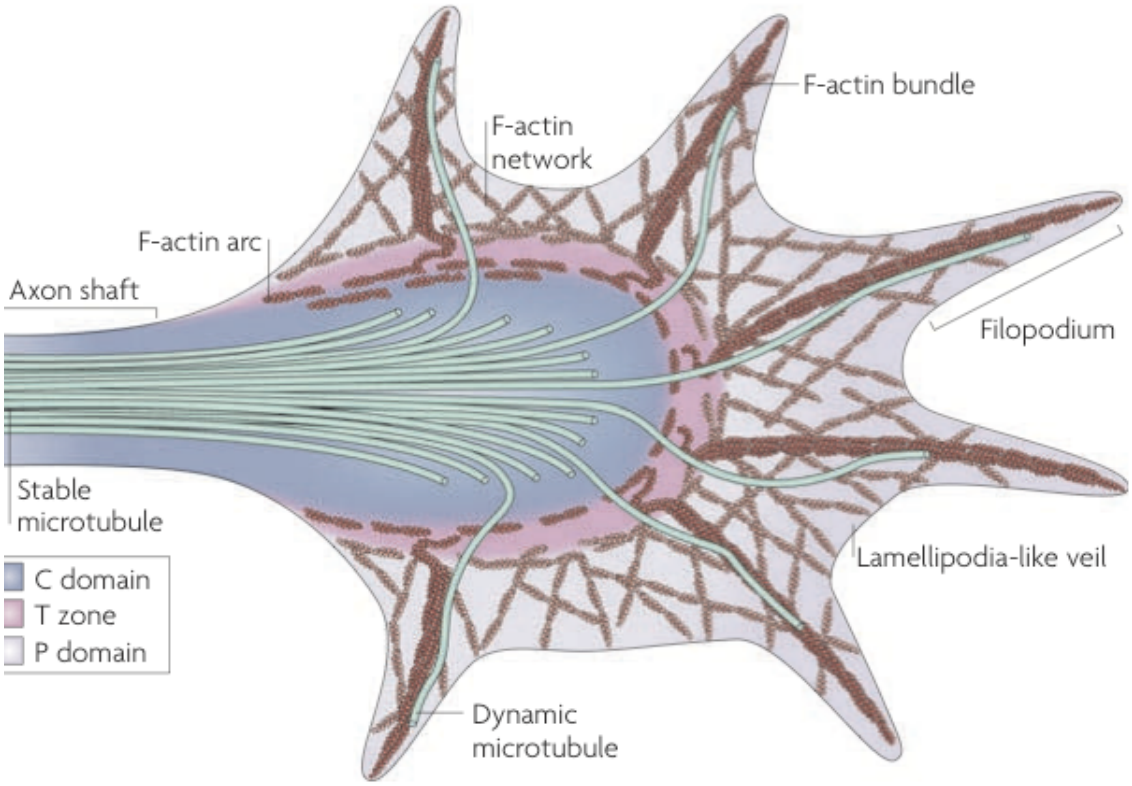

gure 1.1 Representative diagram of a growth cone. Note the central (C) domain, minated by microtubles, and the peripheral (P) domain, where actin dynamics in opodial and lammelipodial structures plays a central role instead–although some single crotubules still intrude. The region between these is sometimes called the transitional (T) main. Reprinted from (8).

been distinguished: the ephrins, the netrins, the slits, and the semaphorins, along with numerous cell-adhesion proteins and morphogens that are known to act in a guidance role (1, 15). Each family, in turn, is associated with a complementary family of receptors: Eph, DCC/UNC5, Robo, and Plexin, respectively.

Although there is considerable diversity within each of these families--some being wholly secreted, others membrane-bound, and acting over a variety of distance scales--there are structural motifs that are conserved and also a general tendency for each family to exert an attractive or repulsive influence on developing axons (1, 15, 16). For example, the netrins are frequently attractive cues, drawing axons to grow in the direction of increasing cue concentration, while the semaphorins are mostly repulsive, directing axon growth away from the location of secretion. In some cases the generally attractive or repulsive nature of a cue may be altered or even reversed by so-called modulatory cues, or by the type of receptor being expressed–as in the case of netrins, which in spinal cord development are attractive while axons grow towards the midline and then, due to expression of different receptor types, become repulsive after reaching or crossing the commissure. Furthermore, axon guidance receptors may be bi-directional, as in the case of the Ephs, able to both receive and send signals (1, 3, 15, 16).

The semaphorins, a particularly large and well-studied family of cues, and distinguished by the presence of the "sema domain", a 500-residue, seven-bladed beta propeller structure, as well as several Ig-like repeats and PSI-domains. Their receptors, the plexins (17), are single-pass transmembrane proteins that feature an ectodomain consisting of a similar arrangement and composition of subdomains to that of semaphorin (1, 6, 18). It is thought that the sema domains are naturally inclined to dimerize in an

edge-to-edge manner, giving a plausible mechanism of ligand recognition and receptor activation (15, 19-21).

There are about 20 semaphorin types in higher vertebrates, distributed in five numbered classes (3-7; 1 & 2 in invertebrates only), and nine plexins, with four classes. Perhaps the most abundant and best-studied of the subgroups is the Type 3 semaphorins, especially soluble Sema3A, the first semaphorin discovered; these are secreted by guidance substrates--such as glia, cells of the midline, and other axons--and bind to Plexin A receptors (particularly Plexin A1). Sema3A's interaction with Plexin A requires a co-receptor, Neuropilin-1 or -2, though other plexins can transduce semaphorin guidance signals by themselves, for example Sema4D with Plexin B1 (22, 23).

The plexin intracellular domain has an unusual structure, consisting of four main elements: a C1 domain, a rho-binding domain (RBD), a C2 domain, and an N-terminal helix. From both sequence analysis and the crystal structures of both plexin A3 and B1, it is apparent that the C1 and C2 domains rest together in a somewhat intertwined conformation and constitute a Ras-GTPase activating protein (Ras-GAP). As is typical of GAPs, that of plexin is marked by two conserved catalytic arginines (24-26). Plexin is unusual in the intercalation of the RBD between its two GAP domains, and among guidance receptors in directly interacting with small GTPases (26, 27). The RBD is capable of binding such Rho GTP-binding proteins as RhoD, Rac1, and Rnd1, with accompanying large variations in GAP activity--ranging from inhibition to strong activation, as assessed by cell contraction assays (28-31).

Though the exact mechanisms of plexin signal transduction remain unknown and are no doubt complex, they are thought to exist at rest in an autoinhibited conformation

for which the ectodomain plays a key role (32). Two main upstream requirements have been proposed for their full activation, while at least three main downstream effector pathways are recognized. The upstream requirements have been described as logically "AND-gate like" in that they must be simultaneously realized in order for full signaling to take place (20, 25, 29, 33). In the first place, receptor clustering must be induced (or halted, depending on the account), by semaphorin binding at the extracellular domain; in the second place, a suitable Rho protein in a GTP-bound state must interact with the plexin RBD (30, 34, 35).

Following activation of plexin, the guidance signal is thought to be relayed by three possible pathways:

1) activation of the plexin Ras-GAP, leading to effects on such diverse functions as PTEN activity (36), phosphorylation of cofilin by LIMK1 (14, 37), GSK-3 activation (38), and integrin adhesion (18, 25, 33);

2) binding of collapsin-response mediator proteins (CRMPs), which may subsequently be modified by phosphorylation or oxidation in order to influence GSK-3β activity or microtubule disassembly (27, 39, 40); or

3) activation of MICAL (Molecule Interacting with CasL) leading to direct chemical modification and disassembly of F-actin and hence, growth cone collapse or steering.

1.3 MICALs.

MICAL was discovered initially in lysates of COS-7 cells as an interaction partner of both CasL, a large multifunctional scaffolding protein involved in actin

bundling (and from which the name MICAL derives: Molecule Interacting with CAsL), and vimentin, a protein abundant in intermediate filaments (41). Further, MICAL was determined to interact through the SH3 domain of CasL, via a PPKPP motif near its C-terminus, and mutation of the lysine of this motif was sufficient to abolish interaction. Association with vimentin also appeared to depend on the C-terminus of MICAL, though other regions of MICAL, notably its CH domain could also interact with CasL in isolation (41).

MICAL is a 118 kDa, 1048 residue protein found in a wide range of species including flies, mice and humans. There is one isoform in Drosophila and three in mice and humans (42). MICAL displays a distinct and diverse combination of conserved domains, linked by stretches of much more variable sequence (Fig. 1.2). In order from the N-terminus, these include a flavin-binding monooxygenase domain (MO; a.a. 1-484), the only known enzymatically active component of the protein; a calponin homology domain (CH; a.a. 516-617); a LIM domain (a.a. 690-752); a proline-rich region which includes the PPKPP motif (a.a. 822-827); a glutamate-rich region (a.a. 856-876); and finally, a C-terminal domain (CTD) containing a predicted coiled-coil structure with an Ezrin-Moesin-Radixin (ERM)-like sequence (a.a. 876-1048, 5, 40).

Of these, the most intensely studied regions of MICAL so far have been the MO and CTD. In a series of groundbreaking experiments shortly following the discovery of MICAL as an interaction partner of CasL, Kolodkin et al. (5) independently identified MICAL in a yeast two-hybrid screen and confirmed it by co-immunoprecipitation as a binding partner of the plexin A C2 domain in *Drosophila*. Furthermore, genetic knockouts identified MICAL, and particularly the MO domain, as of critical importance

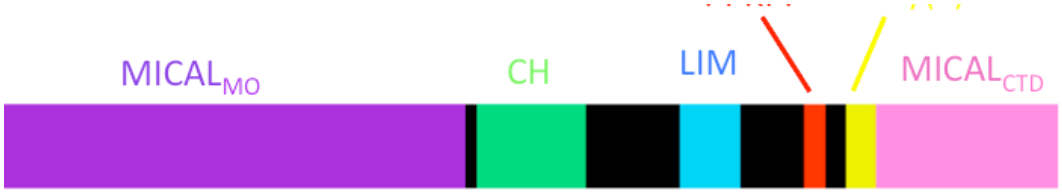

F

2a, domain diagram of MICAL-1 protein. MICAL$_{MO}$ is the enzymatically active ygenase domain; CH is a single calponin-homology domain; LIM is a single zinc-IM motif; PPKPP is the proline-rich region that binds to CasL SH3 domain; Poly(E) glutamate repeat of uncertain function; and MICAL$_{CTD}$ is the predicted coiled-coil hat interacts with plexin intracellular C2 domain.

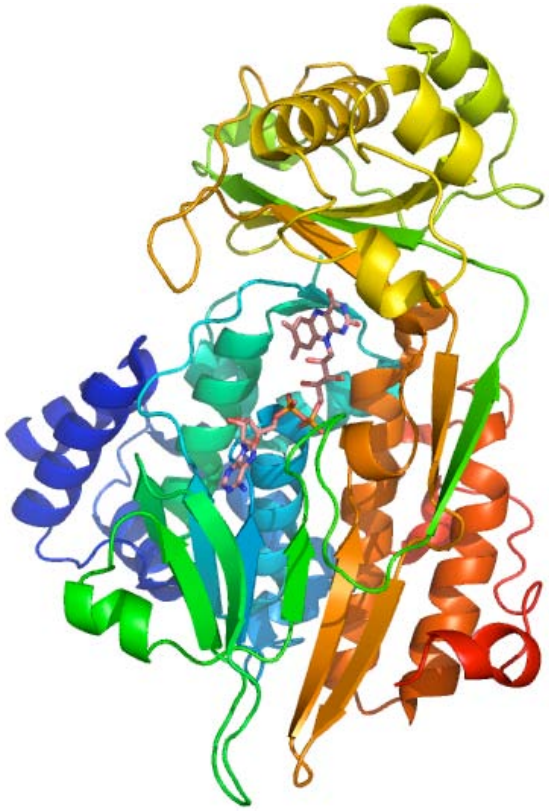

e 1.2b. Structure of the monooxygenase domain of MICAL-1. Note the extensive space surrounding the FAD, which is thought potentially capable of nmodating a protein side-chain as substrate. From PDB file 2BRA.

for proper axon guidance in flies and for response to Sema3A in cell cultures, with knockouts showing adult lethality and serious nerve de-fasciculation deficits similar to plexin knockouts. MICAL overexpression, conversely, produced excessive de-fasciculation similar to that seen in plexin overexpression (5).

In the same work, MICAL's likely status as a flavin-monooxygenase also is implicated on several lines of evidence. First, sequence analysis revealed a GxGxxG motif characteristic of the dinucleotide-binding regions of flavoprotein monooxygenases, and mutagenesis of this to WxWxxW abolished guidance function (5). Second, purified MICAL proteins exhibited a yellowish color and an absorption peak at 425 nm characteristic of flavoenzymes. Third, the known monooxygenase inhibitor EGCG abrogated axon repulsion by Sema3A in a manner highly similar to MICAL knockout (5). However, it is worth noting that EGCG was subsequently found to cause human fl-MICAL to precipitate, so this "inhibition" may actually be due to non-specific damage to the enzyme (43, 44).

X-ray crystallography and kinetics data have since given insight into the structure and catalytic activity of the MICAL MO domain and decisively confirmed its status as a flavoenzyme (42, 46). The structures of the other domains have been resolved only by NMR (CH and LIM), (45) or not at all (proline-rich and CTD). The MO domain shows only distant sequence similarity but large structural resemblance to two other families of flavoproteins, the aromatic hydroxylases and amine oxidases, although the binding pocket containing the flavin is considerably larger than these, suggesting an unusually large substrate, possibly a protein side chain (40, 42, 46).

Kinetics data shows that MICAL-MO consumes NADPH with a 10-times larger

rate for a given concentration than NADH. Product inhibition by $NADP^+$ is also observed (42). Interestingly, the MO is capable of directly reducing O_2 at a high rate (possibly as high as $77s^{-1}$, 42) to generate H_2O_2, sometimes described as a "NADPH oxidase" reaction (43, 44, 47), (Fig. 1.3). This reaction is of uncertain significance but hypothesized to play a role in signaling.

While hydrogen peroxide is normally thought of as a dangerous reactive oxygen species like superoxide and hydroxyl radical, recent studies (48-50) have indicated that the picture is considerably more complex, with the classic toxic effects of oxidative stress associated with H_2O_2 only appearing at a level well above that necessary for redox signaling. Studies in COS-7 cell lysates have shown strong H_2O_2 production in the presence of constitutively active MICAL constructs (40).

Aside from its interaction with vimentin, the significance of the MICAL CTD was first appreciated as the area of the protein responsible for its interaction with plexin, it being sufficient for the observed co-IP with Plexin C2 domain (5). Further investigation has produced strong evidence that the CTD functions in a dominant-negative, and likely auto-inhibitory fashion. For example, expression of a myristoylated (membrane-targeted) form of the protein was sufficient to create axon guidance phenotypes similar to MICAL knockout (5), and in COS-7 lysates the expression of a similar construct containing residues 761-1048 was able to abolish Sema3A-induced contraction (40).

Further work in *Drosophila* bristles has shown that the plexin-interacting (CTD) region, and for that matter the entire sequence of MICAL excluding the MO domain, is sufficient to cause changes in actin polymerization behavior consistent with a dominant-negative (51). Conversely, deletion of the CTD produces constitutively active MICAL

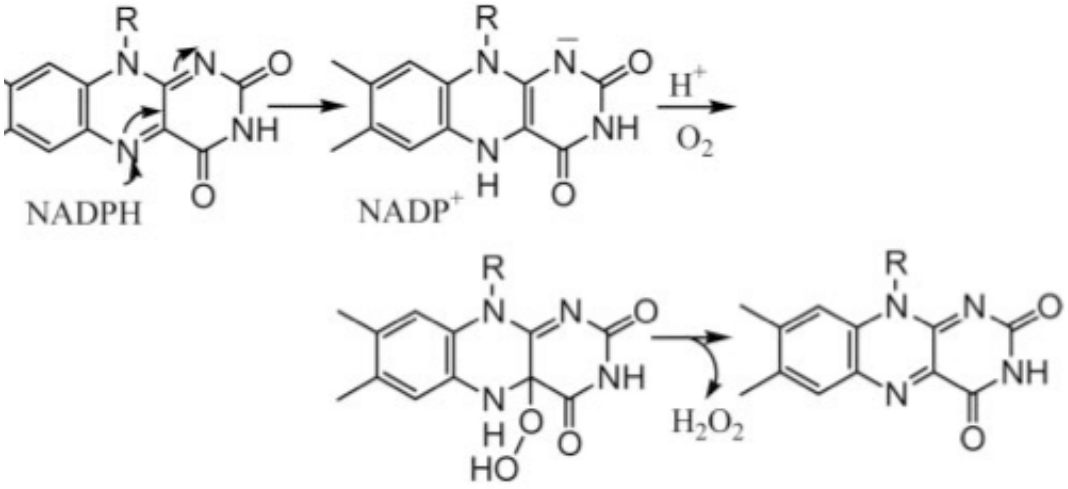

re 1.3 Proposed mechanism of the MICAL NADPH-oxidase reaction. NADPH is to convert FAD to $FADH_2$, which then reacts with dioxygen. In most oxygenases the resulting C4a-hydroperoxide is protected from bulk solvent but in AL it is vulnerable under certain circumstances, decomposing to H_2O_2. It is thought n the presence of the appropriate protein substrate this reaction is averted, in favor f sulfoxidation of key actin residues. Reprinted from (42).

constructs as measured by H_2O_2 production, cell contraction, axon guidance behavior, and bristle morphology (40, 51, 52). CTD deletion also leads to a decrease in the number of cells exhibiting actin stress fibers, as does mutation of key alanines to prolines to disrupt the CTD's coiled-coil structure (53).

In turn, rescue of these constitutively active, overexpression-like phenotypes is possible by co-expression or direct addition of the pure CTD region; for example, H_2O_2 production in cell lysates is restored to normal levels (40). Finally, overexpression of the full-length form of MICAL (fl-MICAL)--that is, with a functional MO domain but the CTD attached and intact--generally results in limited or no phenotypic change, further suggesting that the natural state of the protein is autoinhibited (5, 53). In vitro, fl-MICAL in lysates and as purified protein is found to consume NADPH at a far slower rate than any constructs that omit the C-terminal region (40, 54).

The CTD is notably absent in the mammalian MICAL-2 isoforms, which unlike the other two, appears to be primarily nuclear in localization and function and is constitutively active (53, 55). Hence it must be regulated by some other mechanism. However, chimeric proteins combining the C-terminus of MICAL-1 with the MO- and CH domains of C2 show a reconstitution of the autoinhibited state seen in MICAL-1 and -3 (53).

Altogether, these results suggest that fl-MICAL exists in an autoinhibited state under normal conditions in the absence of semaphorin signaling. It appears plausible then, given the known concomitant roles of the CTD as auto-inhibitory domain and as the plexin-interacting region, that activation of plexin, presumably in the AND-gate like fashion described above, makes available binding regions on the plexin C2 intracellular

region which then competes the CTD away from the MO, allowing full MICAL activity to mediate growth cone collapse (56).

The role of the other components of the MICAL molecule remains obscure. For instance, although the typical role of CH domains is actin-binding, this typically happens in pairs of cooperating CH domains. The single MICAL CH domain, on the other hand, appears to add no actin-binding capacity; the MO domain alone binds actin as well as $MICAL_{MO\text{-}CH}$ (44). Hence, its importance has only recently begun to be understood to play a necessary role for correct localization of MICAL to the region of growth cones, effective rescue of actin dynamics in fruit fly bristles and possibly axon guidance (51) as well as for binding of CRMP proteins (40). As for the other domains of MICAL, the LIM domain contains only a single zinc-finger and its function remains mostly unclear (44), while the glutamate-rich region, being very short, seems not to have any vital function, though it may conceivably provide electrostatic interactions with certain basic patches elsewhere on the MICAL molecule.

1.3.1 Mechanism of action of MICAL.

Regardless of the question of autoinhibition or the regulatory and binding functions of the various subunits (in which the CTD appears to play a special part), the exact chemical mechanism of MICAL monooxygenase activity in semaphorin signaling and growth cone collapse is still somewhat debated, although recent experiments have clarified new possibilities. It was proposed early on that MICAL may function entirely through production of H_2O_2 as a signaling molecule (42).

However, many facts also suggest that MICAL's physiological function may include, or even be limited to, direct chemical modification of a specific target molecule,

very possibly a protein side chain: the size of the active pocket, the potential toxicity of free H_2O_2 production at the level observed (at least for the non-autoinhibited enzyme), the areas of positively charged residues surrounding the entrance to the active pocket suggestive of a binding, as well as the fact that the known flavoenzymes most structurally similar to MICAL (aromatic hydroxylases and amine oxidases) produce H_2O_2 only as an adventitious leakage in the absence of substrate site (44, 42, 46), all support such a possibility. This has led to a search for potential substrates, although a small-molecule search among a number of amino acids, aromatic compounds and polyamines turned up no candidates, with many acting as inhibitors (43, 44).

In general, the distinction between direct substrate modification and modification by the presumably extremely high local peroxide concentrations generated close to the enzyme has been difficult to settle definitively. Although the most recent evidence weighs on the side of direct substrate modification, H_2O_2 signaling cannot be excluded (40, 44, 57).

In cell lysates, co-IP experiments show that semaphorin signaling induces CRMP binding to MICAL via the MO and LIM regions, and that co-expression of these two creates increased cell contraction reminiscent of semaphorin signaling (40). However, Amplex Red measurements revealed in this case that the addition of CRMP leads to a dramatic reduction of H_2O_2 production by normally constitutively active MICAL, feeding the surmise that CRMP is a direct substrate (44).

Other studies with CRMP have shown that this protein may be modified by MICAL through oxidation at Cys504, leading to the formation of a disulfide-linked dimer (58). This dimerization may be essential to downstream control of actin dynamics, as

mutations in either Cys504 of CRMP or Cys32 of THX (which exchanges with CRMP to reduce it back to the monomeric state) showed abrogation of normal Sema3A response (58).

These same studies also detected, using HyPer, an oxidation-sensitive GFP-based fluorophore, a rapid time-dependent increase in H_2O_2 production near the membrane following Sema3A stimulation that, along with the majority of cell contraction, is dispelled by knockdown of either MICAL-1 or -3 with siRNA (58). Immunoprecipitation also showed the appearance of the CRMP dimer within minutes following Sema3A stimulation, but only in the presence of active MICAL. Thus, the possibility that MICAL's H_2O_2-producing capacity is an essential part of semaphorin-plexin signaling remains very much an open one (58).

Perhaps the most critical and widely discussed advance in the search for a MICAL substrate came from a series of biophysical observations published in 2010-11 (51):

Firstly, it was found through in-vitro co-sedimentation that MICAL has actin-binding properties, which could assist in its modification of F-actin dynamics. For example, this raises the possibility of regulation of the actin-binding property by axon guidance signaling, possibly through the CTD displacement mechanism proposed earlier. MICAL monooxygenase could then, due to its extreme proximity to actin, either oxidize it through H_2O_2 production or direct modification of a side chain.

Secondly, when measured by NADPH consumption, it was found that in the presence of F-actin, constitutively active MICAL constructs (specifically, $MICAL_{MO\text{-}CH}$) exhibit a >100-fold increase in rate and in k_{cat}/K_m, further increasing the likelihood of F-

actin being a direct substrate of MICAL (43, 59). This acceleration strongly supports the suspicion that F-actin is the physiological substrate of MICAL--although it may still be due to a conformational change upon actin-binding, for example, that places the flavin ring in a more exposed position for its reaction with O_2.

Thirdly, these same MICAL constructs are capable of disassembling F-actin, and oppose the polymerization of G-actin. In co-sedimentation experiments, G-actin was stably polymerized, then combined with NADPH or both NADPH and $MICAL_{MO\text{-}CH}$. Ultracentrifugation to pellet F-actin revealed that while $MICAL_{MO\text{-}CH}$ alone, or NADPH alone or with BSA control did not affect actin's polymerization state, NADPH with $MICAL_{MO\text{-}CH}$ converted most, though notably not all, F-actin into G-actin (or, according to electron microscopy, fibers sufficiently small to elude ultracentrifugation). In addition, pyrene-actin timecourses also show dramatic effects on actin polymerization state by NADPH with $MICAL_{MO\text{-}CH}$, whether the MICAL is added at the beginning of, or well after the G-actin has had a chance to polymerize (59).

That the disassembly reaction does not go to completion, leaving residual F-actin even with large excesses of NADPH and long after addition of MICAL, remains somewhat of a puzzle, though one of disputed significance. Aggravating the issue is the fact that MICAL does not show distinct two-phase behavior with regard to the NADPH consumption rate that would be expected if an extremely fast actin-modifying reaction took place first, giving way to a far slower NADPH oxidase reaction; instead, the reaction rate remains moderately high throughout. Some groups (43, 44) claim this as evidence of "substrate recycling" whereby an equilibrium is achieved between MICAL modification, disassembly and actin re-polymerization; other data implies that a chemically permanent

modification is at work in the disassembly process by MICAL, meaning there is no measurable equilibrium.

In concert with these biophysical findings, genetic work in *Drosophila* bristles (which in fly morphogenesis are initially patterned upon processes of F-actin governed by Semaphorin/plexin signaling in a manner reminiscent of axonal guidance) showed dramatic defects in actin patterning upon overexpression, constitutive activity, or knockout of MICAL (51, 52). In the absence of MICAL signaling, the actin fibers appeared overly thick and rigid, and therefore formed abrupt ruptures instead of following the normal curvature of a wild-type bristle. Excessive signaling on the other hand converted the bundled and linearly oriented wild-type actin structure into a fragmented meshwork, with many points and branches, consistent with MICAL disrupting the actin polymerization more thoroughly (51). Confirming the link with semaphorin signaling, similar phenotypes appear when plexin mutations are introduced. The CH and MO domains appear to be essential to proper bristle formation, while as in earlier work the CTD acted in a dominant-negative fashion and constructs lacking it were constitutively active (51, 53).

Additional results from mass spectroscopy accompanying these discoveries aimed to determine the exact actin modifications involved in MICAL treatment, and the possible mechanism of their reversal. $MICAL_{MO\text{-}CH}$-treated actin was found to be consistently heavier by 32 daltons, consistent with the addition of two oxygens; these modifications localize to two methionine residues in the D-loop of the actin molecule, M44 and M47 (M46 and M49 in mammalian actin) (55, 59, 60). To further investigate these modifications, mutations of either or both methionines to leucine were made and

their behavior after MICAL treatment was examined. Strikingly, mutations involving M44L all produce MICAL-resistant actin, which does not disassemble or show reduced polymerization when treated with $MICAL_{MO\text{-}CH}$ (though no control was reported with H_2O_2) (59).

Intriguingly, modification of M47 appears to have no effect whatsoever on F-actin susceptibility to MICAL; its role therefore remains unclear. How to square the fact that MICAL shows quantitative modification of two distinct residues--of which only one appears necessary for MICAL actin disassembly--with claims that MICAL is a "specific" modifier of actin is somewhat uncertain, and has yet to be thoroughly discussed or investigated. Hence, it is generally considered that the modification of M47 is simply a by-product of the modification of M44, due simply to its relative proximity on the D-loop region, especially given that the M47L actin mutant shows no resistance to MICAL-based disassembly (59).

1.3.2. Unresolved questions in MICAL function.

How to square sulfoxidation, a stable chemical modification that does not spontaneously reverse itself under the conditions of the cell--and particularly not at a rate remotely commensurate with which the forward reaction is carried out by MICAL--with the apparent substrate recycling and lack of two-phase kinetics other groups have observed is one puzzle of MICAL's mechanism of action on actin dynamics that remains to be untangled.

An equally pressing question, given that this particular kind of stable modification has been observed and its effects are by this point well documented--M44L cells show a bristle phenotype similar to MICAL-/-, while yeast containing M44C were non-viable (44,

59)--is whether actin modified by methionine oxidation by MICAL is permanently modified and simply degraded or regenerated in some way--and if so, how.

Insight into this has come from experiments published by two groups, which both found that the selenoenzyme MsrB, a methionine sulfoxide reductase, is capable of restoring the polymerizability of MICAL-treated actin, and argue for its role as the physiological regulator of MICAL-based F-actin disassembly (52, 60). In this work, mass spectroscopy of actin treated first with MICAL and then MsrB shows the loss of the 32 Da originally found to be added by MICAL, indicating that MsrB is indeed reducing methionine sulfoxide at both Met44 and Met47.

Importantly, given that MsrB is exclusively stereospecific to the *R* enantiomer of methionine sulfoxide--MsrA acts only on the *S* form--the finding that MsrB can completely reverse the disassembly and modification of actin by MICAL shows that MICAL, in addition to being markedly accelerated in the presence of F-actin, also modifies it stereospecifically. Together these add support to the idea that F-actin is a direct substrate of MICAL rather than being modified by locally high H_2O_2 concentrations. However, there are conflicting reports on whether actin treated with H_2O_2, which is achiral and hence should show no inherent preference for *pro*-R or *pro*-S oxidation of methionine, shows partially (60) or negligibly (52) restored polymerization upon MsrB treatment.

In vivo, expression of MsrB appears necessary for a normal bristle phenotype and for correct nerve fasciculation in *Drosophila*, with MsrB deletion producing phenotypes reminiscent of MICAL- or plexin- overexpression. MsrB overexpression, on the other hand, appears capable of rescuing signs of MICAL overexpression (52), though the

reports disagree somewhat on the effects of MsrB overexpression; one observes clear changes in bristle phenotype and muscle organization similar to MICAL deletion (52), while the other finds no change in F-actin polymerization in HeLa cells (60).

Such evidence, on balance, appears to lay out an important regulatory role for MsrB in axon guidance and actin remodeling as a purposeful antagonist of F-actin disassembly by MICAL. On the other hand, a relatively small number of proteins are currently thought to be regulated by methionine oxidation (61, 62); possibly the most well known of them is CamKII. Moreover, recent mouse models have shown that simultaneous double knock-out of both MsrA and MsrB is wholly viable and produce minimal phenotypic abnormalities, mostly involving dietary requirements for methionine; no neurological or axon guidance issues were reported (61).

This raises doubts about the true necessity of MsrB as a regulator of actin oxidation state and function and possibly, by extension, re-intensifies questions as to the true role of MICAL in mammalian systems. Therefore, despite impressive and suggestive results on some fronts, the status and importance of MICAL in actin dynamics and particularly axon guidance remains to a large degree unresolved.

As well, the status of MICAL as a physiologically important actin modifier depends not on the behavior of $MICAL_{MO\text{-}CH}$, which is constitutively active, but on the full-length form, fl-MICAL, which is thought to be modulated by semaphorin/plexin signaling in a complex and sensitive way. Although it has been shown that deletion of fl-MICAL can phenocopy that of plexin, evidence that overexpression of fl-MICAL produces strong phenotypes is contradictory at best. In the work of references (51) and (52), the expression of an additional copy of fl-MICAL seemed to produce noticeable

abnormalities, while in references (40), (53) and (60) it either did not or the effect was modest. Further, the original findings on MICAL linking it to plexin signaling showed ambiguity in the abundance of overexpression phenotypes of fl-MICAL and even in the phenotypic difference between knockout and overexpression: while “a large fraction of these MICAL GOF motor axon guidance phenotypes are consistent with increased defasciculation”, Kolodkin et al. admit that "GOF defects in some cases are quite similar to the defects we observe in MICAL mutants and defects reported in PlexA GOF mutants" (5).

There is also a general lack of kinetic and in vitro studies of the behavior of fl-MICAL. What data there is suggest dramatic differences between MICAL orthologues across species, with human $MICAL_{MO\text{-}CH}$, for instance, proving much more active than the *Drosophila* orthologue (44).

Therefore, an investigation of the behavior of the full-length MICAL protein, particularly towards F-actin, and with comparison to the behavior of $MICAL_{MO\text{-}CH}$, is a necessary step in establishing its mechanism of action and activation. In addition to this, the hypothesis of how fl-MICAL is activated--with an AND-gate like mechanism involving plexin dimerization, GTP-bound Rnd1 binding, remains unconfirmed in vitro. In the following experiments, using purified proteins in vitro, several aspects of MICAL activity were examined: its actin-binding, actin-disassembling, and rate acceleration in the presence of F-actin, as well as its reaction to added plexin and Rnd1.

In general, I find that in contrast to the $MICAL_{MO\text{-}CH}$ used in most published experiments thus far, fl-MICAL does not display the expected disassembly activity in the presence of F-actin. This much is consistent with the theory of autoinhibition, except that

the presence of F-actin does produce a sizable increase in NADPH consumption with no decrease in relative H_2O_2 production, suggesting that actin alone is sufficient to lift autoinhibition of the monooxygenase domain to a significant degree.

The plexin-Rnd1 results also, while partly supporting the existing theory, introduce ambiguity. In accord with the AND-gate model, these two factors are found capable of stimulating fl-MICAL monooxygenase activity, but they differ from the model in that they only appear to work in the *absence* of F-actin. It is possible that some specific factor other than these, as yet unidentified, is necessary for activation of F-actin disassembly by fl-MICAL.

There is also some evidence that the CTD, in purified form, is able to displace $MICAL_{MO}$ and $MICAL_{MO\text{-}CH}$ from F-actin fibers, lending support to the autoinhibitory model. However, under some conditions of experiment these results show a weak effect, that might not account for the degree of activity and enzymatic control needed for MICAL's posited role in signaling.

Chapter 2: Initial Cloning, Expression and Purification.

2.1 Introduction.

The process of reconstituting the hypothesized systems of MICAL function in vitro required acquiring the DNA for the genes, then successful expression of protein, and purification of the following proteins: $MICAL_{MO}$, $MICAL_{MO\text{-}CH}$, and fl-MICAL; CRMP; the intracellular domain of Plexin A1; mouse Rnd1; and a construct of the MICAL C-terminal region, called $MICAL_{CTD}$.

Techniques used in the cloning stage typically included PCR with Pfu polymerase, restriction digestion, clonase reaction and TOPO cloning. Clonase is a technique devised by Invitrogen to allow efficient, frame-conserving integration and removal of gene inserts into a variety of plasmids known as "donor vectors", using recombination between attP sites. TOPO cloning is a method that uses the topoisomerase activity of Taq polymerase to rapidly integrate the insert in the position of the 3' thymidine in the target sequence 5'-(C/T)CCTT-3' in a rapid (5 min), ligation-free reaction.

For expression, standard BL21 cell lines were rendered competent by re-suspending the cells on ice in 10 mM PIPES, 55 mM $MnCl_2$, 15 mM $CaCl_2$, and 250 mM KCl, and 10 mM MgSO4, pH 6.8, spinning and re-suspending once more, adding DMSO to a final concentration of 7%, and quick-freezing in liquid nitrogen.

2.2 MICAL-2 Cloning

PCR amplification of mouse MICAL-2 was attempted, using MICAL-2 cDNA. AccuPrime Pfx polymerase and SuperMix were used. Primers, dissolved to 100 nM, were of the following: for forward, without stop codon (NS); forward, with stop codon (S), and the reverse primer (Table 1). Reactions produced 350-550 ng/μL of DNA according to

	CTG GAG TCA CGG GTG-3'	constructs containing C1 domain
), SalI	5'-CCG ATA GTC GAC TCA GCT GCT CAG GGC CAT TGT-3'	Antisense primer for all plexin-A1 constructs containing C2 domain
), NheI	5'-CCG ATA GCT AGC ATG CAG CAG ATT GAC TAC AAG-3'	Sense primer for plexin-A1 RBD subclone
, SacI	5'-CCG ATA GAG CTC TCA CTT GCT GCC ACG GTC GCC-3'	Antisense primer for plexin-A1 RBD and C1-RBD subclone
, BamHI	5'-CCG ATA GGA TCC CCG GCA GCA AGA TGG TCT CT-3'	Sense primer for plexin-A1 C2 domain subclone
(A_), BamHI	5'-TTA CGA GGA TCC GAA GCG ATC GAA AAA-3'	Sense primer for subcloning of $MICAL_{CTD}$
(A'_), BamHI	5'-TAT GCC GGA TCC TCT AAC ATG CAG CCG-3'	Sense primer for subcloning of $MICAL_{PPPCTD}$
(A"_), BamHI	5'-TTA CGA GGA TCC CCG CTG CCG CCG CTG-3'	Sense primer for subcloning of $MICAL_{CTD}$ lacking
(_B), SalI	5'-TAT CGT GTC GAC TTA CGC CGG CAT TTC ACG-3'	Antisense primer for subcloning of original $MICAL_{CTD}$ construct
(_B'), SalI	5'-TAT CGT GTC GAC TTA CAG TGC ATC GCG CTG-3'	Antisense primer for subcloning of pre-truncated CTD (CTD24)
PP_)	5'-CTG AAT GAA ATC GAA CCG CCG ATG CGC GAA CTG GAA-3'	Forward mutagenic primer for disruption of CTD coiled-coil
_PP)	5'-TTC CAG TTC GCG CAT CGG CGG TTC GAT TTC ATT CAG-3'	Reverese mutagenic primer for disruption of CTD coiled-coil
_), BamHI	5'-ATA CTA GGA TCC CGT GCA CCG CAA CCG-3'	Sense primer for amplification of mRnd1
b), SalI	5'-ATA GAT GTC GAC TTA GAC CGG AGA TTT CGG-3'	Antisense primer for amplification of mRnd1

st of primers produced for cloning and construct production.

A_{260} measurement, and were purified using a QIAquick PCR purification kit. However, very little DNA eluted after the purification (~2.5 ng/μL), not enough to appear on a 1% agarose/ethidium bromide gel.

After repeating the PCR reaction and purification attempt with similar results, it was determined that this was due to formation of primer dimers (Fig. 2.1), which inhibited DNA extension. On the other hand, PCR of the small GTPase Rab1, carried out simultaneously, proceeded well, as seen on agarose gel. To confirm that the original cDNA was correct, it was run in an agarose gel; the resulting band indicated a length of 6 kb, much longer than expected. A new cDNA was therefore grown from culture as a mini-prep, and PCR was run again. To reduce the risk of primer dimer formation, dimers were used at reduced concentration. This time, robust amplification was observed by agarose gel for both the "S" and "NS" versions.

In order to transfer the purified PCR product into suitable destination vectors (Fig 2.2), TOPO cloning was attempted. PCR product was mixed with TOPO salts, water, and destination vector mixed gently and incubated at room temperature for 5 min and placed on ice. The usual transformation procedure was then used: 2 μL of the reaction was then added to 50 μL competent *E. coli* CG5 maintenance cells, incubated another 20 minutes on ice, heat-shocked for 35 s at 42 ºC and then returned to the ice. The transformed cells were then added to 500 μL TB, shaken at 37 ºC for 1 hr, and then plated on selective agar.

No transformants were observed from the first of these attempts, so the clonase technique was tried as well, with destination vectors pDEST 14, 15, 17, and 49. Entry clone (mMICAL-2), destination vector and clonase reaction buffer were combined in TE buffer (pH 8.0) and incubated at room temperature for 1 hour. Proteinase K was then

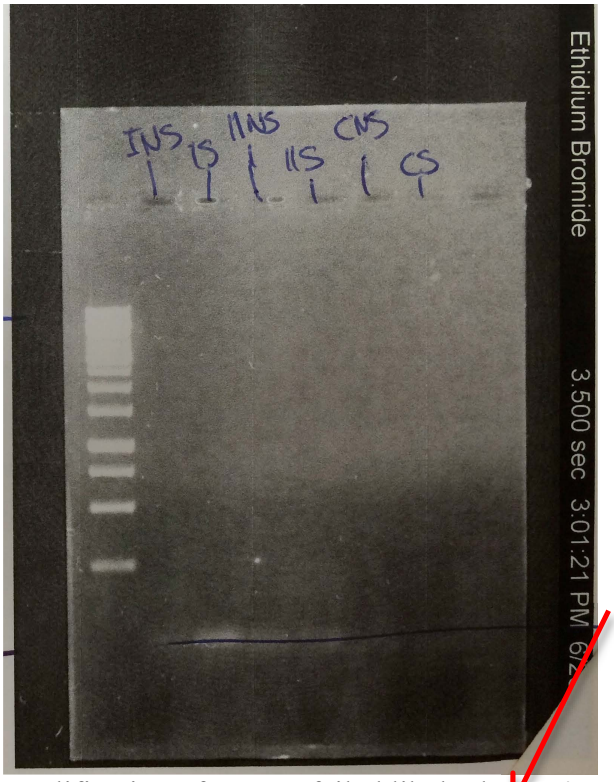

2.1. Initial PCR amplification of CRMP failed likely due to formation of dimers the original primers.

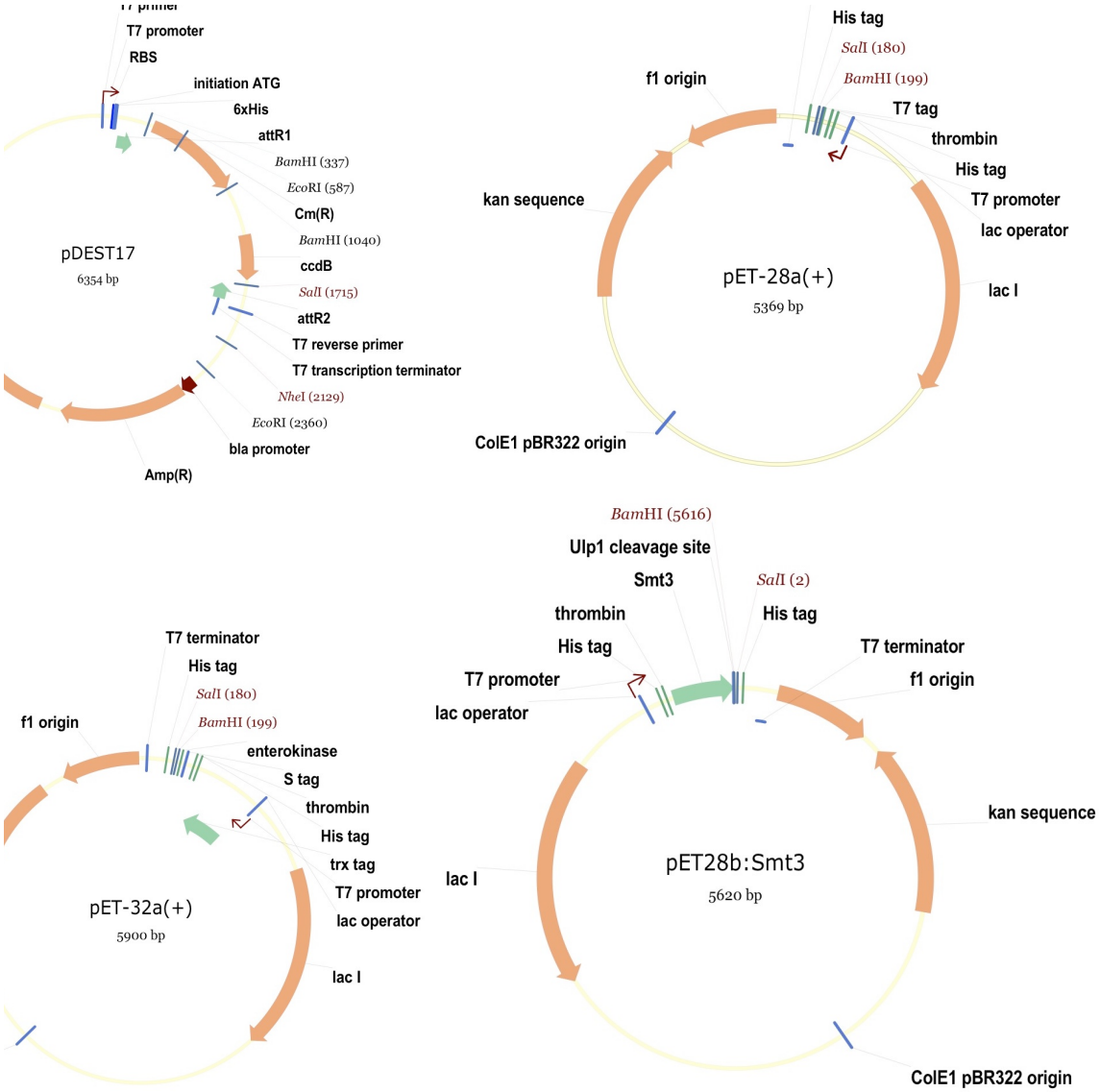

ıplified maps of the main vectors used for construct production and protein expression:
'28a, pET32a, and pSmt3.

added, and the mixture incubated a further 10 min.

Initially this method, too, generated no transformants. However, after varying the ratio of PCR product to vector, this reaction appeared successful, with hundreds of colonies observed from 100 μL transformed cells per plate. Rab1, curiously, still did not transform. The colonies were grown in LB medium overnight and mini-prepped. Restriction with BamHI and agarose gel showed a plasmid length of ~6 kb, close to the predicted value (Fig. 2.3).

At the same time, continued efforts with TOPO cloning appeared to succeed, but upon restriction digestion with BamHI the plasmid appeared, unexpectedly, to break into two fragments of about 4.5 and 1.5 kb (Fig. 2.4). These transformants were therefore deemed unusable as well. TOPO cloning was repeated anew, searching for a suitable target vector for the MICAL-2 PCR product. To speed this process, sectors of agar plates were streaked with different colonies following transformation, and the colonies PCR amplified in search of a band similar to the expected insert. However, no bands were observed by agarose gel after PCR.

Eventually, after continued repetition, bands of the expected 3 kb length were obtained by double restriction of the product of miniprep samples of TOPO plasmids (Fig. 2.5). However, when these miniprep samples were submitted for sequencing it was found that, although they carried considerable areas of sequence alignment with the expected, large tracts were missing, including TEV sites. In light of these ongoing difficulties, further attempts to clone MICAL-2 were halted.

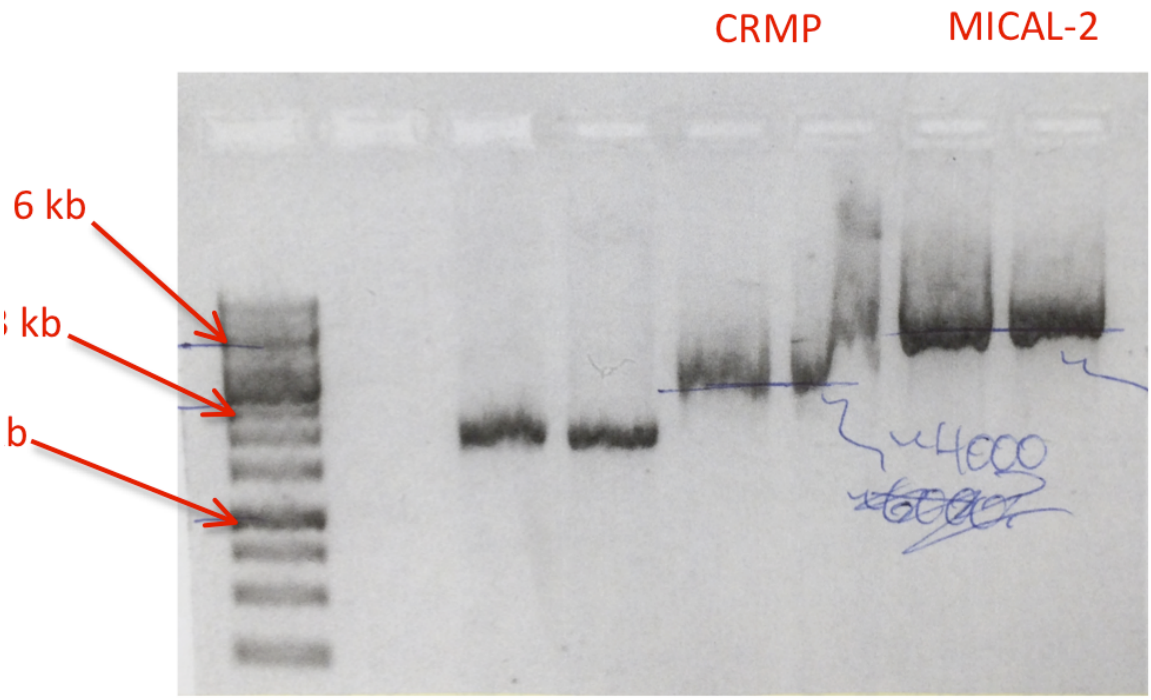

re 2.3. Apparently successful initial TOPO cloning. Cleaved plasmid masses correspond RMP (~4 kb) and MICAL-2 (~6 kb).

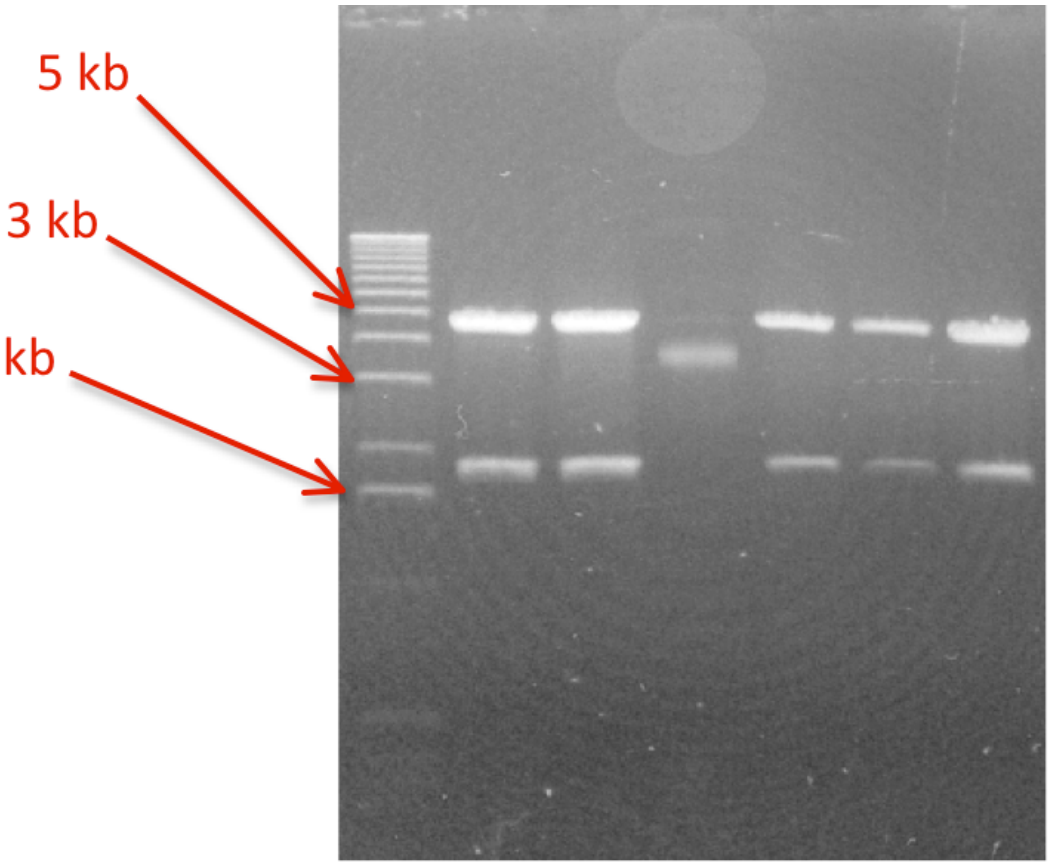

ure 2.4. Single digestion with BamHI unexpectedly causes the MICAL-2 containing
smid to break into two fragments, indicating an error in the sequence.

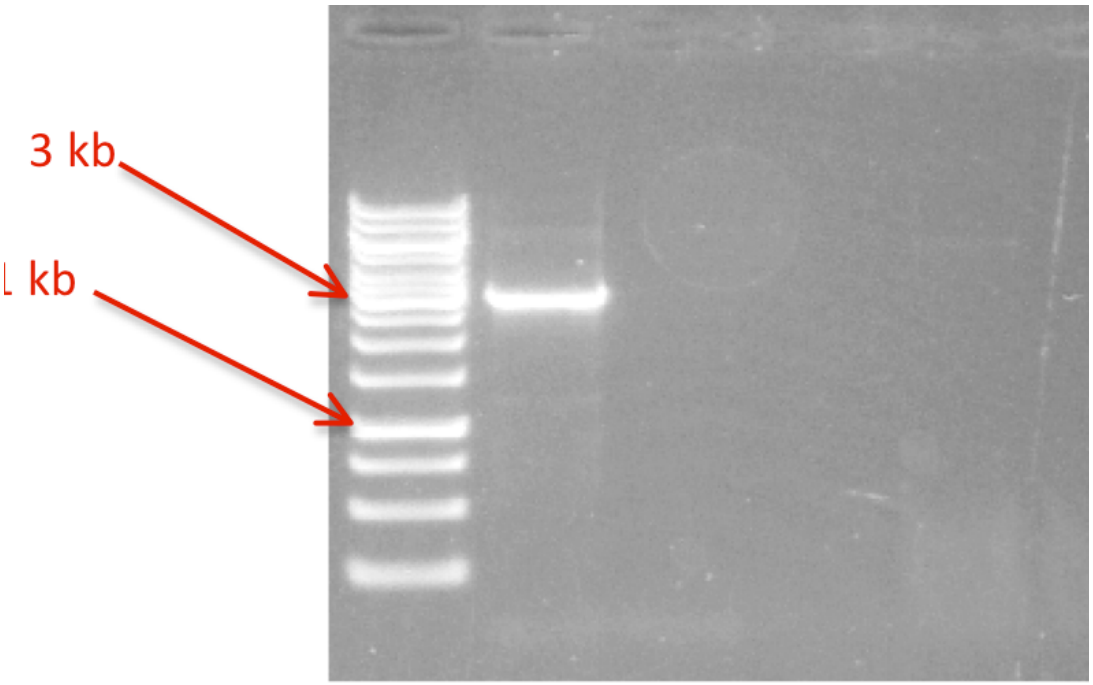

gure 2.5. Successful PCR product of MICAL-2.

2.3. MICAL-1 cloning and purification.

Initially, mouse fl-MICAL-1 DNA was obtained from American Tissue Culture (ATCC; Gene ID NC_000076.6) and cloned into a vector which affords an N-terminal GST tag cleavable with thrombin pET48 --Novagen Inc. (Fig. 2.2). MICAL-1 monooxygenase ($MICAL_{MO}$) clone was also available. Both were in BL21 expression cell cultures. In preparation for expression and purification, 4 L LB media was made and titrated to pH 7 with NaOH, and 1mL aliquots of 1 M IPTG were also prepared for induction of cultures. At the same time, plates of LB agar were prepared for future selection experiments, containing 25 μM kanamycin sulfate, 100 μM ampicillin sodium salt, or 34 μM chloramphenicol (dissolved in ethanol). Some plates also contained both kanamycin and chloramphenicol, or ampicillin and chloramphenicol.

After autoclaving, each liter of LB was combined with 100 mg ampicillin, 100 μg FAD, and 0.15 g DTT (final concentration 1 mM). An inoculation culture of fl-MICAL was set up overnight. In the morning, after 1 hr shaking at 210 rpm and 37 ºC to bring the media to growth temperature, inoculation was carried out and A600 was measured every 30 min. Upon reaching A600 of 0.6, the media was moved to 20 ºC, a timepoint sample was taken and the remainder induced with 1 mM IPTG overnight. The final absorbances of the culture were measured to be ~5.0, based on 10-fold dilutions to keep within the linear range of the spectrometer. The cultures were washed with benzamidine 1 mM and PBS buffer (140 mM NaCl, 2.7 mM KCl, 10 mM Na_2HPO_4, 1.8 mM KH_2PO_4, and pH 7.3), re-centrifuged and the pellets frozen at -80 ºC.

For resuspension of the pellet, pellets were broken by microfluidization in the

following way: pellets were thawed on ice, and pellets from each 1 L of culture were resuspended with 35 mL of the appropriate buffer for purification of the protein, but with the addition of 5 mM $MgSO_4$, 10 μg/mL DNAse, and a tablet of EDTA-free Complete protease inhibitor cocktail (Roche pharmaceuticals). The mixture was gently resuspended with a glass rod and two presses of a dounce homogenizer, stirred at 4 ºC for 10-15 min. and broken using two passes through the microfluidizer with 75 psi of air pressure. (Unless otherwise stated, all pellets were processed in this way.)

The lysate was clarified by 30 min. spinning in a SS34 rotor at 10,000 rpm, the supernatant filtered using a millipore 0.22 μM filter Stericup. Glutathione beads and elution buffer were prepared according to manufacturer's instructions, beads were added and shaken with the supernatant overnight. Elution was carried out with a gradient of glutathione. However, when the fractions were loaded on SDS-PAGE gel, no expression was observed. One possible cause of failure was thought to be low dissolved oxygen, due to a persistent plateau in A600 reading early in the growth phase. Subsequent cultures showed a similar difficulty, with A600 values that were slow to increase or even regressed slightly.

Another GST column purification of the fl-MICAL pellet showed significant amounts of product around the expected ~130 kDa mass when run on a 4-15% SDS-PAGE gel (Fig. 2.6), suggesting the growth deficiency may not be important to yield. Thrombin digestions of the fractions that were candidates for containing GST-MICAL1-fl were carried out, and free GST was removed by addition of recharged GST beads. The flow-through was collected, centrifugally concentrated and analyzed by SDS-PAGE (Fig 2.7). The expected band was visible, but very weak, with an abundance of lower-mass

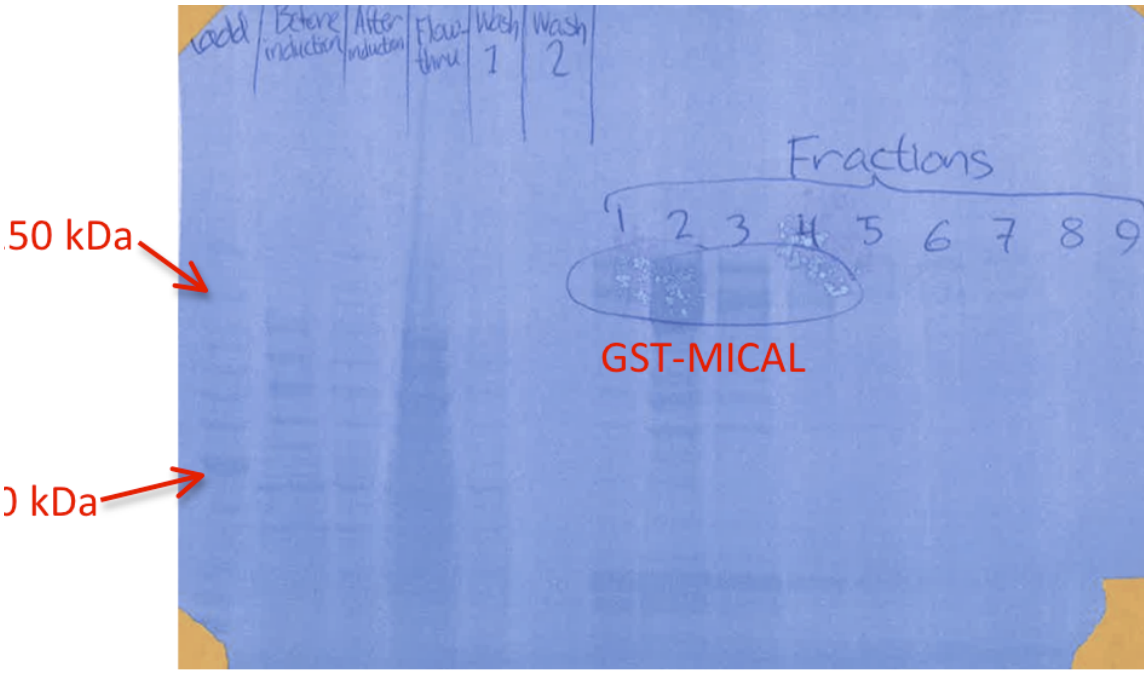

gure 2.6. Elution of fl-MICAL from GST beads.

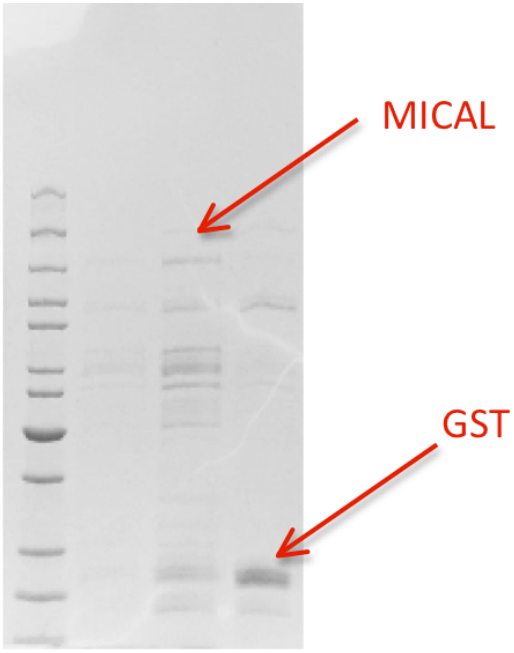

ure 2.7. Following GST tag cleavage and removal, MICAL is found only in poor
ld and contaminated by lower-mass components.

congeners, most likely degradation products.

Due to ongoing difficulties in GST-tag based purification, MICAL1-fl (2-1048) sequence with Q78K modification to eliminate an internal TEV-cleavage site was codon-optimized for *E. coli* expression and synthetized by Genscript Inc including a N-terminal TEV site (MTEVQ78K) was cloned into a pET-28 vector, which instead affixes an N-terminal 6xHis tag for affinity chromatography (Fig 2.2). Further induction attempts were carried out in large batches (6L) or, ideally, a fermentor with automated pO_2 regulation, at 20 ºC. Expression appeared to be counterbalanced strongly by protein degradation, as yields proved highly dependent on the amount of time of induction, with timepoints showing expression clearly underway within 4 hours of induction but completely lost by 20 hours. At best, this afforded small but manageable yields of 6xHis-fl-MICAL protein (0.5 mg/L) which could then be collected by passage through a His-trap column, elution of non-specific binding proteins at 10% (50 mM) imidazole, followed by elution of the fl-MICAL itself at 50% imidazole. Following dialysis or desalting into 20 mM Tris pH 8.0, fl-MICAL protein was purified by binding and elution from a SourceQ anion exchange column using a 0-1.0 M NaCl gradient.

2.4 CRMP cloning.

Mouse CRMP1 cDNA was successfully PCR amplified, producing the expected band around 1.7 kb. The product was gel purified and TOPO cloning was carried out. Initial cloning produced very few or no colonies, and those there were, when grown in minipreps, produced no DNA. Upon repetition and optimization of the protocol with an increased number of colonies was observed, and when grown in minipreps and restriction digested with BamHI revealed a plasmid of about 3.5 kb, the expected size. However,

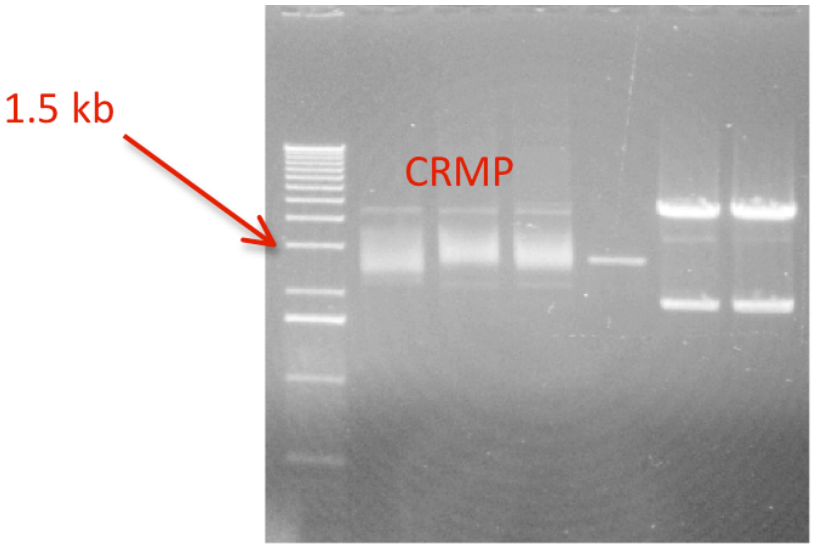

ure 2.8. PCR of CRMP frequently produced a smear of products of approximately the ired length instead of a single pure band.

this band was contaminated and proved unusable (Fig. 2.8)

2.5 Plexin expression, purification, and constructs.

Plates were streaked with cells carrying clones of mouse Plexin-A1 intracellular domain (from ATCC, GenBank NM_008881) in pDEST-15, gift of Dr. Mario A. Bianchet. Seven such colonies were grown in 10 mL LB medium with ampicillin to an A600 of 0.6, glycerol stocks were made by adding 15% glycerol to 1 mL and freezing at -80 ºC, and the remainder was induced with 1 mM IPTG for 3 hr at 37 ºC. At the end the culture was pelleted, sonicated and the expression assessed by SDS-PAGE. Although a band was expected with the plexin intracellular domain's mass of 75 kDa, no difference in general induction before or after IPTG was observed, and the 75 kDa band was not distinct (Fig. 2.9).

New 10 mL starter cultures were begun from the glycerol stock and used to inoculate 1 L each of LB medium with ampicillin, and induced for a longer duration (5 hr). This time the band at 75 kDa was more distinct, but did not show any increase from the addition of IPTG. However, incubation overnight of the cell lysate with Ni-NTA beads and elution with 200 mM imidazole, 20 mM Tris, and 0.5 M NaCl allowed recovery of a moderate amount of plexin from one of the seven clones (Plex2, Fig. 2.10). This plexin as eluted was relatively impure, consisting of two bands of slightly varying mass (~72 and 75 kDa) and two smaller, also closely spaced bands.

The 6xHis tag in the construct required cleavage at a TEV site for removal. TEV protease was grown at 37 ºC and induced overnight at 20 ºC in 2 L Terrific Broth, pelleted, and frozen. The next day pellets were broken and passed through a HisTrap and

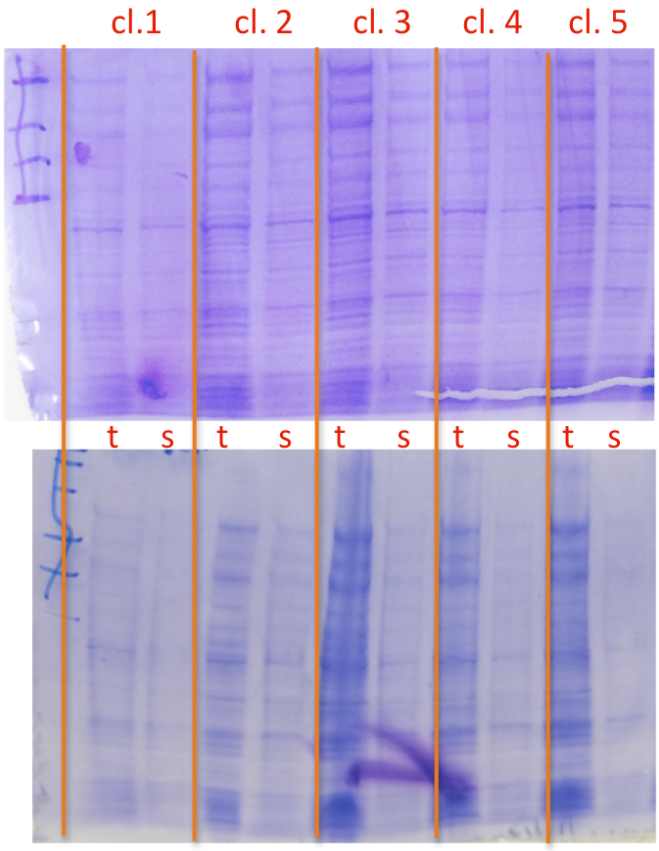

gure 2.9. Expression attempts of the initial TOPO plexin-A1 constructs showed no lucibility. Top, five separate clones before induction. Bottom, the same clones after 3h cubation with 1 mM IPTG. (s, t = soluble and total fraction)

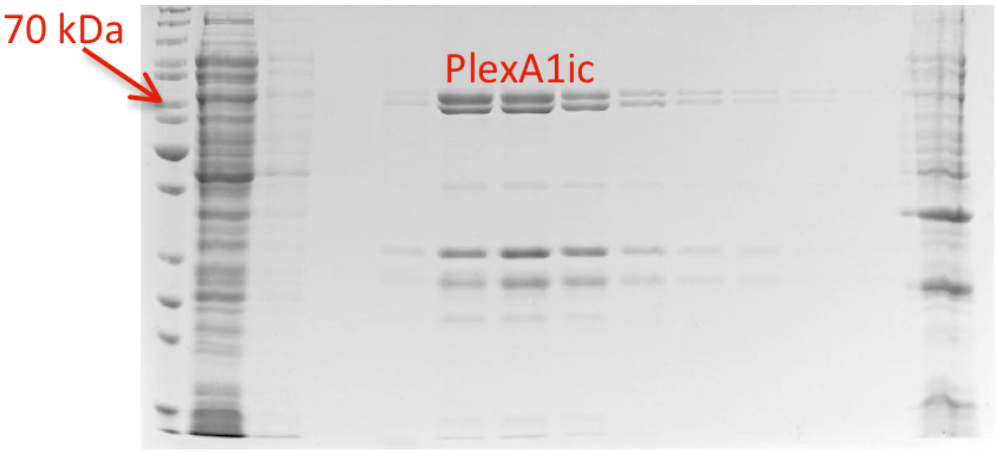

re 2.10. Despite rather poor solubility limited amounts of plexin-A1 intracellular ain could be obtained by elution from Ni-NTA beads.

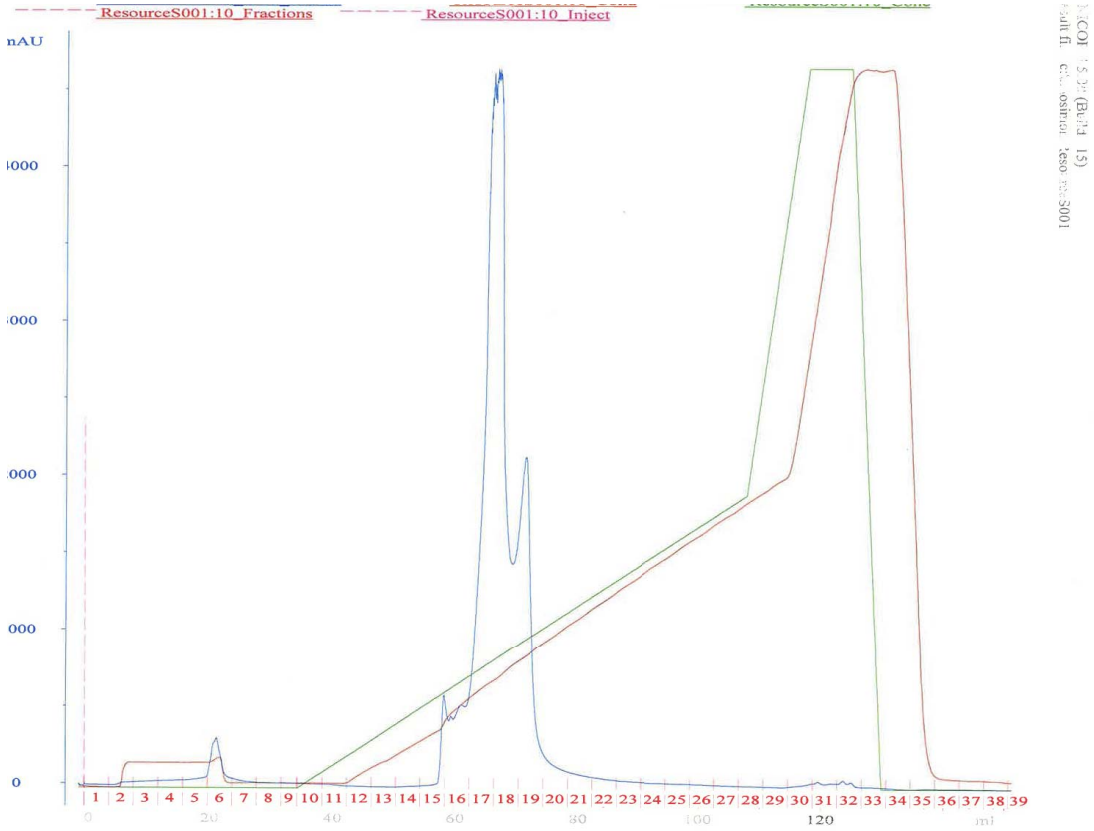

gure 2.11. TEV purification by SourceS readily produces a highly pure product that ıtes as a sharp peak.

eluted, affording ~90% pure TEV in tens of mg quantities. The TEV was desalted to 50 mM Tris, 10 mM NaCl, 10% glycerol, pH 7.5 and subjected to further purification on a MonoS column, eluting in a sharp peak (Fig. 2.11) and then frozen for storage.

In an attempt to increase the yield of plexin, the Plex2 construct was grown to much higher cell densities before inducing (A600=1.5). Also longer induction times, and reduced amounts of IPTG (0.5 mM) were tried, and showed the same basic problem of poor inducibility and low yield. The other six Plex clones, 1 and 3-7, were also test-induced under these circumstances and showed no advantage over Plex2. In fact, surprisingly, it was found that leaving out IPTG altogether had no effect on the level of plexin expression, and even slightly increased it (as assessed by the Bradford assay). SDS-PAGE gels showed no increase in the 75 kDa band in either the soluble or the total fractions (as separated by tabletop centrifugation), with no trend of increase from 0 to 3 hr after addition of IPTG (Fig. 2.12).

As it was clear that little or no useful plexin-A1 expression could be achieved with the present construct in pDEST 15, cloning into pDEST 17 and pDEST 49 were attempted instead. The clones were grown in 10 mL cultures to an A600 of 0.6 and induced with IPTG. However, these constructs too showed constant leaky expression of numerous proteins and some plexin, with no induction evident either from SDS-PAGE gel or by Bradford assay. Ni-NTA beads were added to the lysates of these test inductions in order to concentrate and purify the plexin by elution but very little was recovered.

Further attempts to purify plexin from the Plex2 construct met with these same obstacles, particularly the appearance of twin bands for plexin, probably due to proteolytic degradation since removal of the 6xHis tag did not convert one into the other.

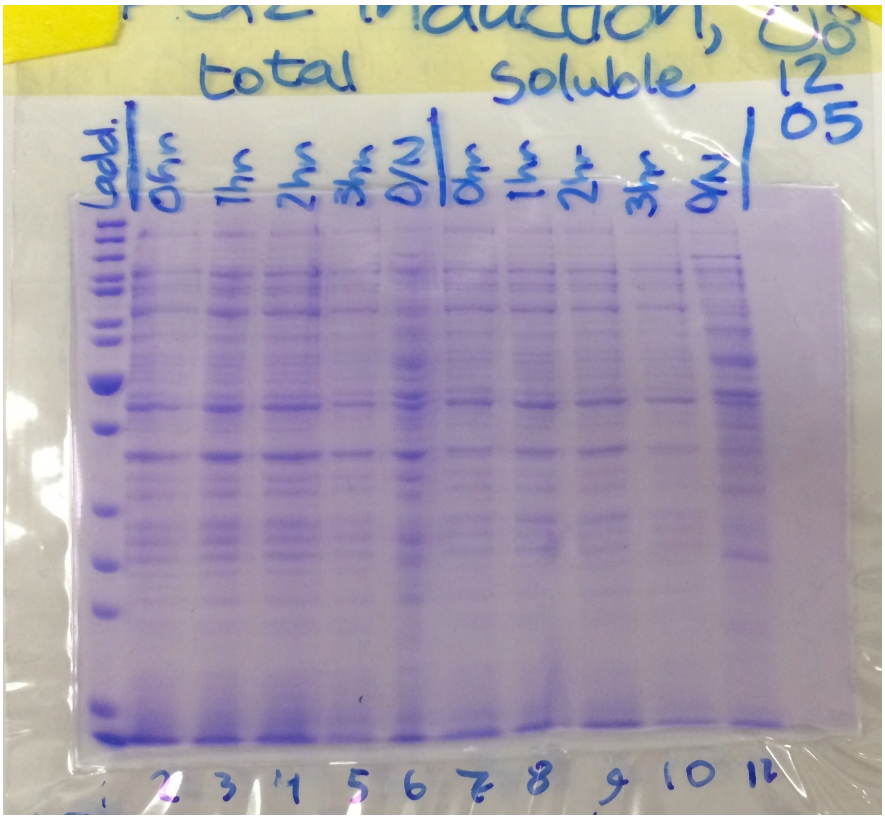

ure 2.12. Like the TOPO construct, Plex2 construct shows no appreciable increase in
ression, although a modest constitutive expression is observed.

Eventually the TEV cleavage step was discarded in the interest of increasing the yield of the fusion protein. Also, TY medium was tried (per liter, 16 g tryptone, 10 g yeast extract 5 g NaCl, 2% glucose), to boost induction; inductions at higher A_{600} and low temperature (18 ºC), and added glucose upon induction to assist the LacZ system. Anion exchange (MonoQ) was attempted in order to purify out a single band. None of these measures had any noticeable effect on plexin induction or yield.

At this point, the Plex2 construct, as well as the clonase technology and pDEST vectors on which it was based, were abandoned in favor of traditional cloning methods. The pDEST 17 vector with plexin insert was grown in a maxi-prep, concentrated 10-fold using QiaexII beads, the plexin-A1 gene was excised from pDEST 17 using BamHI and NotI and ligated into a variety of pET system vectors. The circular plasmid ran as two distinct bands of uncertain mass but BamHI cleavage at one site produced a single band at the expected mass, suggesting the two bands represented different supercoiled states. Cleavage with both BamHI and EcoRV produced two fragments of the expected lengths (4.5 and 1.9 kb, Fig. 2.13).

Cloning of the plexin-A1 insert was carried out in pET 28, pET 32, pET 42 between the BamHI and either EcoRI or NheI sites. Cloning was tested in the Vector NTI software (Invitrogen, v. 10.3.0), which allowed restriction sites to be chosen and maps of the intended constructs built. EcoRI was used where possible with BamHI to avoid the sequential digestion required when using NheI. For pET28a(+), SacI and NheI were used. Because this plasmid includes both N- and C-terminal 6xHis tags, PCR amplification of the plexin insert was carried out using two sets of primers (Table 1), depending on whether the antisense primer contained a stop codon. Amplification produced a band on

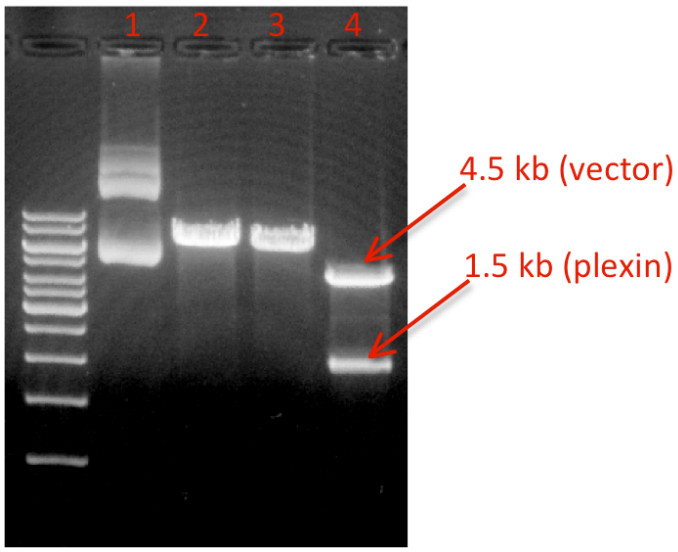

igure 2.13. Excision of the PlexA1$_{IC}$ gene from pDEST17 with BamHI and EcoRV :oduces bands of the expected length (1.5 kb for plexin, 4.5 kb for rest of vector). Lane uncut vactor; lane 2, BamHI digest; lane 3, EcoRV digest; lane 4, digested with both ızymes.

agarose closely matching the expected 1.8 kb.

Competent GC-5 cells were transformed with pET28a and grown in miniprep, providing an ample stock of the destination vector. The plexin PCR product was purified, and both it and pET28a were digested with NheI and SacI. Ligation was carried out using a 6:1 insert:vector ratio and GC-5 cells were transformed with the product. The colonies produced by transformation with ligations where the plexin insert lacked a stop codon were far more numerous than those with a stop codon, but both were collected and grew normally, with normal DNA yields (~10 ng/μL). SacI digestion was carried out on all clones and assessed by agarose gel, confirming that most colonies were successful ligations with the expected length (Fig. 2.14).

However, digestion of the stop-codon versions--which should cut in the middle of the insert as well as at two sites within pET28a, thus giving three distinctive bands--showed only a single cleavage, with a single diffuse band as the product. Ligation was repeated, using a 3:1 insert:vector ratio. Of the twelve clones grown in miniprep, following double digestion with SacI and NheI, only two showed the two expected bands (Fig. 2.15); these were labeled "S27" and "S31". Both were sequenced, revealing that S27 was unusable but S31 perfectly matched with plexin-A1 intracellular region ($PlexA1_{ic}$) ligated into pET28a, with the exception of a T-to-C transversion that proved silent for that codon.

The pET28a: $PlexA1_{ic}$ clone S31 was transformed into BL21 cells and inducibility was assessed by induction of a small sample, sonication of the pellet, separation into soluble and total fractions and SDS-PAGE, revealing a very clear band showing induction at 75 kDa. However, this expression appeared entirely in the total

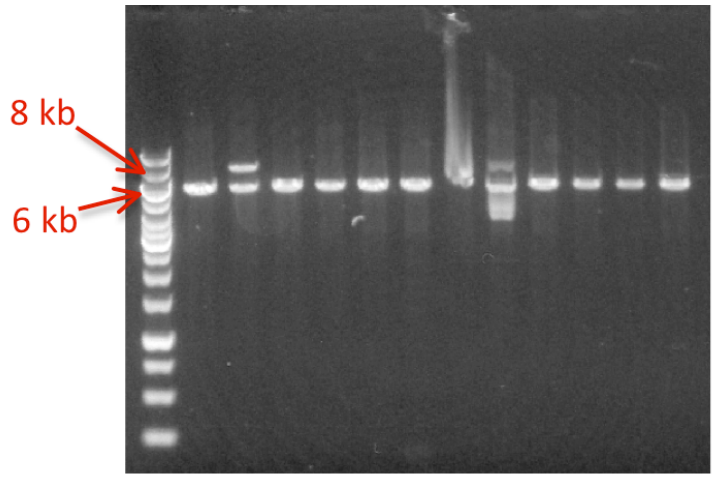

igure 2.14. Ligation of PlexA1ic into pET28a proceeded successfully. Cleavage with acI reveals bands of the expected total mass of 7.1 kb.

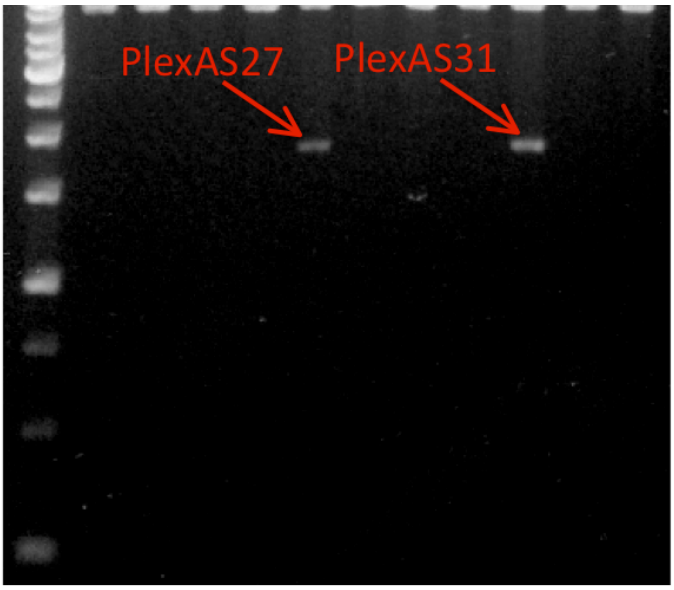

gure 2.15. Double-digestion of PlexA1$_{IC}$: pET28a ligation revealed two clones of tentially correct sequence, labeled “PlexAS27” and “PlexAS31”. DNA sequencing vealed PlexAS31 to be an exact match to the desired sequence.

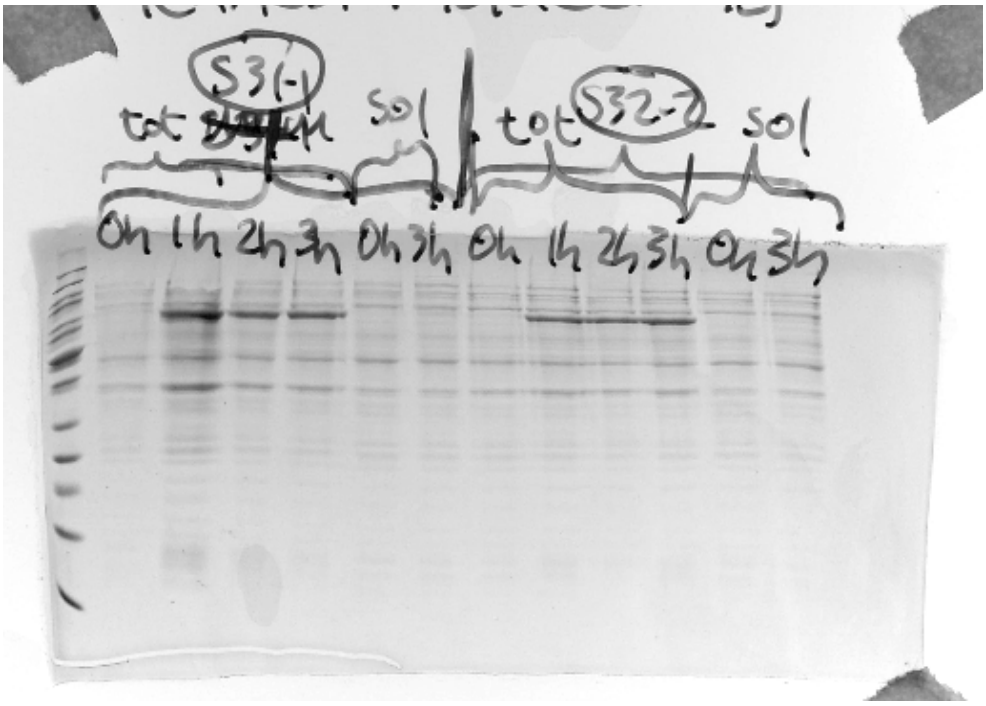

ure 2.16. First successful demonstration of inducibility of PlexA1$_{ic}$, using the xAS31 : pET28a construct. Note however that virtually no plexin is found in the ıble fraction.

fraction, with only a minute amount remaining soluble (Fig. 2.16). In an attempt to resolve this solubility problem, inductions were tried at lower temperatures, both for 4.5 hours: 25 ºC and 18 ºC. The lower temperature only marginally improved the amount of soluble $PlexA1_{ic}$ as measured by Bradford assay, and negligibly as viewed by SDS-PAGE (Fig. 2.17). Proceeding with Ni-NTA beads to collect what soluble protein there was, eluting and then dialyzing overnight with thrombin to remove the 6xHis tag afforded both very low yield of $PlexA1_{ic}$ and incomplete tag cleavage.

In the hope of recovering more of the insoluble fraction of plexin, or at least solubilizing it so that it could be quantitated, pellets were grown at 25 ºC and broken using 0.3% v/v Triton X-100, 5% v/v glycerol (also 50 mM Tris, 150 mM NaCl, 0.1% ß-mercaptoethanol, pH 8). This increased the amount of $PlexA1_{ic}$ that eluted from Ni-NTA beads, however it was unusable, precipitating once the detergent was dialyzed away. The solubilizing detergent CHAPS at 0.1% w/v was also tried, with a similar result.

For the small amount of $PlexA1_{ic}$ that could be recovered in the soluble fraction, thrombin digestion of the 6xHis tag continued to be a problem, with only partial digestion. As a control a small amount of another thrombin-cleavable fusion protein, Tc-SPPS, was expressed and purified and treated with the same amount of thrombin. Cleavage was complete for this protein, indicating that the problem did not lie with the thrombin stock or the procedure used (Fig. 2.18).

Given the hydrophilicity of histidine, it was thought that an additional, C-terminal 6xHis tag might improve the solubility. A construct lacking the antisense primer stop codon, called NS36, was isolated in the same manner as S31, found to be of correct sequence, and cloned into pET28a. Like the S31:pET28a construct however,

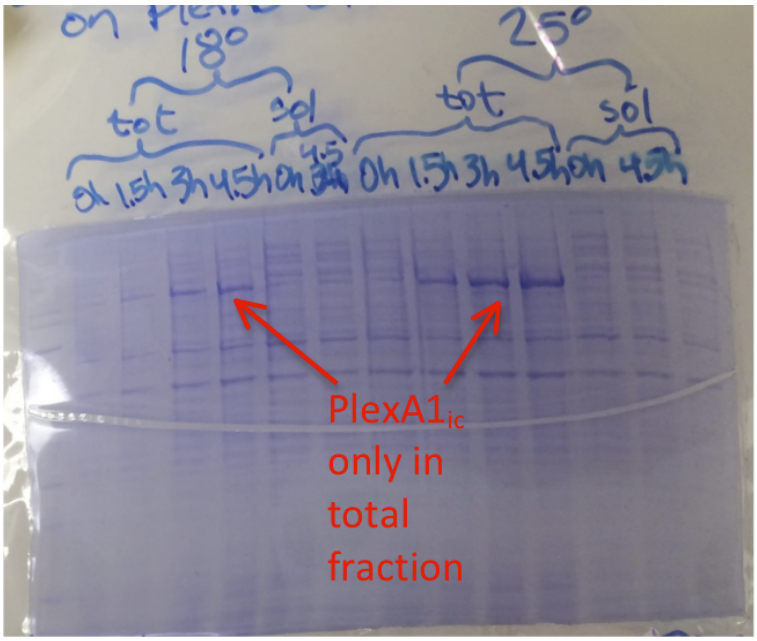

gure 2.17. Reduced-temperature induction of the PlexAS31 construct does not prove the solubility issue.

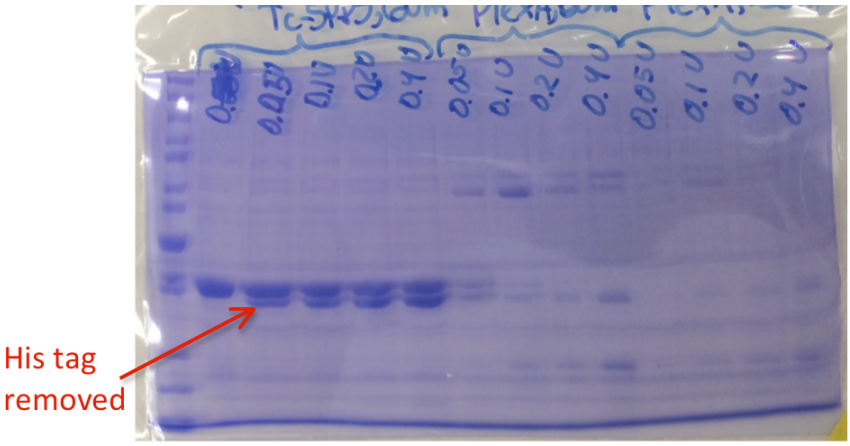

ɡure 2.18. Incomplete removal of the 6xHis tag by thrombin was a common problem ɒurification of the PlexAS31 constructs. Successful removal of 6xHis tag from Tc-PS by the same sample of thrombin suggests a problem of structural inaccessibility of cleavage site in the case of plexin.

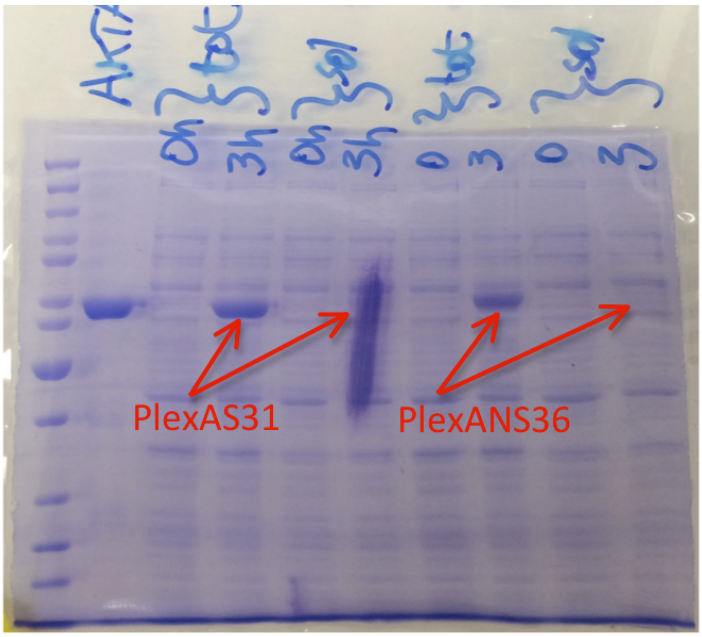

gure 2.19. In contrast to the PlexAS31 clone, in which a stop codon prevented
ınslation of the C-terminal 6xHis tag, the PlexANS36 clone contained both N- and C-
·minal 6xHis. The additional tag afforded no major improvement in purification or
lubility.

NS36:pET28 exhibited strong inducibility but no soluble plexin product was observed (Fig. 2.19).

On the hypothesis that plexin was misfolded and that this was impeding solubility and thrombin cleavage, 6M guanidine hydrochloride was used to gradually unfold, then refold the plexin (. 2 mL of 6xHis- PlexA1$_{ic}$, eluted from Ni-NTA beads at a concentration of 0.27 mg/mL, was dialyzed into 6M guanidine HCl for 6 hr and then back into Tris + NaCl buffer, pH 8. Thrombin digestion was not improved, even at a level of 5 U/mL, indicating that either the problem is not one of misfolding, or that the protein does not successfully re-fold.

In any event, as a small fraction of plexin could be extracted in the soluble fraction, larger induction volumes (>4L) were used and these larger pellets were lysed, shaken overnight at 4 ºC with Ni-NTA beads, eluted with 200 mM imidazole and dialyzed to remove the imidazole and salt for anion exchange. Typically 1/3 of the total protein would precipitate during this dialysis step, and much of the rest during SourceQ purification. This left a small amount (~3 mg) of highly pure, though uncleaved 6xHis-PlexA1$_{ic}$ (Fig. 2.20).

As solubility and cleavage inefficiency continued to render production of adequate amounts of PlexA1$_{ic}$ for kinetic studies or crystallization problematic, it was decided to move the plexin gene into another plasmid, a pET28b in this case, specially modified by inclusion at the N-terminus of a yeast SUMO protein sequence and downstream Ulp1 protease cleavage site (Gly-Gly-Ser, Fig. 2.2). This vector, known as pSmt3, was a generous gift of Dr. Christopher Lima, Sloan Kettering Institute. Ulp1 protease is readily expressed and purified and was already available (courtesy of Dr.

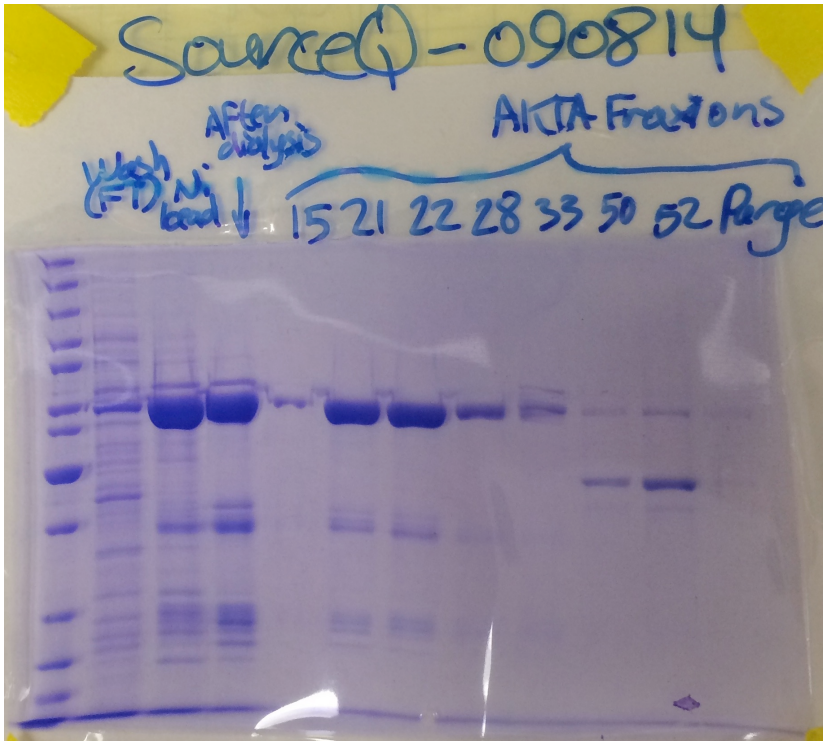

ure 2.20. SourceQ purification of the product of the PlexA1$_{ic}$: pET28a induction. hough the large majority of the product was insoluble and much of the remainder ically precipitated, small quantities could be obtained in pure soluble form by anion hange.

Krisna Duong-Ly).

The PlexA1$_{ic}$ insert was excised from pET28a using SacI and NheI. To accommodate the fact that the SUMO sequence was already inserted into pSmt3 using an NheI site, the forward plexin primer was changed to incorporate a BamHI site instead. PCR, agarose gel purification, restriction of both the PCR product and pSmt3 with BamHI and SacI, and ligation were carried out. Sequencing of the clones revealed several with perfect fidelity to pSmt3: PlexA1$_{ic}$, and these were transformed to GC-5 cells, grown in miniprep, and then used to transform BL21 cells. They readily induced and showed not only higher yield than all constructs previously tried, but far more protein remained soluble. SUMO tag removal with Ulp1 also proved much more straightforward (Fig. 2.21). Purification by SourceQ readily separated Ulp1-cleaved PlexA1$_{ic}$, giving a single very sharp peak. However, when removing salt by dialysis following elution, PlexA1$_{ic}$ became unstable and approximately 80% precipitated. This was thought to be due in part to intolerance of low salt, combined with the highly soluble and stabilizing SUMO tag.

Buffers were further optimized, and it was found that plexin stability post-Ulp1 cleavage was considerably improved by addition of 0.2 M glycine and 5% glycerol to the buffer, and pH adjusted to 7.3-7.7. At least 50 mM NaCl remained necessary for long-term protein solubility however; brief periods of desalting sufficient to load an anion exchange column were tolerated, but storage of hours or more invariably produced precipitation. Surprisingly, addition of DTT also appeared to induce precipitation.

To increase yield and possibly the folding of the protein, expression was carried out at 16 ºC overnight (~16 h), which significantly increased the yield (>8 mg/mL of SUMO- PlexA1$_{ic}$) and also reduced the tendency of the protein to precipitate at later

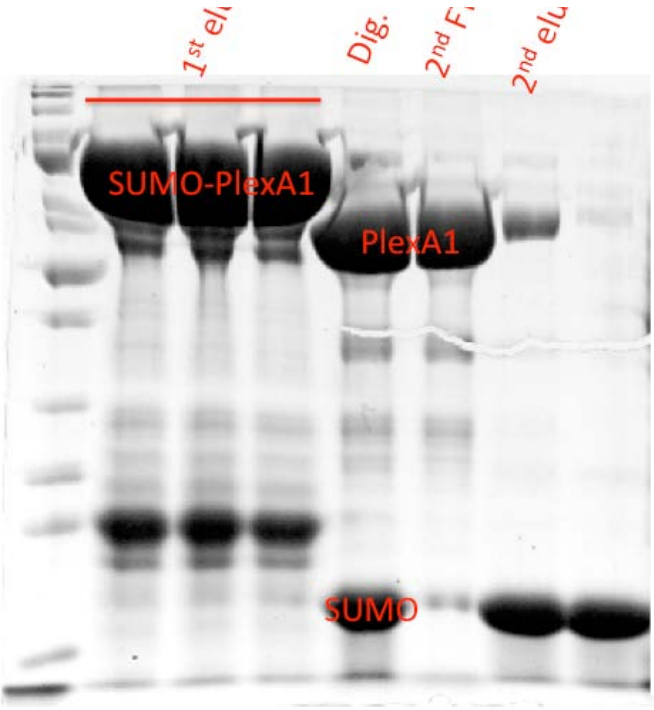

gure 2.21. Cleavage of the SUMO-PlexA1$_{ic}$ fusion by Ulp1 proceeds almost antitatively, and after dialysis to remove imidazole from the initial His-tag step, JMO is easily removed by shaking with Ni-NTA beads. The result is PlexA1$_{ic}$ (2nd ') sufficiently pure that further affinity chromatography is often not necessary.

stages of purification. It was also found that due to the extremely high expression of SUMO- PlexA1$_{ic}$, anion exchange was not necessary for purification; instead the fusion protein was retrieved from the lysate using Ni-NTA beads, eluted, cleaved with Ulp1, desalted to remove imidazole, and treated with Ni-NTA beads again to remove the SUMO tag (which contained the only 6xHis tag in the fusion protein). The result, as estimated from SDS-PAGE gel, was protein of >95% purity. This combination of methods was deemed very satisfactory and was used for all plexin subsequently produced.

2.5.1 Plexin-A1 Intracellular Domain Subcloning.

To examine the interactions between these domains and other proteins, especially fl-MICAL, it was necessary to express isolated subdomains of PlexA1$_{ic}$ as well. Four new constructs were chosen, consisting of combinations of the three main parts of PlexA1$_{ic}$ (C1 domain, RBD, and C2 domain). These were delineated by the choice of four primer sites within the PlexA1$_{ic}$ gene: α, A, B, and ω (Table 1), with the following rationales:

C1 alone. Between primer sites α and A (a.a. 1286-1496). The structures of Plexin-A3 and -B1 intracellular domains (25, 26) show the C1 and C2 domains closely intertwined with the RBD more loosely tethered between them. Furthermore, given that C2 is the region of plexin known to interact with fl-MICAL (5, 40), this suggests that plexin activation involves a significant shifting of the domain structure to expose or create an fl-MICAL binding site. Planned experiments centered around examining whether this could physically interact with the C2, and also whether it could act as an inhibitor for fl-MICAL activation by plexin, by competing the C2 away from the plexin-interacting region of fl-MICAL.

C1–RBD. Between primer sites α and B (a.a. 1286-1670). Similar to the purpose of C1, but with the RBD included, in case this was necessary for reconstitution of plexin activation, or for C1 binding to C2.

RBD alone. Between primer sites A and B (a.a. 1496-1670). The RBD alone was considered a valuable subject for structural determination in itself and in combination with purified Rnd1, with which it is known to bind. This was subsequently achieved by Buck et al. in Plexin B1 (34, 35).

C2 alone. Between primer sites B and ω (a.a. 1670-1910). As the region of plexin thought to facilitate the activation of fl-MICAL, specifically through binding to the C-terminal autoinhbitory domain, this region of plexin was of particular interest. Under current understanding, it seemed plausible that this subdomain might in isolation mimic a constitutively activated plexin molecule, its MICAL-binding region being completely unhindered by C1 or RBD. It thus could be sufficient to titrate the C-terminus away from its auto-inhibitory position, which would then be measurable as an increase in NADPH consumption (or F-actin disassembly).

The C1, C2, RBD, and C1-RBD segments of PlexA1$_{ic}$ were amplified by PCR (with 5% DMSO), giving bands of the expected length (Fig. 2.22) and restriction digested and ligated into pET28a. Both PCR from the purified plasmid and sequencing confirmed error-free incorporation of the insert for the case of the RBD and C2, while successful amplification and ligation of C1 alone proved elusive.

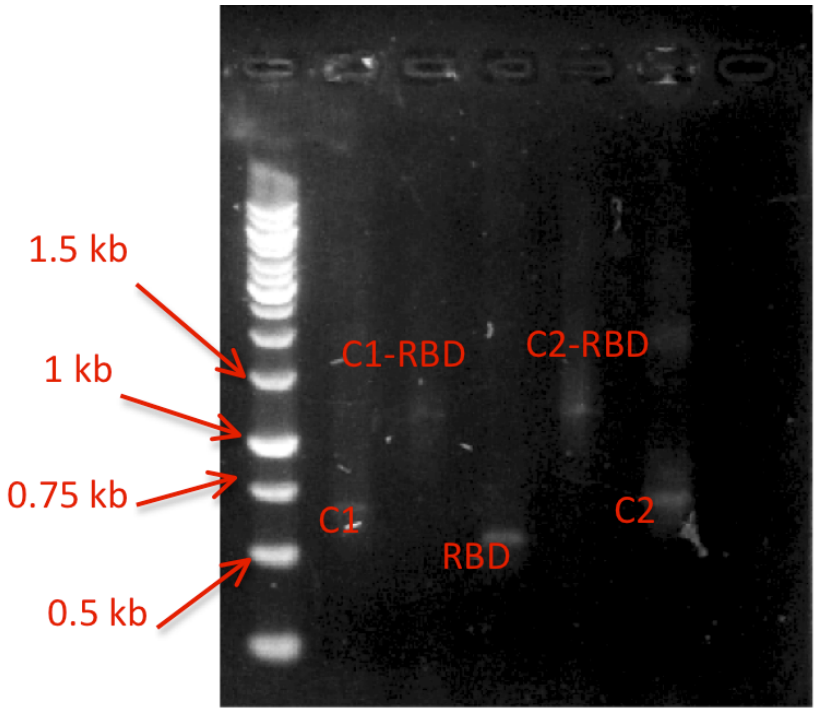

ure 2.22. Five subclones of PlexA1$_{ic}$ successfully amplified by PCR.

However, when incorporated into BL21 cells and induced, the pET28a:RBD plasmid showed no trace of induction on gel, while Bradford measurements indicated a decrease in total protein upon induction in both soluble and total fractions. After numerous efforts to modify the induction conditions in which no sign of the expected band could be found, some expression was observed but the protein remained insoluble even in detergent (0.3% w/v CHAPS). It was concluded that the protein was inherently unstable. Similar difficulties were encountered in the cases of C1–RBD, and C2; C1–RBD, which expressed well, was not soluble.

It was judged that of the four subclones, C2 was the most interesting and further attempts focused on producing and studying it alone. Cloning into pSmt3 and PGEX-5x-1 was carried out and sequencing revealed several clones with no sequence abnormalities. SUMO-C2 (and to a lesser extent GST-C2 fusion), visible as a band at 37 kDa, expressed robustly at 17 ºC for 20 h, with a slightly more acidic LB medium (no added NaOH), producing 7 mg/L, an amount similar to that observed for SUMO- PlexA1$_{ic}$. Following cleavage of the SUMO tag, however, the free C2 proved highly insoluble, with near-complete loss of the protein. A subsequent search for stabilizing buffer conditions, varying salt, pH, and glycerol levels, showed no improvement in this situation.

This suggested that the isolated C2, normally found in an intertwined configuration with the C1, depends on intramolecular interactions with the other subdomains for stability, or in this case, with SUMO. This dependence incidentally raises questions as to the validity of studies that have featured expression of the isolated C2 domain to outline plexin-MICAL interactions, such as (5) and (33). In any event, all experiments requiring PlexA1$_{ic}$ C2 henceforth were carried out with the uncleaved fusion.

2.6 MICAL C-terminus (and variants).

6xHis-tagged $MICAL_{CTD}$ (a.a. 843-1048) was originally cloned from codon-optimized MICAL-1 gene and ligated into a PRO-EX plasmid by Dr. Tsu-Lan Yeh. Cells grew well under ampicillin resistance and induction (17 h at 18 ºC) produced a large increase in protein expression. However this expression contained a vast number of non-specific bands; although overall solubility appeared satisfactory in 150 mM NaCl, 20 mM HEPES pH 8, 0.1% Triton, the problem of non-specific bands was not reduced appreciably by binding and elution from Ni-NTA, suggesting that many of the bands were degradation products still containing the original affinity tag.

Further attempts at expression optimization were unavailing, so new primers to the CTD were generated and the gene was amplified from the original stock of codon-optimized fl-MICAL1. The gene was restriction digested and ligated into pSmt3. Induction was extremely successful, producing in some cases >15 mg/mL of SUMO-CTD fusion protein product in ordinary LB after 3 hr at 37 ºC. Binding and elution with Ni-NTA beads was unproblematic and, furthermore, Ulp1 cleavage produced none of the solubility difficulties occasionally seen with plexin and its subdomains such as C2.

As with plexin, because the overwhelming majority of protein produced in induction was SUMO-CTD, little purification was subsequently needed. However, anion exchange using MonoQ was helpful in removing SUMO and residual impurities. Buffer conditions were 50 mM Tris pH 7.3, 5 % glycerol, 0.2 M glycine, 30 mM NaCl for buffer A, and 900 mM for buffer B. SUMO eluted in a sharp peak at 19% B, while the elution of CTD was centered around 38% B but eluted in a complex profile, with a wide undulating plateau with three absorbance maxima (Fig. 2.23).

Notably, the CTD thus purified consisted of two bands of very similar mass, 24 and 27 kDa as judged by the SDS-PAGE ladder (Fig. 2.24). This two-band problem was also observed with the intact SUMO-CTD fusion, ruling out the possibility of unwanted proteolysis by Ulp1. Since a monodisperse product was desired, efforts were made at isolating one or both of these bands; they were generally not successful, as gel filtration lacked sufficient resolution to completely separate proteins differing by only 3 kDa. On the other hand, SDS-PAGE of the fractions from MonoQ anion exchange demonstrated that a small shoulder of "24 kDa" band eluted before the "27 kDa" began to appear, although the vast majority of the two coincided. This difference proved too modest to reliably exploit, and varied considerably from one pellet to another despite efforts to closely control the conditions of induction and pellet lysis and identify factors that could increase the ratio of "24 kDa" to "27 kDa" through slower induction, lower temperature, added glucose, addition of 1 mM TCEP during lysis, and so on.

It was unclear at this point which of the two bands corresponded to the "correct" sequence, although their near-identical anion exchange elution profiles suggested very similar sequences. N-terminal sequencing bore out this supposition, showing that both bands begin with exactly the same five amino acids--EAIEK, the intended sequence--and that therefore the difference must involve the C-terminal end.

The predicted mass of the CTD product was 24 kDa, suggesting the lighter band

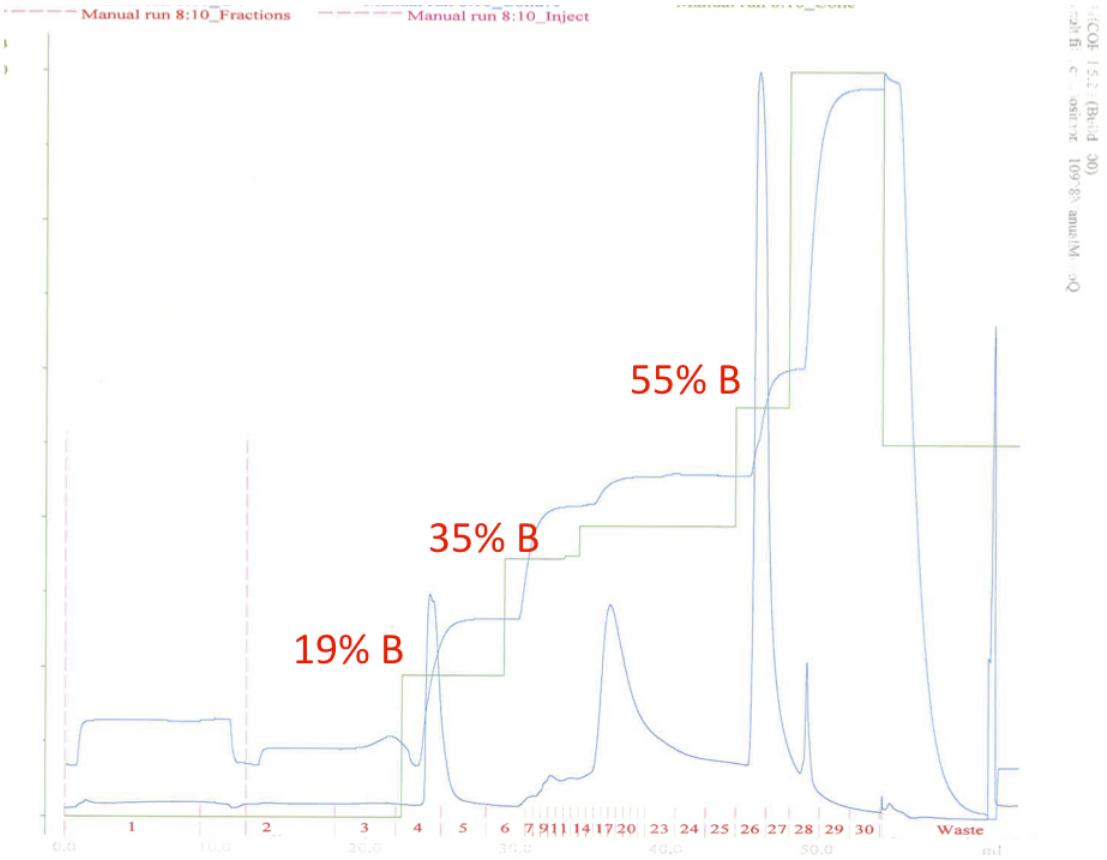

ɡure 2.23. A typical MonoQ separation of MICAL$_{CTD}$ product. Chromatogram shows MO eluting from column in a sharp peak at 19 % B, while CTD begins eluting at 34.6 B. A final large peak emerges at 55% B. Clearly visible in the gel of the fractions low) are the two separate lengths of the MICAL$_{CTD}$ product. Although the two bands re extremely hard to separate in large amounts, the lighter “24 kDa” band in some es would elute slightly before the heavier “27kDa” band, allowing a small amount of nodisperse product to be collected.

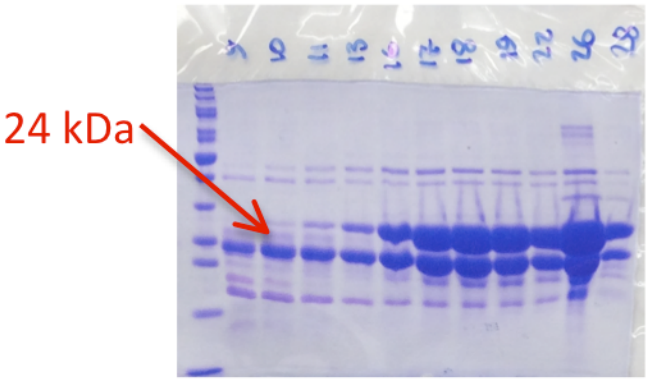

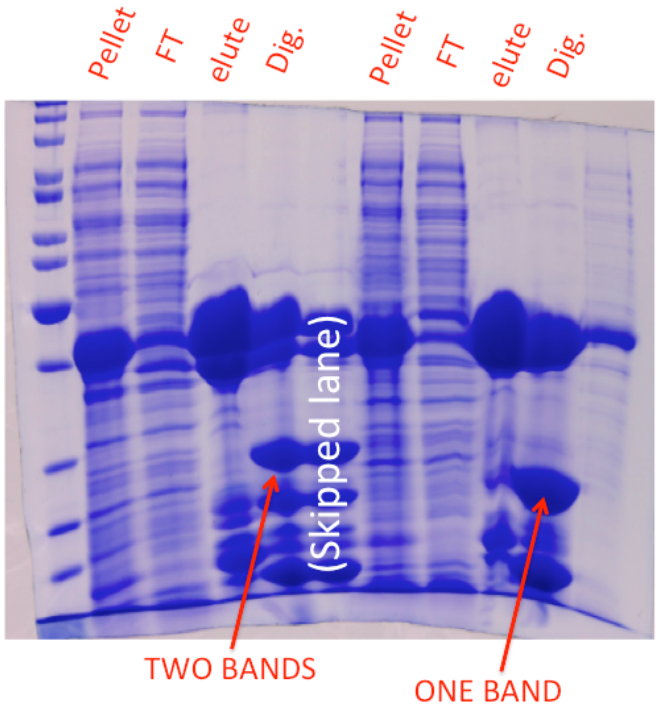

gure 2.24. Original MICAL$_{CTD}$ construct when digested to remove SUMO reveals
'o bands at approximately 24 and 27 kDa. A newer construct, designed to pre-
ıptively remove the last 14 a.a. of MICAL, produces a single band, allowing
ystallization trials.

was correct, but read-through of a UAA stop codon appeared unlikely. It was also observed that a mixture of the two bands, if left to stand at room temperature for several days, would gradually convert to the shorter, "24 kDa" form. (This phenomenon proved to be of little use, as the protein was rendered ineffective by such conditions.) This, taken together, suggested proteolytic cleavage, however the presence of protease inhibitor cocktail (Complete; Roche, Inc.) and PMSF did not reduce the observed quantity of the shorter band.

To resolve the identity of the two products, the bands were separated by running on SDS-PAGE, transferred to PVDF membrane, cut out and sent for mass spectrometry. This analysis showed that the longer band was in fact the complete form, while the shorter was formed by loss of the C-terminal 14 residues (Fig. 2.25). Searches of UniProt suggested no unique protease cleavage consensus sites in that region, so it may be that the truncation is due to a halt in protein translation which sometimes leads to premature termination.

Once it was clear that the "27 kDa" was the complete sequence attempts were made to purify it instead, but although usually more abundant, this proved more difficult than obtaining "24 kDa", since the latter always eluted first, contaminating the second product. Instead, a new construct was made to overcome the problem. Since the shorter product of $MICAL_{CTD}$ (called CTD24) had appeared to have the same potency, a new primer was designed to pre-emptively truncate the 14 residues in question, thus ensuring a monodisperse product. This product, cloned in pSmt3 as with the original CTD DNA, was expressed and purified with similar ease and in similar quantity to the latter. Moreover, SDS-PAGE gels indicated the product consisted of a single band (Fig. 2.24).

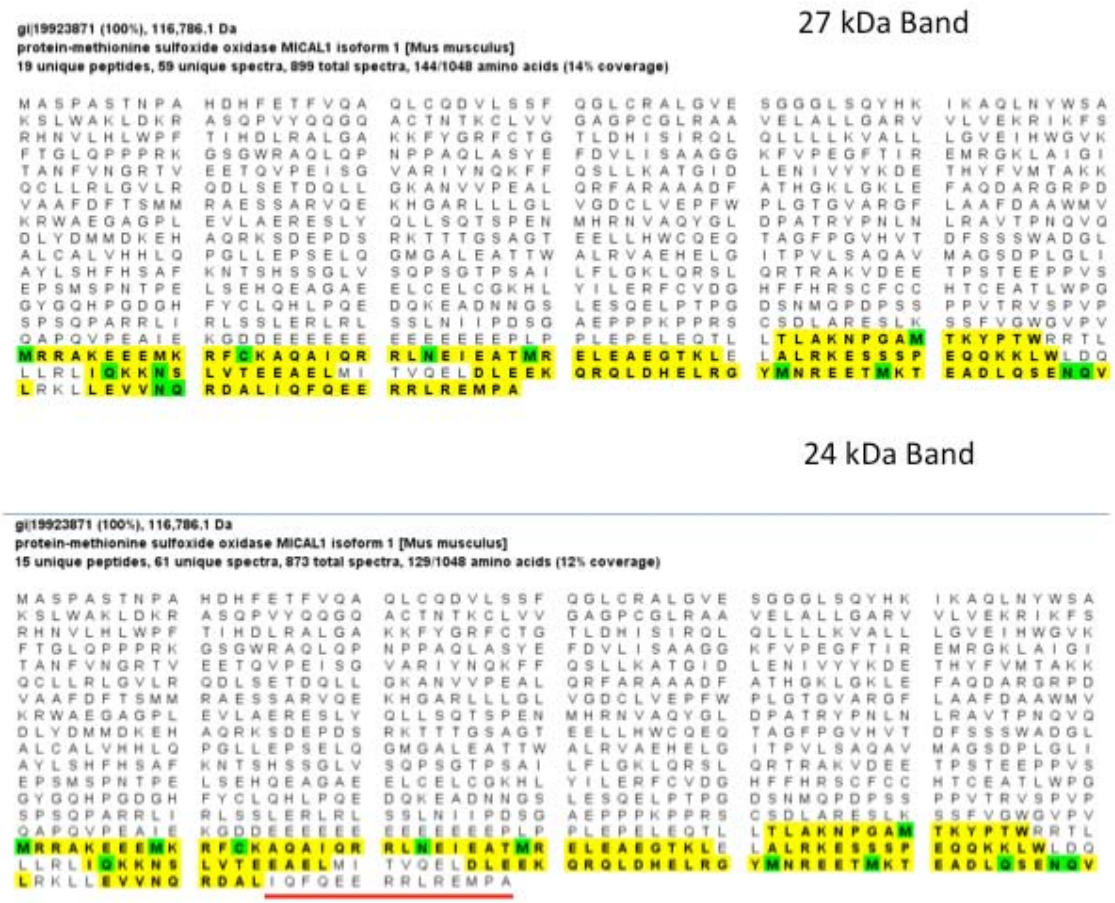

gure 2.25. Mass spectrometric analysis of the "24 kDa" and "27 kDa" bands produced r the MICAL$_{CTD}$ construct. Both clearly derive from the intended sequence of MICAL-1, but the "24 kDa" version has suffered a 14-a.a. truncation (red line).

In addition to the original SUMO-MICAL$_{CTD}$ (SUMO-CTD) and SUMO-CTD24 constructs, three variants on the CTD were pursued. The first, called "PPPCTD" (a.a. 769-1048) included the proline-rich, SH3-domain-binding region of MICAL1. It was thought that, due to this region's interactions with CasL in particular, its inclusion may help modulate the auto-inhibitory function of the MICAL CTD itself.

Another, shorter version of the MICAL1 CTD, "CTDnoE13" (a.a. 875-1048) omitted the 13-glutamate stretch at the N-terminal end of the CTD. This, it was hoped, would give clues as to the role of this unusual sequence feature in MICAL1 autoinhibition, and possibly in the stability of the CTD itself.

Finally, a double mutant was made containing A934P & T935P point mutations. These lie in the heart of the (predicted) coiled-coil helices of the CTD and so, by disrupting them with prolines, this protein was intended as a control to confirm the necessity of this structure for proper inhibition. Though cloning proceeded without problems and sequence was verified, none of these three constructs (except PPPCTD, in pET28a--Fig. 2.26) showed detectable protein expression and they were not pursued further. PPPCTD proved highly difficult to render soluble and was not pursued further.

2.7 Rnd1.

As one of a small group of GTP-binding proteins known to bind and activate the RBD of Plexin-A1, expression of Rnd1 is likely a necessity for any effort to reconstitute plexin activation. Rnd1 was originally ordered from Open Biosystems as a clone in a pDNR-LIB vector, which was then excised and ligated into pET28a. This expressed well

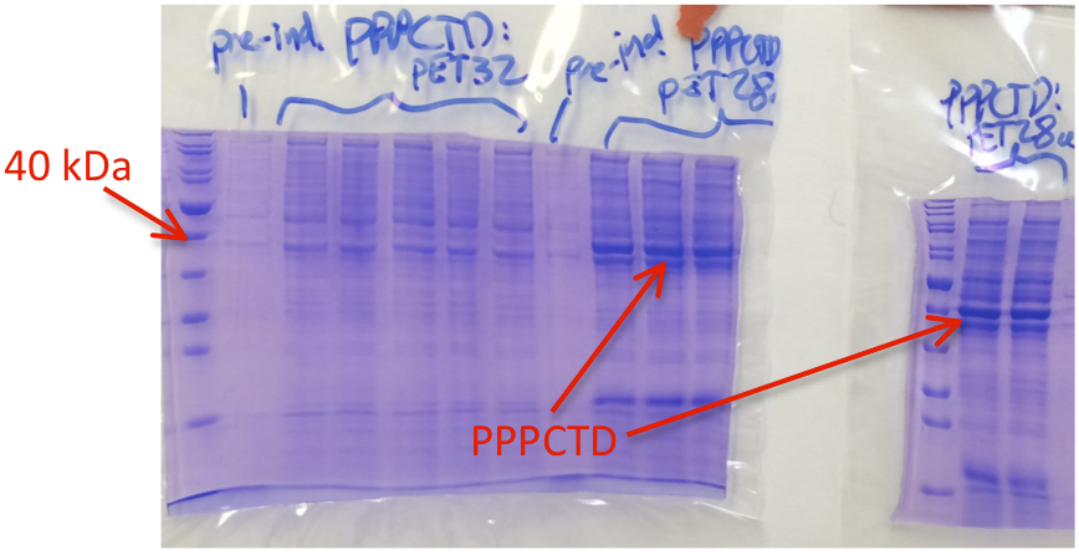

igure 2.26. Successful induction of the C-terminal MICAL "PPPCTD" construct, ɔmprising both the proline-rich and coiled-coil domains.

but proved completely insoluble, even under buffer conditions under which Rnd1, far from being unstable, is known to crystallize (35, 63).

It has been documented that rho-family GTPases, contrary to the general rule that such smaller proteins are often more stable and easier to crystallize, are actually very sensitive to buffer conditions and presence of ligand (64). It was therefore supposed that addition of GTP might, upon binding, lock the protein into a stabler conformation and allow solubilization. This, as well as urea refolding attempts, met with no success. Further analysis of the sequence revealed that the sequence on which the construct was based (with Entrez accession number BU048531), despite being labeled as "mouse Rnd1", did not represent the physiological protein; in particular, a lengthy repeat of very hydrophobic residues--cysteines and valines--had been incorporated at the C-terminus.

Once this problem was recognized, the correct sequence (NP_766200.1) was located, and this time synthesized in codon-optimized form by GenScript. Residues 5 to 200 of 232 were used for this construct, as this version had been previously crystallized and shown to bind GTP (35), and was therefore expected to be more stable. Initially, cloned into pET28a, no growth was observed; after the product was validated by sequencing, it was transferred into pET 22a, 32a, 42a, and pSmt3. All save pET32a showed no expression, and pSmt3 did not even produce colonies. pET32a, however, expressed vigorously after 15 h at 16 ºC (Fig. 2.27).

The product of pET32a expression is a fusion, containing an N-terminal thioredoxin (THX) tag, and this may have aided solubility. The fusion was easily removed from the lysates by nickel affinity beads due to an internal 6xHis tag, and cleavage by thrombin proceeded smoothly with 5 U/mg of enzyme, which was halted

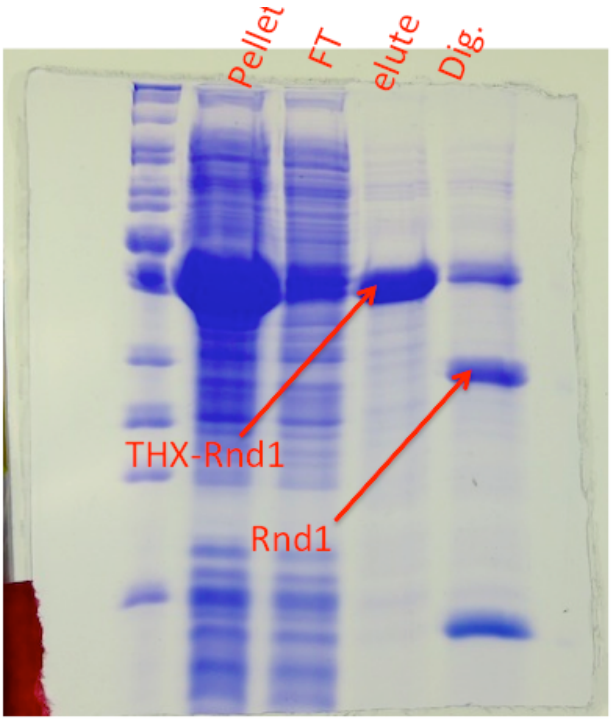

gure 2.27. THX-Rnd1 fusion expresses readily in pET32a vector, and thrombin avage proceeds smoothly, and both products are fully soluble and retrieved in good ·ld.

after overnight digestion at 4 ºC with PMSF. Buffer conditions were the same as published for crystallization: 50 mM Tris HCl, 150 mM NaCl, 5 mM $MgCl_2$, 5 mM DTT, pH 7.5. The THX-6xHis tag was easily separated from Rnd1 by anion exchange chromatography over a gradient of 0.1-1.0 M NaCl, with THX eluting at 8 % buffer B (90 mM NaCl) and Rnd1 at 17 % B.

Excellent yields (~8 mg/L) and purities (>95%) were achieved by these methods, and as a final step, Rnd1 was loaded with GTP by incubation overnight at 4 ºC in 3 mM GTP (Sigma) After concentration to 5 mg/mL, 15% glycerol was added and the stocks were flash frozen and stored at -80 ºC.

	quantity	specificity		
exA1-intracellular pET-28a	good (>5 mg/L)	very good	poor	73 kDa
exinA1-RBD in pET-a	none seen	n/a	n/a	20 kDa
exinA1-C1 in pET28a	poor	n/a	n/a	30 kDa
exinA1-C1-RBD in T28a	poor	n/a	n/a	50 kDa
exinA1-C2 in pSmt3 UMO)	good (>5 mg/ L)	very good	Fair before cleavage, poor afterwards	37 kDa
exinA1-intracellular pSmt3	very good (>10 mg/L)	very good	Excellent, still good after cleavage	85 kDa
CAL_{CTD} in pSmt3	excellent (>15 mg/L)	good, except forms two similar-mass bands	excellent	38/35 kDa
D24 in pSmt3	excellent (>15 mg/L)	excellent—single band can be highly purified	excellent (>25 mg/mL)	35 kDa
d1 in pET-32a	very good (>8 mg/L)	very good	very good	36 kDa
F-2α PAS-B in OEX (GST tag)	good t (>5 mg/L)	very good	good before cleavage, poor after	37 kDa

ıble 2. Summary of constructs produced.

Chapter 3: Results.

3.1 HPLC/gel filtration.

A key aspect of the models of plexin activation and also of MICAL auto-inhibition is that they imply physical association of certain proteins. For example, $MICAL_{MO}$ is anticipated to associate with the $MICAL_{CTD}$ and thus be inhibited; plexin is thought to dimerize and also to bind Rnd1 to its RBD region; and the C2 domain of plexin has been identified by co-immunoprecipiation (5, 40) as the region whereby it interacts with MICAL-CTD, lifting auto-inhibition. These aspects were investigated by HPLC and gel filtration experiments.

To detect the formation of a complex between MICAL1-CTD and $PlexA1_{ic}$, after zeroing with buffer, a standard curve was produced by injecting 1:1, and 6:1 molar mixtures onto a Bio-Rad HPLC column at a rate of 1 ml/min. Volumes of elution for each peak were measured and plotted, and fitted to a logarithmic curve. Next, freshly cleaved SUMO-CTD and SUMO- $PlexA1_{ic}$ were injected and elution volumes were measured for all of the major peaks observed (Fig. 3.1). These were compared to the peak profile created by a 1:1 molar mixture of the two proteins.

Results in all three cases showed a very clear peak for SUMO (12 kDa) which, consistent with its small size, eluted last at 13.6 mL and thus functioned as a standard. For plexin alone, there was also a large and distinct peak at 9.3 mL, indicating a mass of 66 kDa, close to the actual mass of 70 kDa. Results with CTD alone were more complex and difficult to interpret. Instead of the expected single peak for a 24 kDa protein, which should elute ahead of the heavier $PlexA1_{ic}$ but well before SUMO, there were instead two very large peaks at 8.8 mL and 6.4 mL, corresponding to masses of 79 and 215 kDa

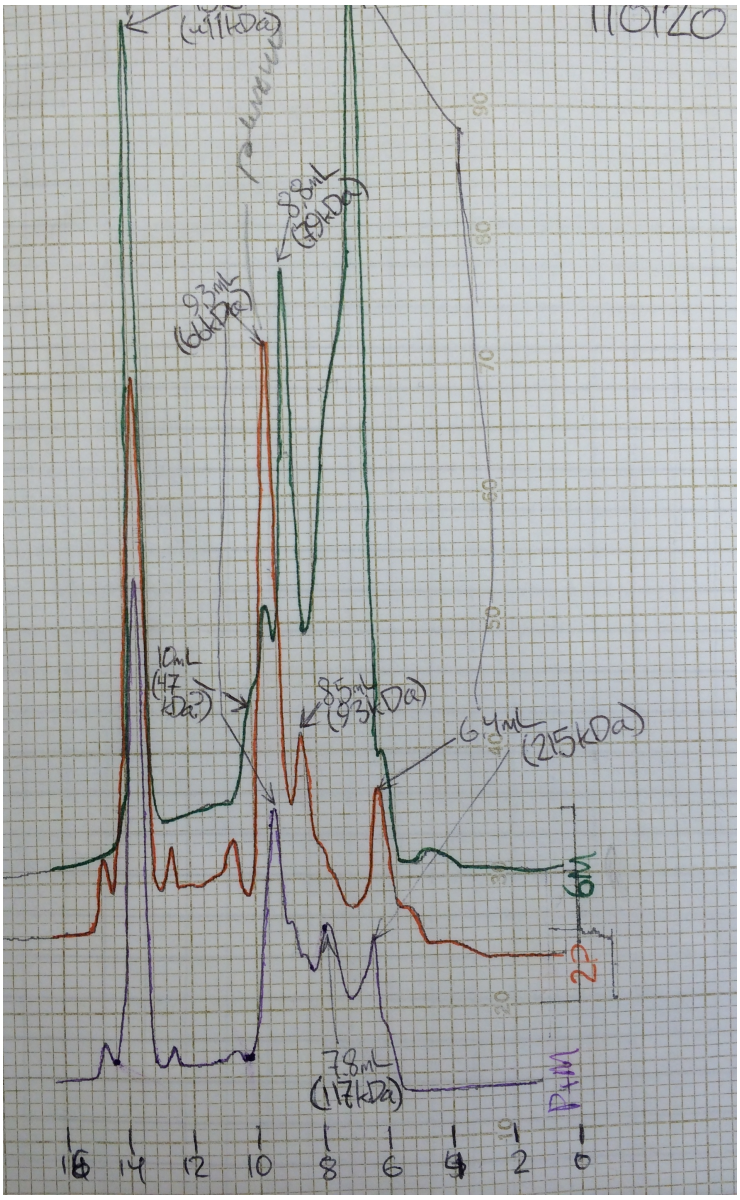

gure 3.1. Initial HPLC experiments showing calculated MW corresponding well to :xin ("P", ~66 kDa), and SUMO (~11 kDa). $MICAL_{CTD}$ ("M") on the other hand pears to exist as oligomers with peaks at roughly 79 and 215 kDa.

respectively. These large values are indicative of the formation of large oligomers (trimers and above) by the CTD.

The combination of PlexA1$_{ic}$ and CTD, notably, showed some changes in these features, with the intensity of the plexin peak reduced by half relative to SUMO; the large 215 kDa peak observed in the CTD alone reduced by three-fourths and the 79 kDa became indistinguishable. This suggests that PlexA1$_{ic}$ is able to disrupt aggregates of CTD, perhaps in favor of formation of a complex. At the same time, a moderately strong peak appeared at 7.8 mL, not seen in either component preparations. This new peak however corresponded to a mass of 117 kDa, too large to be accounted for by a 1:1 plexin:CTD complex which would be only 94 kDa (although a 1:2 complex would give 116 kDa, a close fit).

Subsequent experiments, however, showed no new peaks appear upon combination and of the two proteins, arguing against formation of a complex (Fig. 3.2). This may not be inconsistent with the models of plexin activation however, since no GTP-bound Rnd1 was present in these experiments.

Further HPLC experiments showed that addition of 20 mM BME could change the distribution of oligomers, dramatically shifting the preponderance of CTD from the 215-kDa band to the 79-kDa. However, the fact that the CTD construct in question only contains one cysteine makes it uncertain how redox-sensitive oligomers larger than dimers could be formed.

Related attempts were made with size-exclusion FPLC, both to confirm the HPLC results and to address the difficulties in separating the two MICAL-CTD bands. No significant separation was achieved, although the elution profile bore a mild resemblance

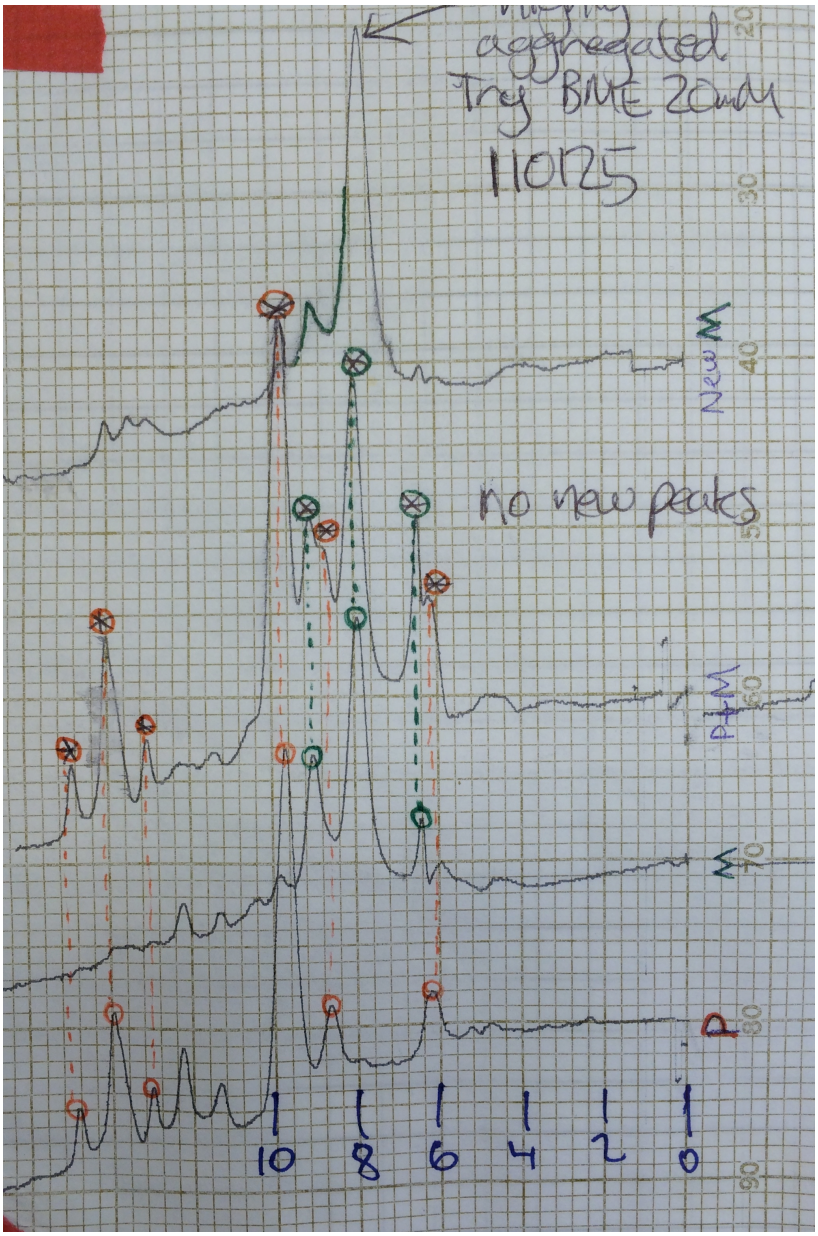

igure 3.2. Further HPLC experiments show distinct profiles for PlexA1$_{ic}$ (orange eaks, “P”) and MICAL$_{CTD}$ (green peaks, “M”). However, the 1:1 molar mixture of ıese two samples reveals no major new peaks that would suggest a complex.

to that from HPLC, with three main "humps" rather than peaks (Fig. 3.3). SDS gel however indicated that the two latest-eluting of these contained little or no protein, suggesting that all CTD actually traveled as the 215-kDa oligomer.

Another subject of importance was whether the interaction of CTD with the rest of the MICAL molecule could be detected as a complex. Therefore, three experiments were carried out on a Superose 6 column, with 200 μL containing one or both of 1.5 mg/mL of CTD and 3 mg/mL of $MICAL_{MO}$. Although the CTD continued to run as a heavier-than-expected oligomeric form, eluting ahead of the 54 kDa $MICAL_{MO}$, a small, early-eluting peak was observable ahead of both the CTD and $MICAL_{MO}$ peaks (Fig. 3.4), suggesting that enough monomeric CTD remained available in solution to produce significant amounts of the expected complex with $MICAL_{MO}$.

The activation of plexin is supposed to be partially dependent on its dimerization (33). Since many of the kinetics experiments were to be carried out under the supposition that this dimerization can be made spontaneous by adding enough plexin to the solution, it was important to confirm that the plexin concentrations used in those experiments were sufficient to produce a significant amount of the dimerized form.

Standards used were vitamin B12 (1 kDa), myoglobin (17 kDa), ovalbumin (44 kDa), gamma-globulin (158 kDa), and thyroglobulin (670 kDa), while the sample consisted of 500 μM of $PlexA1_{ic}$ at 2 μM concentration. Next to the main plexin peak--whose calculated mass of 71.5 kDa closely corresponded to the actual value of 70.1 kDa--was a significant "shoulder" peak whose center (as detected by AKTA UNICORN 5.0 software) corresponded to 157.5 kDa, very close to the expected 140 kDa for a dimer, and comprising about a fifth of the total protein.

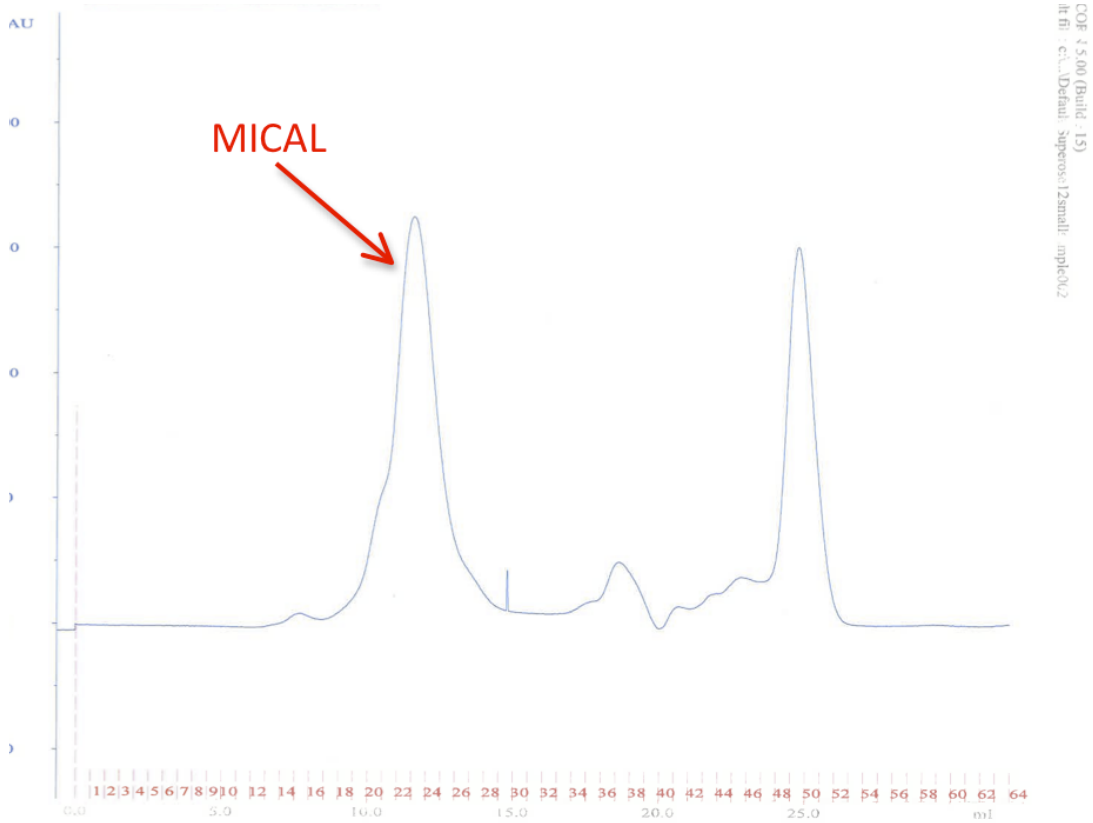

gure 3.3. Consistent with HPLC, Superose12 analysis of MICAL$_{CTD}$ also suggests ·ge oligomers with the main peak eluting close to the void volume (about 12 mL). vo other peaks are strongly apparent but contain little or no protein when assessed by)S-PAGE.

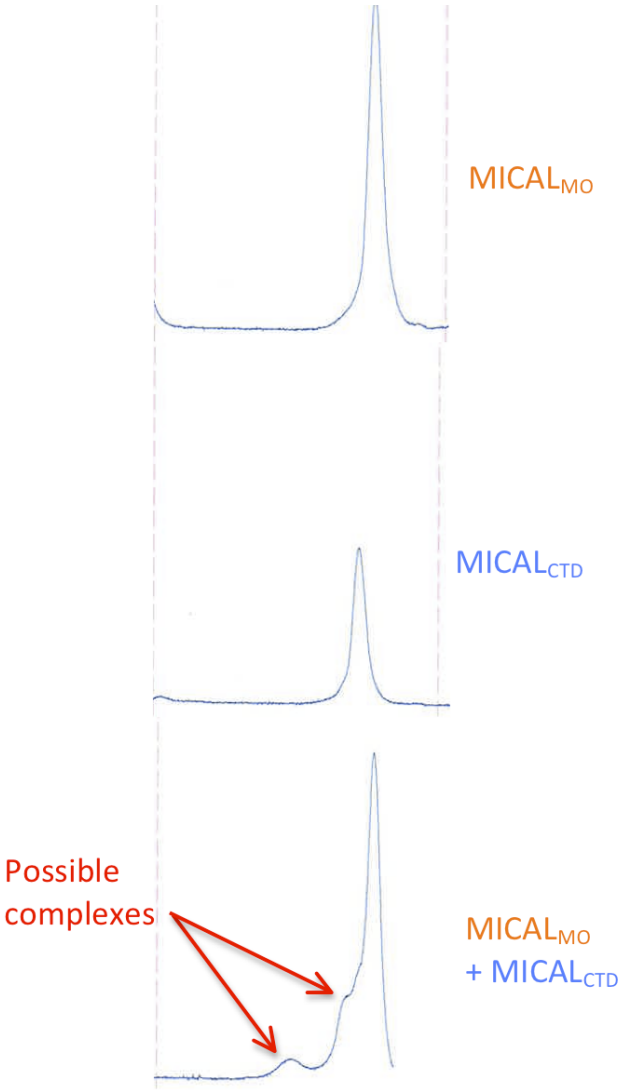

igure 3.4. Analysis of complex formation between MICAL$_{CTD}$ and MICAL$_{MO}$. Three ɔnsecutive Superose6 injections are shown. First, MICAL$_{MO}$ and MICAL$_{CTD}$ are run ɛparately. The latter again runs as an oligomer, eluting in a smaller volume than the 54 Da MICAL$_{MO}$ despite having half the molar mass. When the two are combined, two ɪrlier-eluting peaks are observed. Duration of each experiment is 25 mL (one column ɔlume).

3.2 Kinetics.

Central to the question of the effect of F-actin and the MICAL-CTD on the activity of the MICAL monooxygenase is the rate of NADPH consumption by the latter. This is readily monitored due to the strong absorption at 340 nm of NADPH, which is absent in the reaction by-product, NADP. Briefly, the proteins involved in the experiment in question were combined at 10/9 desired final concentration, then fresh NADPH was prepared at 10x desired concentration (after A340 measurements to check for degradation). Each 100 μL cuvette was rinsed thoroughly with ddH_2O and ethanol, dried with pressurized air, and 99 μL of the desired protein mixture was added; the spectrophotometer was blanked, and 11 μL of 10x NADPH added to start the reaction, then vigorously mixed by pipetting up and down for 5 s to homogenize the mixture as quickly and thoroughly as possible. Reaction progress was then monitored spectrophotometrically for 15 min and each reaction was carried out in triplicate. In general, experiments consisted of five triplicates at [NADPH] ranging from 10 to 150 μM. The results for the different protein mixtures were as follows, (in all cases with [MICAL] = 0.1 μM):

a) $MICAL_{MO}$, $MICAL_{MO\text{-}CH}$, and CTD.

In the presence of increasing amounts of MICAL-CTD, both $MICAL_{MO}$ and $MICAL_{MO\text{-}CH}$ showed very strong (Kd ~ 300 nM) inhibition, underscoring the hypothesis that MICAL-CTD is an auto-inhibitory domain.

*b) $MICAL_{MO\text{-}CH}$ alone, and with F-acti*n.

As reported elsewhere (43, 59, 65), $MICAL_{MO\text{-}CH}$ showed a large increase in NADPH consumption in the presence of F-actin, suggesting that this is at least one

physiological substrate of the enzyme. However the observed acceleration, while large, was substantially less than some reports, which claim a >100-fold increase.

c) fl-MICAL alone, and with F-actin.

fl-MICAL consumed NADPH about ten-fold slower than the constructs lacking the CTD did under similar conditions (Fig. 4.1a). This reduced activity is consistent with an auto-inhibited state owing to the CTD, perhaps blocking substrate access. Unexpectedly however, this auto-inhibited state could be largely abolished by addition of F-actin, whereupon the enzyme showed kinetics about 40% as fast as the CTD-free constructs (Fig. 4.4). Since F-actin can activate fl-MICAL, it appears that physiological activation of fl-MICAL's F-actin disassembly function may involve *displacement of another inhibitory molecule*, not of the CTD itself.

d) fl-MICAL with $\text{PlexA1}_{\text{ic}}$ *and Rnd1*GTP.*

When 1 μM $\text{PlexA1}_{\text{ic}}$ was added to fl-MICAL, a roughly 30% increase in velocity was observed. Inclusion of Rnd1*GTP in the mixture led to nearly a doubling of velocity. Both effects were considerably larger than that seen with lysozyme controls (Fig. 4.6b), suggesting that these two factors can indeed significantly activate the auto-inhbited MICAL monooxygenase. Surprisingly however, no increase in velocity was detectable from these two factors when F-actin was already present (Fig. 4.7a). Thus, it is unlikely that these factors alone are sufficient for the activation of F-actin disassembly under physiological conditions.

e) fl-MICAL with CasL SH3 and F-actin.

CasL is known to interact both with MICAL and with vimentin, raising the possibility that it plays a role in activating fl-MICAL's monooxygenase to disassemble F-

actin in the interior of cells. But, contrary to expectations, the presence of 1 μM of CasL SH3 inhibited the NADPH consumption of fl-MICAL on F-actin by about six-fold.

(For more information, see "Methods" section of Chapter 3.)

3.3 Co-sedimentation.

It is known that MICAL is an actin-binding protein, and in particular the $MICAL_{MO}$, $MICAL_{MO\text{-}CH}$, and $MICAL_{MO\text{-}CH\text{-}LIM}$ have been shown to co-sediment with F-actin. Given the reported auto-inhibitory role of the MICAL CTD region (5, 40), it seemed plausible that this region might control the actin binding of MICAL as well as its monooxygenase activity.

To test this, 1 μM MICAL construct, 3-5 μM of MICAL-CTD, and 5 μM of G-actin were combined in a G-actin buffer of 5 mM Tris, pH 8, 0.2 mM $CaCl_2$, mixed by pipetting up and down, and then initiating actin polymerization by adding 5 μL 10x polymerization buffer (500 mM KCl, 20 mM $MgCl_2$, 10 mM ATP) to a total volume of 50 μL. Samples were incubated at room temperature for 25-30 min to allow polymerization to reach a steady state, and ultracentrifuged at 100,000 g in a TLA-100 rotor for 25 min. Supernatants were carefully pipetted from the top to avoid disturbing the pelleted actin fraction, which was then solubilized by addition of 50 μL of Laemmli buffer and vigorous pipetting. Both pellets and supernatants were then briefly incubated at 95 ºC before processing by SDS gel to assess the protein constituents of the fractions. This methodology had already been employed in (59) to show that $MICAL_{MO\text{-}CH}$ is capable of binding and disassembling F-actin in vitro.

The first experiments, conducted with the original CTD construct, clearly show a displacement effect, with both the $MICAL_{MO}$ and $MICAL_{MO\text{-}CH}$ completely associating

with the F-actin pellet under ordinary conditions but the reverse taking place when CTD is present (Fig. 3.5). There was variation in the strength of the effect depending mostly on the batch of $MICAL_{CTD}$ being used, but it was possible to reproduce the result repeatedly (Fig. 3.6), including with $MICAL_{MO\text{-}CH\text{-}LIM}$ (Fig. 3.7), although in the case of that construct the batch variability issues were more significant. In particular, the pre-truncated CTD (CTD24), while producing a single clear band and in theory identical to the shorter band produced by the original construct--which in turn had been isolated in small amounts and shown to be effective at actin displacement--seemed somewhat less effective at actin displacement.

The CTD24 product showed a wider range of displacement potency, and was far more likely to co-sediment with the actin or even to pellet by itself. Investigation of the purification method by MonoQ showed that, while the original CTD product eluted over a very broad peak or combination of peaks and appeared indistinguishable by gel, different regions of this peak behaved very differently in terms of displacement of $MICAL_{MO\text{-}Ch}$ from F-actin, and their own adhesion to F-actin: CTD that eluted from the MonoQ at the first broad peak at 34.8% buffer B (343 mM NaCl) was active, as was that from 39% B, while CTD that eluted at 55% B did not block actin binding and itself stuck to actin (Fig. 3.8). Some of the variation could be attributed to differences from one MICAL batch to another, with significant amounts of MICAL pelleting on its own in some cases. However, introducing an initial centrifugation step to remove this insoluble MICAL fraction, though it did produce a well-behaved MICAL that bound F-actin and did not pellet on its own, neither eliminated nor greatly improved the CTD effect

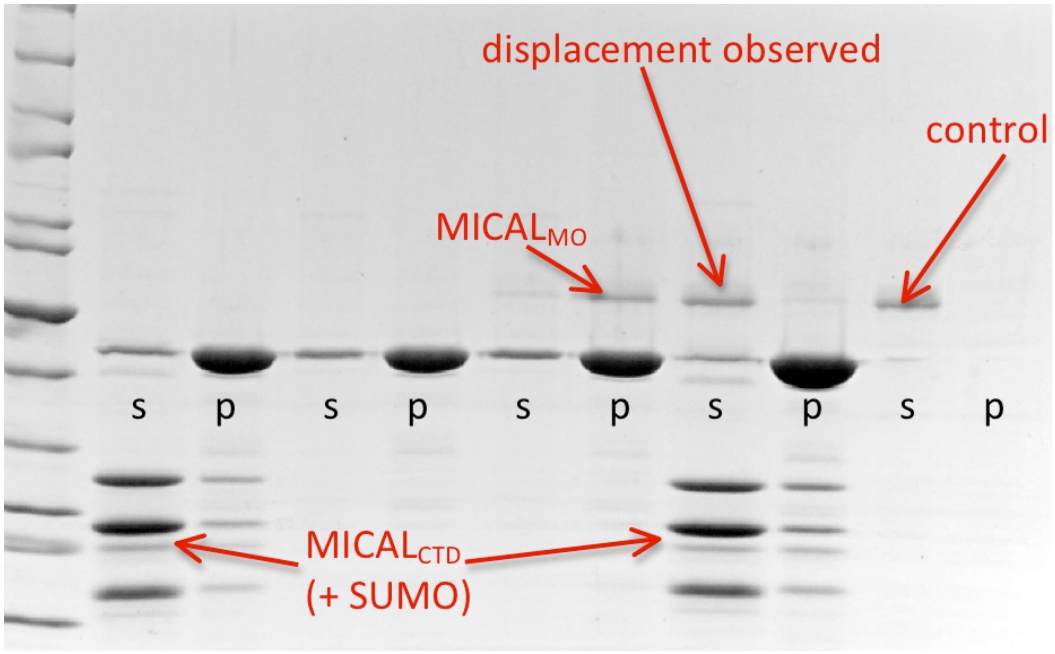

ure 3.5. Evidence of MICAL$_{CTD}$'s ability to abrogate F-actin binding by MICAL. ile MICAL$_{MO}$ readily binds F-actin and pellets with it, addition of MICAL$_{CTD}$ (here l containing SUMO from Ulp1 cleavage as well as both 24 kDa and 27 kDa products) ufficient to almost completely drive MICAL$_{MO}$ into the supernatant (s). Control eriment shows that MICAL$_{MO}$ does not pellet spontaneously.

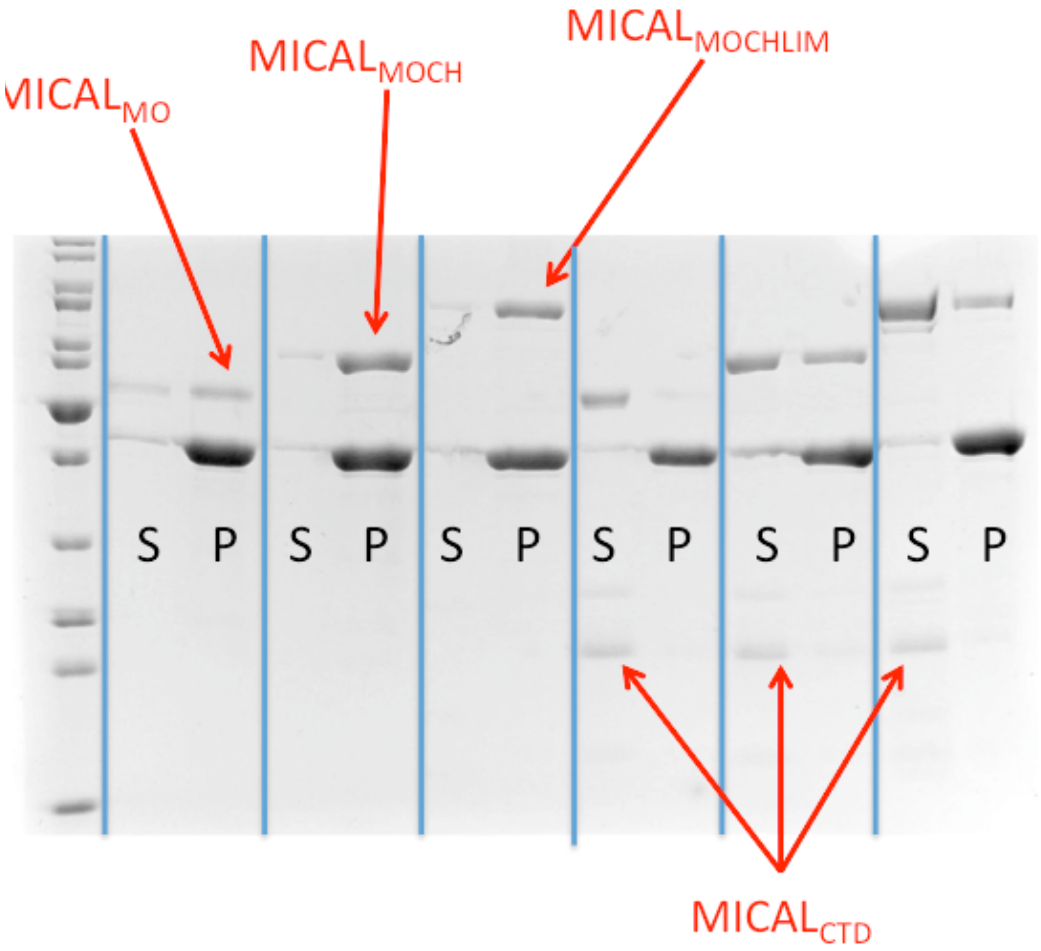

Figu

3.6. Smaller quantities of MICAL$_{CTD}$ still suffice to displace significant amounts of CAL constructs from F-actin, including MICAL$_{MO}$, MICAL$_{MO-CH}$, and MICAL$_{MO-CH-}$

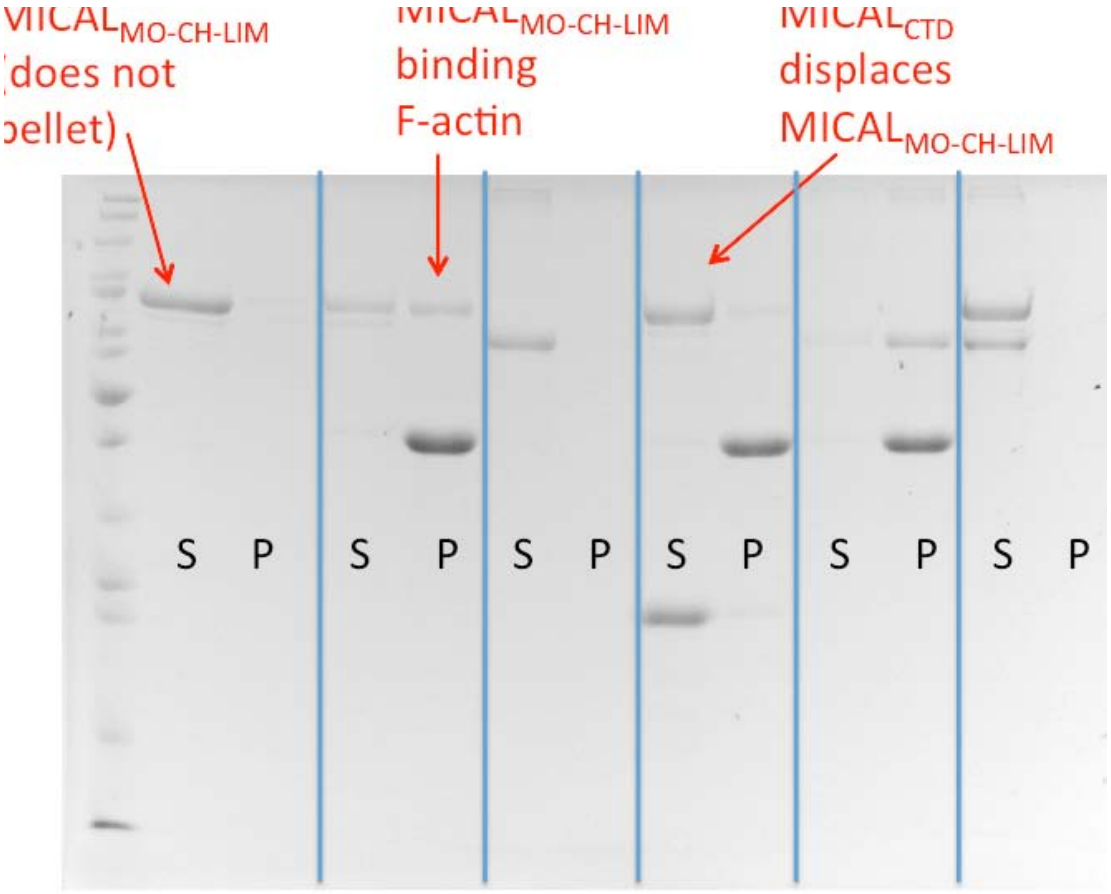

gure 3.7. Single-band CTD24 readily displaces $MICAL_{MO\text{-}CH\text{-}LIM}$.

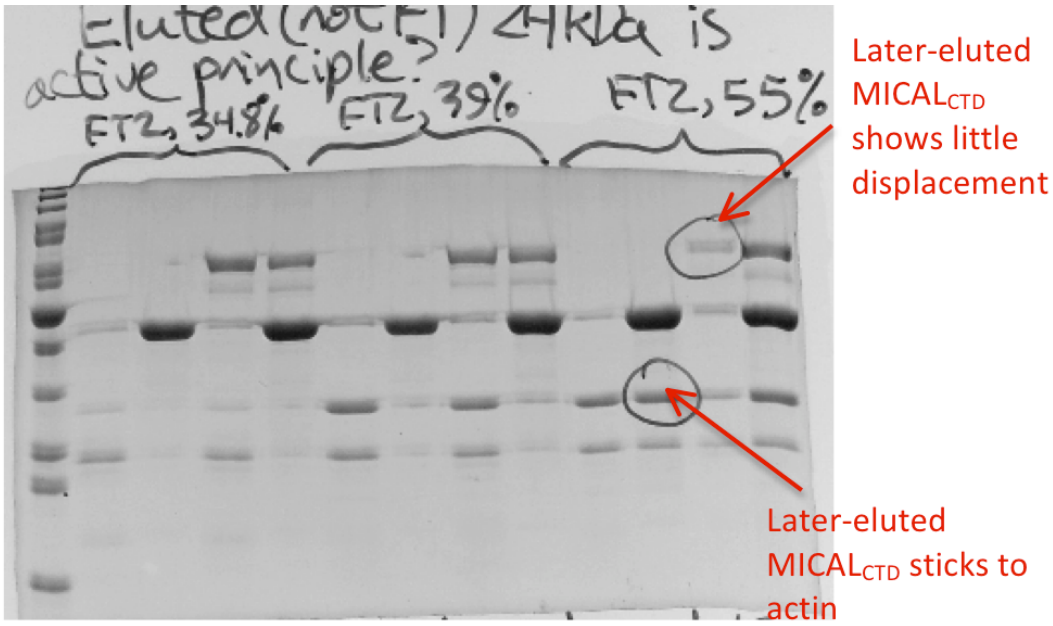

ure 3.8. The lower-weight product of MICAL$_{CTD}$ expression, when purified, is ficient to produce F-actin displacement. On the other hand, although MICAL$_{CTD}$ tes through the range of 34-55%B, the actin displacement ability of the MICAL$_{CTD}$ reases greatly toward the end of this range, with later-eluting protein sticking to F-in and showing minimal displacement.

observed in the remaining soluble fraction (Fig. 3.9).

Moreover, even such commonplace procedures as flash-freezing with glycerol for storage, or 48 h storage at 4 ºC seemed able to convert the CTD into a non-displacing form that precipitated by itself at 100,000 g and was useless for actin-displacement. The behavior, wherein active samples of the protein might remain stable for weeks and then within 1-3 days convert to the ineffective form (at an accelerating rate, Fig. 3.10), suggested an autocatalytic process of misfolding.

To address the question of whether the displacement effect as observed owed to the CTD protein's structure itself or just to the intense negative charge of the polyglutamate stretch which precedes the predicted coiled-coil, the polyglutamate stretch was synthesized as a peptide ("E13") and the co-sedimentation experiment was conducted using it instead of the CTD. No displacement of $MICAL_{MO}$ was observed by the E13 peptide in these experiments.

Since the binding of MICAL constructs to F-actin remained a robust observation throughout these experiments, a series of increasing MICAL concentrations was undertaken to quantify the stoichiometry of this interaction. Densitometry showed near-complete binding to 5 μM F-actin for concentrations of $MICAL_{MO}$ up to 1 μM; thereafter, a steadily increasing fraction of the total was found in the soluble fraction, with 50% of the MICAL remaining in the soluble fraction at an initial concentration of $K_d \sim 3.5$ μM (Fig. 3.11). $MICAL_{MO\text{-}CH}$ showed a similar pattern but with a somewhat higher K_d (>5 μM, Fig. 3.12).

Recent evidence shows that MICAL is involved in actin-disassembly (43, 59, 60), and does so through the oxidation of select methionines to (R)-methionine sulfoxide.

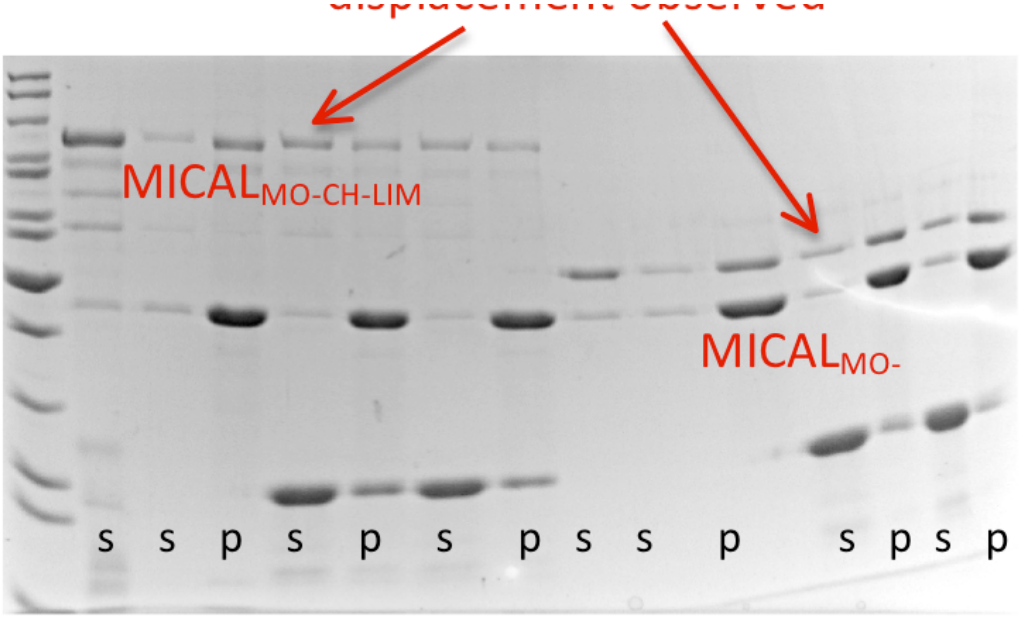

ure 3.9. Due to batch variations in the aggregation state of MICAL protein, an initial trifugation step was added to the actin-displacement protocol to pellet out any ;regate. Supernatants were collected and used in the protocol as normally. placement by CTD24 was still observed.

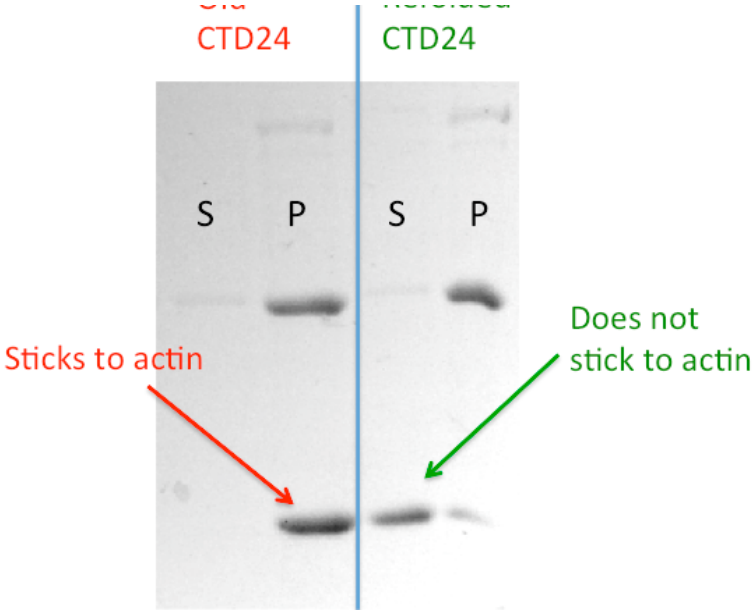

igure 3.10. MICAL$_{CTD}$ and particularly the truncated form CTD 24 convert readily to ı alternate form that does not displace MICAL from F-actin and also co-precipitates ith actin. However, overnight dialysis in 8 M urea and re-dialysis into the original ıffer eliminates this aberrant actin-binding, suggesting successful refolding of the ·otein.

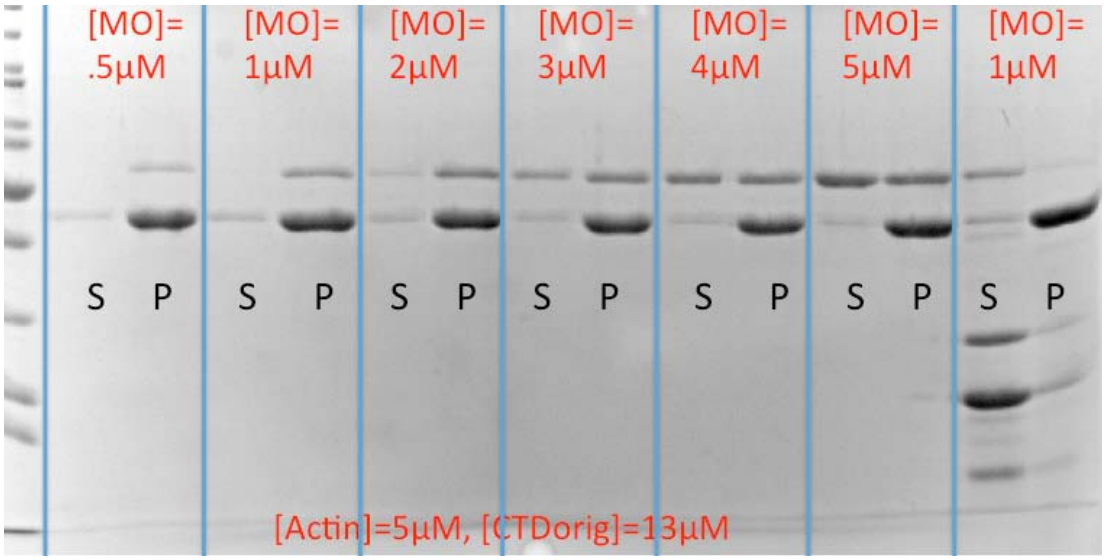

ure 3.11. Concentration series assessing binding of $MICAL_{MO}$ to F-actin. 50% ding and hence K_d is at approximately 4 µM $MICAL_{MO}$, while saturation of the actin gins at approximately 2 µM $MICAL_{MO}$, suggesting 2:5 binding stoichiometry. At ht, $MICAL_{CTD}$ displaces $MICAL_{MO}$ from F-actin.

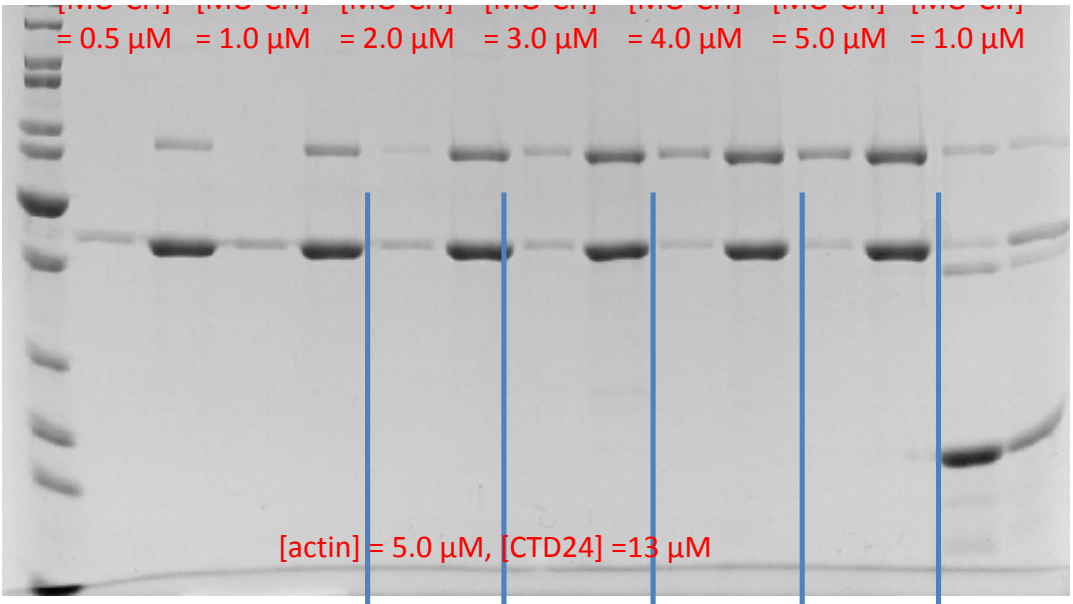

gure 3.12. Concentration series assessing binding of $MICAL_{MO-CH}$ to F-actin. 50% ıding and hence K_d is achieved at >5 µM $MICAL_{MO}$, while saturation of the actin gins at approximately 2.5 µM $MICAL_{MO-CH}$, suggesting 1:2 binding stoichiometry. At ht, CTD24 displaces $MICAL_{MO-CH}$ from F-actin.

The mechanism of this reaction requires consumption of reducing equivalents of NADPH. Indeed, it has been shown in vitro that upon addition of NADPH, F-actin in the presence of $MICAL_{MO\text{-}CH}$ is rapidly disassembled, and ceases to sediment upon ultracentrifugation (59). This methodology was adapted in order to assess the effects of the MICAL-CTD on this disassembly activity: 1 μM of MICAL construct was combined with 5 μM G-actin, polymerization buffer was added and the mixture allowed 30 min at room temperature to fully polymerize, whereupon 50 μM NADPH was introduced and the mixture allowed to incubate 100 min.

The actin-disassembly effect was readily reproduced, with large amounts of actin appearing in the supernatant fraction (Fig. 4.3) compared to control without NADPH. Notably, although at least half and usually a majority of the F-actin was disassembled in each attempt, a significant amount always remained polymerized, possibly supporting the contention that F-actin disassembly by MICAL is a steady-state, rather than an irreversible process. Also, contrary to expectations of its function as an auto-inhibitory domain, addition of CTD even in 5-fold molar excess to MICAL had no noticeable effect on F-actin disassembly by $MICAL_{MO\text{-}CH}$ in the presence of NADPH (Fig. 3.13); the same was true when 1 μM $PlexA1_{ic}$ + 1 μM Rnd1*GTP were present (Fig. 4.7b).

In stark contrast, fl-MICAL showed binding to F-actin but produced no noticeable F-actin disassembly with NADPH, even over timescales up to 4 hr (54). These conflicting results leave the role of the CTD in regulating F-actin disassembly uncertain; it may merely reflect misfolding of the purified CTD, or it may indicate a requirement of some intramolecular interactions not available from the combination of $MICAL_{MO\text{-}CH}$ and CTD, possibly mediated by the LIM or proline-rich regions.

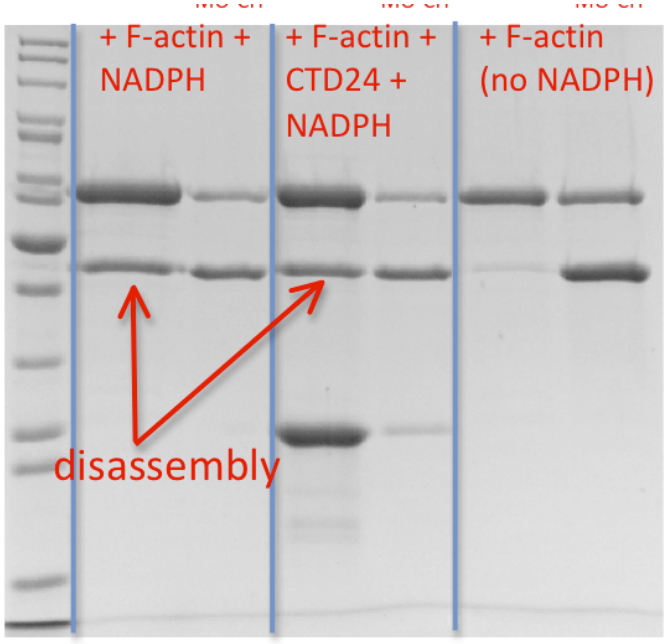

ɡure 3.13. F-actin is disassembled by $MICAL_{MO\text{-}CH}$ in the presence of NADPH. The ːsence of CTD24 has no evident inhibitory effect on this disassembly.

3.4 CTD refolding.

The tendency of CTD to either remain in the supernatant and cause $MICAL_{MO}$ disassociation from F-actin, or to pellet completely and have no effect on $MICAL_{MO}$ association with actin, suggested there may be two distinct phases in which the CTD may exist. In order to convert the pelleting, non-disassociating phase back to the original, restoring the diminished actin-displacement capability of the MICAL-CTD, refolding of the protein was attempted. CTD that had noticeably lost its potency was placed in a 10 kDa MWCO snake skin dialysis membrane and dialyzed overnight into 8 M urea with 5 mM BME, then dialyzed back to the usual buffer of 300 mM NaCl, 50 mM Tris, 5 % glycerol, pH 7.5. This procedure produced a marked recovery of the actin-displacement ability of the MICAL-CTD (Fig. 3.14). In addition, refolded CTD ceased to co-precipitate with actin. In connection with this idea, denaturing lysis was investigated as a way of breaking the pellet and refolding all the harvested protein at once, thus increasing the initial potency. In contrast to refolding of the already purified protein, this method produced no noticeable change in displacement by the CTD so produced and it was abandoned.

Effectiveness of refolding tended to vary dramatically from batch to batch and especially with the construct being used. While the original CTD construct with its two-band product showed major improvement in actin displacement and a decrease in actin co-sedimentation upon refolding, in the case of the pre-truncated CTD24 construct frequently halting of co-sedimentation of the CTD24 was observed, but with limited improvement in its displacement efficacy.

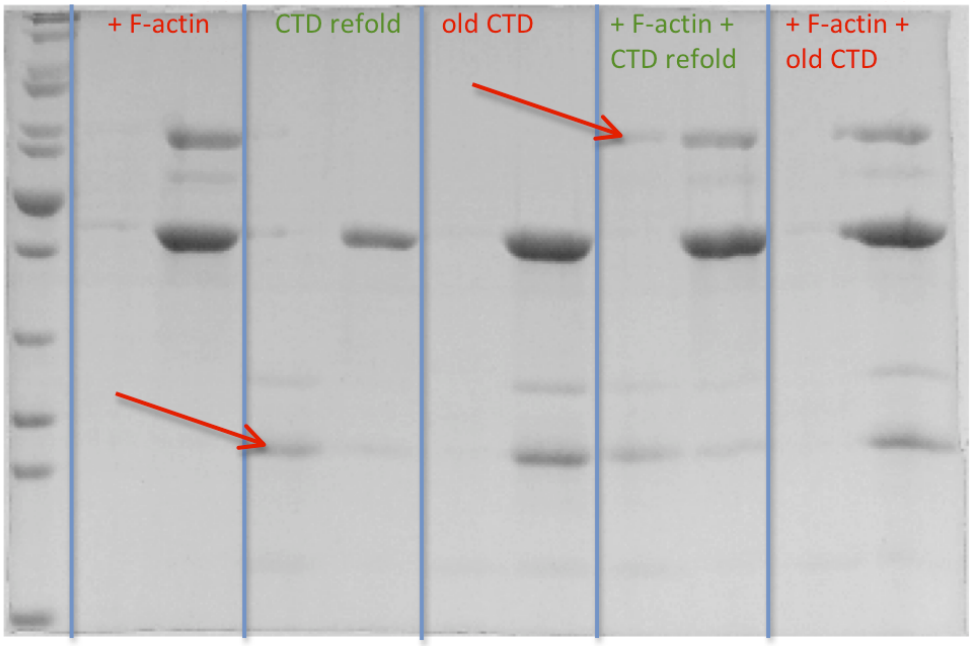

ɡure 3.14. $MICAL_{CTD}$ within a few days typically loses its ability to displace MICAL ıstructs from F-actin and begins to adhere to F-actin. The urea re-folded $MICAL_{CTD}$ ains the ability to displace MICAL $_{MO\text{-}CH}$ from F-actin (arrows).

3.5 H_2O_2 production measurements.

It is understood that the molar ratio of NADPH consumption to hydrogen peroxide production in the NADPH oxidase reaction of $MICAL_{MO}$ is 1:1, both on mechanistic and experimental grounds (44). However it follows from similar grounds that, if MICAL does indeed use reducing equivalents to oxidize methionine residues on actin, this should be accompanied by a substantial drop in H_2O_2 production per NADPH. However, the standard Amplex Red assay for H_2O_2 has been found to produce artifactually high readings in some cases (65) and also requires a more complicated procedure to compare the two, since all NADPH must be removed before it is carried out. Instead, a non-enzymatic assay based on the peroxide-driven oxidation of Fe(II) ion to Fe(III), coupled to binding with xylenol orange to produce a violet product (absorption peak at 560 nm), was employed.

To distinguish the differences in H_2O_2 production by MICAL with or without its auto-inhibitory domain intact, and also how the presence of actin alters this production, four distinct formulations were used in the experiment, labeled C1, C2, D1, and D2 for brevity. Their compositions were as follows: C1 contained 0.1 μM $MICAL_{MO\text{-}CH}$, 50 mM KCl, 2 mM $MgCl_2$, 1 mM ATP, 100 mM NaCl, and 20 mM Tris, pH 7. C2 was identical to C1, except for the inclusion of 5 μM of F-actin. D1 was identical to C1 except in containing 0.1 μM fl-MICAL instead of $MICAL_{MO\text{-}CH}$, while D2 was identical to D1 except for the inclusion of 5 μM of F-actin.

Standard curves were prepared using each of the four preparations, combined with 0, 2, 4, 6, or 8 μM H_2O_2, each in triplicate. The H_2O_2 stock was measured in triplicate as well, based on an absorption coefficient of 43.6 /M/cm at 240 nm. 10 μM of each

preparation was added to 100 μM of xylenol orange working reagent, allowed to incubate at room temperature for 30 min., and the absorbance at 560 nm measured.

Initially, difficulties were encountered concerning the reproducibility of the standard curves, without which quantitation of H_2O_2 production would be impossible. However it soon became apparent from repeated attempts to create definitive standard curves for each of the four formulations that this lack of reproducibility stemmed almost entirely from the variability of the y-intercepts due to the combination of small variations in pipetting and instrument drift; the slope of the curves, by contrast, consistently fell within the range 0.009-0.011 A560/μM, with an average value very close to 0.0105 A560/μM. Therefore, this slope value was used henceforth, while for each subsequent experiment, freshly prepared C1, C2, D1 or D2 (to which no NADPH had been added and which thus could be assumed to contain no H_2O_2) was used as the zero for A560 readings, in effect making the y-intercept of the standard curve equal to zero.

Reactions were followed at 340 nm to gauge the NADPH consumption. Because of a slight actin-bundling effect upon addition of MICAL that caused a slow artifactual rise in the measured A340, reaction formulations containing F-actin (C2 and D2) were processed in the peroxide assay in 15 min or less after addition of NADPH to start the reaction, during which time the bundling effect remained less than 5% of total absorbance. In the case of the D1 formulation, on the other hand, the reaction of fl-MICAL in the absence of F-actin proved so slow that a longer time course (45 min) was needed to generate enough H_2O_2 to produce a reliable reading on the xylenol orange assay.

These results, in combination with measurements of total NADPH consumption, consistently showed a drop in the NADPH/ H_2O_2 ratio (in some cases as large as 66%)

for the combination of $MICAL_{MO\text{-}CH}$ and F-actin (C2). All other formulations showed little or no effect on the ratio, suggesting that only MICAL lacking the auto-inhibitiory function was capable of modifying F-actin.

3.6 Pull-down and IP.

As a method of detecting the association of $PlexA1_{ic}$ and MICAL-CTD, pull-down experiments were attempted. These initially focused on the methodology of binding either SUMO- $PlexA1_{ic}$ or SUMO-CTD with an anti-SUMO antibody, collecting and eluting it with protein A beads, then examining the eluate for binding partners. In most of these experiments, the plexin C2 construct--of which small amounts could sometimes be obtained by either leaving the SUMO tag uncleaved, or by expression in a PGEX-5X-1 vector and similarly leaving the GST tag on--was used mostly, as it was thought more likely to provide an open binding site for the CTD. However, the results were generally inconclusive. For example, while SUMO-CTD or SUMO-C2 could occasionally (barely) be observed in the eluted fraction from the protein A beads--implying immunoprecipitation had succeeded--no binding partner (in this case GST-C2 or cleaved CTD, respectively) was seen to accompany it by SDS-PAGE. Various pH conditions (7.5-8.0) and salt concentrations were tried, without significant change in result.

The seeming failure to detect interaction between C2 and CTD may have simply been due to the instability of the C2 domain in the absence of the C1, in light of the close structural interdependence of C1 and C2 in the full intracellular plexin structure (25, 26). Further experiments were therefore attempted with SUMO- $PlexA1_{ic}$. Also, to simplify the procedure, the immunoprecipitation aspect was eliminated by resorting to a pull-down scheme, whereby 6xHis-tagged fusion was incubated with putative binding partner with

no tag. These experiments showed similarly ambiguous results to the immunoprecipitations however.

3.7 Crystallization.

Crystallization trials were carried out on the following proteins and protein combinations: $PlexA1_{ic}$, CTD, CTD24, and $MICAL_{MO}$ with CTD (varying molar ratios). In the case of $PlexA1_{ic}$, in addition to 96-well hanging-drop screens available from suppliers Jena, Qiagen, and Hampton, a sample of $PlexA1_{ic}$ was sent to the Hauptmann-Woodward High-Throughput Screening Center in Buffalo, NY for crystallization screening under oil. None of the conditions screened produced strong signs of crystal formation, though a few examples of crystalline precipitation were investigated but also did not yield improvement. This may have been due to an insufficient concentration of plexin (8.8 mg/mL). Upon publication of the plexin-A3 intracellular domain structure (25)--which shares >80% sequence identity with plexin-A1--further efforts in this area were postponed.

Because of the difficulty in isolating a single pure band from the original CTD construct (and because of the obvious importance of this for crystallization trials), few conditions were screened for the original CTD construct. The CTD24 construct, being easily expressed in large amounts and readily purified as a single band, was tested more thoroughly for crystallization. Surprisingly, even after SUMO tag removal the protein continued to exhibit an extremely high solubility, in excess of 25 mg/mL being achieved. This solubility militated against crystallization or even precipitation however, with only a small minority showing any signs of precipitate even a week or more after the trays were prepared. (This was part of the motivation for attempting the CTD construct lacking the

polyglutamate stretch, as this creates an exceptionally hydrophilic moiety within the molecule.)

Co-crystallization trials using CTD combined with $MICAL_{MO}$ exploring conditions similar to those previously used to crystallize $MICAL_{MO}$ (21% PEG 4000, 0.1 M $Na(CH_3COO)$, 16% glycerol, 1 mM EGTA, pH 5) alone, reliably produced yellow, needle-shaped crystals (Fig. 3.16). However, the formation of these crystals dramatically decreased at molar ratios of more than 1 CTD:6 $MICAL_{MO}$. Since any MICAL-CTD complex is strongly suspected to have a 1:1 stoichiometry, this seemed to argue against their being true co-crystals. Furthermore, their crystal morphology was extremely similar to that of pure $MICAL_{MO}$ crystals. These crystals were very small and when mounted and irradiated using the home X-ray source, showed very poor or no diffraction (>10 Å).

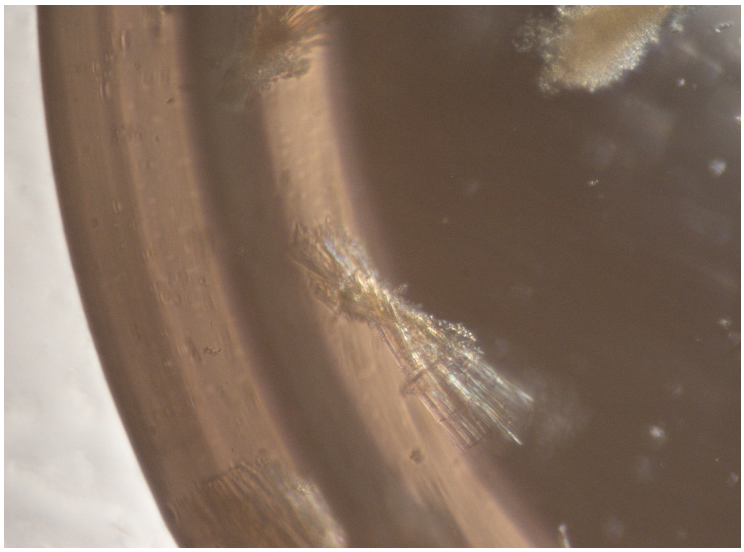

Figure 3.15. Typical crystal obtained during co-crystallization trials with $MICAL_{MO}$ and $MICAL_{CTD}$.

3.8 ITC.

In order to provide complementary evidence for dimerization as well as to determine thermodynamic parameters of the interaction that could not be discovered by HPLC or size-exclusion alone, isothermal titration calorimetry (ITC) was carried out with $MICAL_{MO}$ and MICAL-CTD.

In the first ITC run, zero enthalpy change ($\Delta H=0$) was observed upon addition of CTD in tenfold excess to a solution of $MICAL_{MO}$. However, it was thought that in this case the concentrations of the proteins might have been too small for the heat of their association to be detected; therefore, the experiments were repeated with a tenfold increase in the concentration of both proteins (9.7 μM $MICAL_{MO}$ in the cell; 118 μM CTD in syringe). In this run, too, zero enthalpy change was observed.

This contrasted with the apparent formation of an MO:CTD peak on size exclusion, and with the observations of CTD's ability to displace F-actin from MICAL; on the other hand it supported the HPLC results showing no new "complex" peak and those co-sedimentations where little CTD effect could be observed. It remained unclear how to interpret the result--whether the proteins used in the ITC experiments were somehow damaged, or whether the binding of CTD to $MICAL_{MO}$ was completely entropy-driven.

Chapter 4: Plexin-A1 Intracellular Domain and Rnd1 Together Suffice to Lift Autoinhibition of MICAL-1's Monooxygenase, but not its Actin-Disassembling Activities.

(Adapted from Simon O. et al, 2014)

ABSTRACT.

MICALs are large multidomain proteins implicated in axon guidance, signal transduction and actin remodeling. Moreover, the N-terminal domain of MICAL has a potent monooxygenase activity. Recent studies have put forward a model of MICAL activation and control where MICAL's monooxygenase activity is auto-inhibited by its C-terminal domain (CTD). This inhibition is lifted when Plexin dimerizes, binds small GTPases, and interacts with CTD. Furthermore, work with MICAL lacking the CTD has revealed it to have a potent actin-disassembling activity. Using kinetics measurements, co-sedimentation experiments, and measurements of H_2O_2 production, we find that the combination of GTP-bound Rnd1 and the intracellular domain of Plexin A1 does significantly increase MICAL-1 (fl-MICAL) monooxygenase activity compared to its auto-inhibited state. However, with respect to its actin-disassembling activity we find no discernible effect. Furthermore, we find that Plexin and Rnd1 are not necessary for MICAL binding to F-actin, and that while such binding considerably accelerates NADPH consumption, this activity is not associated with actin disassembly. Based on these observations, we suggest that MICAL may function both in a signaling and actin-modifying capacity.

INTRODUCTION.

In the course of neuronal development in the embryo, or in the re-innervation of damaged tissues, precise location and direction information must be continuously available to extending axons for them to properly innervate their targets. This complex requirement is thought to be met through the establishment and sensing of gradients of a plethora of morphogen and guidance molecules. Several protein families, each comprising dozens of proteins termed "axon guidance cues", are known to serve in this role. Some of the most well-characterized of these include the netrins, slits, ephrins, and semaphorins (1).

Although there is great diversity in the function and expression patterns of these cues, within each family they usually show strong commonalities in their protein structure, their effect on the direction of growing axons (attractive or repulsive), and in the particular corresponding families of receptors with which they interact to exert their effects; furthermore, cues may be secreted or membrane-bound, with some being cleaved from the membrane and thereby serving both roles, depending on the context (16, 15).

The distinctive structure that allows the axon to sense these chemical gradients in the surrounding environment is a highly dynamic structure known as the growth cone. Located at the distal end of the axon, it is marked by an elaborate infrastructure of microtubules and F-actin, kept in dynamic equilibrium between polymerization on one end and disassembly on the other, and such factors as actin rigidity and rate of retrograde movement (1, 14).

While microtubules comprise most of the core of the growth cone, at the outer fringes of the advancing end continually treadmilling F-actin fibers bundle together to

form finger-like outward projections known as filopodia, joined together around their bases by web-like structures, also made of F-actin, known as lamellipodia. Equipped with abundant receptors for the appropriate guidance cues, differing actin polymerization rates on opposing sides of the cone allow it to "steer" its direction of growth with great sensitivity, in response to the concentration gradient of guidance cues (1, 67).

Exactly how a guidance cue's signal is transduced after it binds its receptor--first across the membrane and ultimately into the form of differential changes in actin polymerization--remains an open question. Clues for a possible mechanism, however, have gradually come to light notably in research on one family of these cues, the semaphorins and their companion receptors, the plexins (6, 17).

The semaphorins are a particularly large and well-known group of mostly secreted, mostly repulsive axon guidance cues, whose importance also extends to blood vessel growth, tumor growth and chemotaxis by immune cells (20, 28, 68). They are distinguished by the presence of Ig-like folds and the "sema domain", a seven-bladed beta-propeller (15). Their dedicated receptors, the plexins, are single-pass transmembrane proteins with extracellular sema domains and a distinctive intracellular architecture with known GTPase activating (GAP) function, consisting of two intertwining (C1 and C2) domains of similar structure and sequence with an intervening Rho-binding (RBD) domain (25, 26).

Evidence from many studies (24, 25, 29, 30, 32, 33) indicates that the plexin GAP nominally exists in an autoinhibited "closed" state until binding of small GTPases such as Rnd1 and Rac1 to the RBD; this, combined with dimerization of the plexins brought about by semaphorin binding, leads to activation of the GAP function and

presumably several downstream effects including F-actin disassembly and growth cone collapse (20).

Perhaps the most significant of these known downstream plexin-interacting proteins are those of the MICAL family. The MICALs are a group of large (117 kDa), multi-domain proteins first recognized as an interaction partner of CasL, a large scaffolding protein, and vimentin (41) and later found to associate with Plexins and serve an important role in axon guidance in *Drosophila* (5, 40). MICALs are conserved from flies to mammals, where they are present in one and three isoforms, respectively. Perhaps their most distinctive biochemical feature is the presence in its N-terminal half of an FAD-containing domain (MO, a.a. 1-484) with strong NADPH-dependent monooxygenase activity and structural similarity to aromatic hydroxylases and monoamine oxidases (5, 69, 42).

In isolated form, this MO domain can generate H_2O_2 when NADPH and molecular oxygen are present (47), which may indicate a signaling role. For instance, MICAL-generated H_2O_2 may modify the oxidation state of CRMP2 (Collapsin Response Mediator Protein-2), thereby influencing cell contraction and growth cone collapse (58). However, MICAL-1 also appears to physically interact with plexins and with actin fibers both *in vivo* and *in vitro* (5, 51), and is capable of disassembing actin fibers directly through conversion of key methionines to sulfoxide, with a large concomitant increase in NADPH consumption (59, 65). It remains unresolved whether this function of MICAL involves direct enzymatic modification of actin as a substrate or is due to the production of very large local concentrations of H_2O_2, which are known to oxidize actin, and at the same methionine residues (70-72). However, recent reports indicate that MsrB, a

stereoselective sulfoxide reductase, is capable of fully restoring actin polymerization after MICAL treatment, indicating that MICAL itself modifies actin in a stereoselective way (52, 56, 60).

In addition to its enzymatically active MO domain, MICAL features a calponin-homology (CH) domain (a.a. 516-617); a LIM domain (a.a. 690-752); a proline-rich repeat region (a.a. 822-827), known to bind preferentially bind vimentin and the CasL SH3 domain; a polyglutamate stretch (a.a. 856-876); and finally, a C-terminus predicted to be a coiled-coil/ERM-like domain (CTD; a.a. 876-1040) (67, 44). Extensive evidence now supports a critical auto-inhibitory function for the MICAL CTD in controlling actin-binding, monooxygenase activity, and actin modification (40, 51, 53). In the current model, it is thought that activation of the plexin intracellular domain allows it to bind to the MICAL CTD, uncovering the MO and actin-binding surfaces of MICAL (5, 40, 51). However, such activation has not been directly observed *in vitro* (44).

In this paper, we attempted to validate this model of MICAL activation and control by reconstituting the system using purified proteins.

METHODS.

Genes for full-length mouse MICAL1 (fl-MICAL; a.a. 1-1048) and mouse Rnd1 were synthesized to order by GenScript as codon optimized genes to maximize expression in prokaryotic hosts. Mouse Plexin A1 was obtained in plasmid form from American Tissue Culture. MICAL1 gene and MICAL1-MO-CH (a.a. 2-615, with Q78K mutation to remove a protease site) were cloned into a pET-28a vector (kanamycin resistance; N-terminal 6xHis tag), and Rnd1 into a pET-32a vector (ampicillin resistance;

THX tag with internal 6xHis). Plexin A1 intracellular domain ($PlexA1_{ic}$; a.a. 1302-1912) and the MICAL CTD (a.a. 843-1048) were subcloned into pSmt3 (gift of Christopher D. Lima, Memorial Sloan-Kettering institute), a specially modified pET-28b with an N-terminal 6xHis-SUMO tag and Ulp1 cleavage site. CasL (a.a. 2-74) was obtained from Genescript Inc. in codon-optimized form and cloned into a pGEX-6P2 vector, with N-terminal GST tag.

Following transformation of GC5 maintenance lines, DNA purification and sequencing, standard BL21 expression cultures were transformed with these plasmids and induced with 0.6 mM IPTG. THX-Rnd1, SUMO-CTD and SUMO- $PlexA1_{ic}$ fusion proteins as well as MICAL-MO-CH expressed copiously (>6 mg/L of culture; 3 mg/L for MO-CH) in standard LB medium at 16 ºC for 15 hr, 210 rpm shaking. SH3 expressed at 37 ºC in 3 hr. Owing perhaps to the large size and possible toxicity of the protein, fl-MICAL required TB medium, 20 ºC, 15 hr, 250 rpm in a fermentor and expressed in much lower quantities (~0.5 mg/L).

All cultures were harvested by centrifuging in a GSA rotor at 5000 rpm for 25 min, decanting and re-suspending the pellet in a small volume of 1x PBS, and either flash-freezing in liquid nitrogen or re-pelleting in at tabletop centrifuge at (20 minutes, 3600 rpm in a Jouan Cr 3 22). All pellets were stored at -80 ºC until immediately before use.

Thawing was carried out in the presence of a protease inhibitor cocktail (Complete EDTA-free; Roche), Ca^{2+}, Mg^{2+}, and DNAse. Buffer conditions appropriate to the stability of each protein were maintained: for $PlexA1_{ic}$ and SUMO-CTD, 50 mM NaCl, 0.2 M glycine, 50 mM Tris, 5% glycerol, pH 7.3; for Rnd1, 150 mM NaCl, 50 mM

Tris, 5 mM $MgCl_2$, pH 7.5; for MICAL-MO-CH, 140 mM NaCl, 50 mM Tris, pH 7.3; for SH3, 50 mM Tris, pH 8.0; and for fl-MICAL, 10 mM NaCl, 20mM Tris, pH 8. Pellets were broken by two microfluidizer passes; the resulting lysates were clarified by centrifugation in a (Sorvall SS-34 rotor) at 15500 rpm for 1 hour, and passed through a Millipore 0.22 μm (GSWP) filter.

Proteins were purified by FPLC by binding to a nickel IMAC affinity column (GE global Hitrap) and elution with 10-400 mM imidazole--except for SH3 which was purified by GST-Sepharose using a 0-20 mM glutathione gradient. In the case of SUMO-PlexA1$_{ic}$, the SUMO tag was cleaved by addition of Ulp1 protease in 1:1000 mass ratio to the fusion protein and incubating overnight at 4 ºC. THX was cleaved by addition of 10 units of thrombin per mg of fusion, 2.5 mM Ca^{2+}, and incubation overnight. 6xHis was removed from MICAL-MO-CH and SH3 by overnight dialysis with TEV protease in 0.2 M glycine, 50 mM Tris, pH 7.0. For simplicity, the 6xHis tag was not removed from fl-MICAL.

In preparation for anion exchange, the resulting digests were desalted as necessary using five 5 mL GE Hitrap desalting columns in tandem (total void volume 7.5 mL). MICAL-MO-CH, was loaded onto a Source15S column and eluted with a 0-1 M NaCl gradient. Purification of CTD and Rnd1 (and removal of SUMO and THX tags) was achieved on a MonoQ (1 mL GL) with a 10-900 mM NaCl gradient. For SH3 and fl-MICAL, purification using a SourceQ was found to yield better results. PlexA1$_{ic}$ proved highly pure after desalting and a second run through the IMAC to remove SUMO, making anion exchange unnecessary. All proteins were quantitated by absorbance at 280 nm following denaturation in 6 M guanidine hydrochloride, based on molar absorptivity

coefficients calculated for the protein sequences using the Vector NTI software (Invitrogen, v. 10.3.0).

For co-precipitation experiments, rabbit muscle G-actin (Cytoskeleton, Inc.) was added to a concentration of 5 μM in 45 μL reaction buffer containing 1 μM fl-MICAL or -MO-CH and one or none of the following: Rnd1, 7 μM; PlexA1$_{ic}$, 7 μM; GTP 0.5 mM. 5 μL of 10x polymerization buffer (500 mM KCl, 20 mM $MgCl_2$, 10 mM ATP) was added to initiate actin polymerization. Reactions were incubated at room temperature for 35 min, and ultracentrifuged at 100,000 g for 25 min. Supernatants were carefully extracted and mixed with Laemmli buffer, which was also used to re-suspend the pelleted fractions. Fractions were assessed by SDS-PAGE.

To test for actin-disassembling activity, after the actin polymerization step, 50 μM NADPH was added to the reaction mixture and incubated at room temperature 90 minutes, followed by ultracentrifugation as above.

For kinetics, 11 μL of 1000 nM fl-MICAL was combined in 77 μL MICAL buffer with 11 μL (10 μM Rnd1 + 10 μM PlexA1$_{ic}$ + 1 μM Rnd1, or CTD), and 11 μL of 10x NADPH to give final [NADPH] of 10, 20, 50, 100 and 150 μM. The reactions were immediately mixed by pipetting up and down 16x and 4-minute spectrophotometric time courses taken, using the absorptivity at 340 nm as an indicator of NADPH concentration and consumption. Initial rates were plotted as a function of initial [NADPH] as an index of fl-MICAL activity. Reactions were run in triplicate for each NADPH concentration.

H_2O_2 concentrations were assessed using the Pierce Quantitative Peroxide Assay, aqueous formulation (#23280), in accordance with the manufacturer instructions. Standard curves were generated by measuring triplicates of absorbance at 560 nm after

adding known concentrations of H_2O_2 to each of the four main preparations: fl-MICAL 0.1 μM; MICAL-MO-CH 0.1 μM; fl-MICAL 0.1 μM + F-actin 5.0μM; and MICAL-MO-CH 0.1 μM + F-actin 5.0 μM. As a control, 50 μM NADPH was added to each preparation and the reactions immediately processed with the peroxide assay to stop the enzyme (the working reagent contains 25 mM H_2SO_4, sufficient to denature the enzyme). The same amount of NADPH was added and the reaction allowed to continue for 15 min. A_{340} was tracked to confirm NADPH consumption during this time, and A_{560} was immediately measured at the end for peroxide quantitation. These reactions were performed in triplicate. The molarities of NADPH consumed were calculated and compared with the molarities of H_2O_2 generated.

To confirm that plexin is dimerized under the conditions of these experiments, size-exclusion was carried out with 2 μM PlexA1$_{ic}$ in a buffer of 150 mM NaCl, 20 mM Tris, pH 7, using a 25 mL Superose 12 column. Fractions of the peaks were collected, concentrated using TCA precipitation, and assessed by SDS-PAGE gel.

RESULTS.

1. Kinetics of fl-MICAL and MICAL-MO-CH without actin and the effect of CTD in trans.

In light of the importance attributed to the CTD as an auto-inhibitory domain, MICAL constructs either lacking or containing this domain were tested for NADPH oxidation activity. A greater than ten-fold difference in activity between the full length MICAL construct (fl-MICAL) and one lacking the CTD (MICAL$_{MO\text{-}CH;}$ a.a. 1-615) was observed (Fig. 4.1a). Furthermore, a purified construct of the MICAL CTD (a.a. 843-

1048) proved to be a potent inhibitor of $MICAL_{MO\text{-}CH}$ (Fig. 4.1b).

2a. Co-sedimentation of fl-MICAL and $MICAL_{MO\text{-}CH}$ with F-actin.

Previous co-sedimentation experiments suggested that the CTD, added in trans, may have some capacity to displace MICAL constructs lacking CTD, such as MICAL-MO-CH, from F-actin; this in turn would support a mechanism whereby CTD controls actin binding by MICAL, and thereby also modification and disassembly. We hypothesized that fl-MICAL would be inhibited from binding F-actin in the absence of some other factor(s) that would displace the CTD. To test this, we expressed and purified fl-MICAL and carried out co-sedimentation experiments with F-actin. Surprisingly, we found that fl-MICAL is found entirely in the pellet after ultracentrifugation (Fig. 4.2), implying that it binds F-actin indistinguishably from constructs lacking the CTD. As controls, experiments carried out using fl-MICAL alone in the same polymerization buffer, but lacking actin, showed that all the protein remained in the supernatant, ruling out spontaneous precipitation of fl-MICAL under the conditions of the experiment.

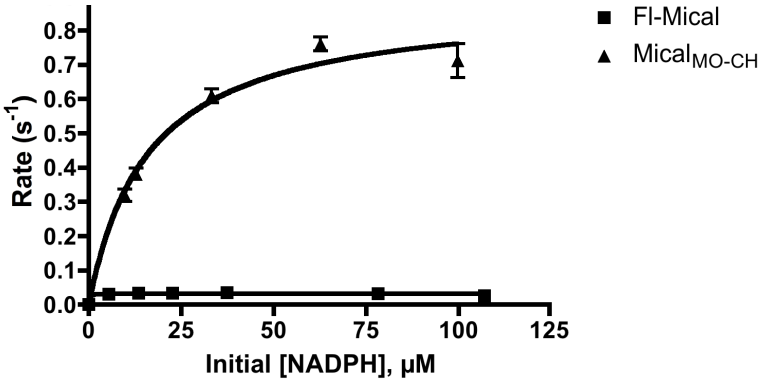

gure 4.1a. Full-length MICAL consumes NADPH approximately 10 times more owly than MICAL$_{MO-CH}$ (or other CTD-lacking MICAL constructs), indicating that e MICAL C-terminal region strongly inhibits the NADPH oxidase activity when esent *in cis*.

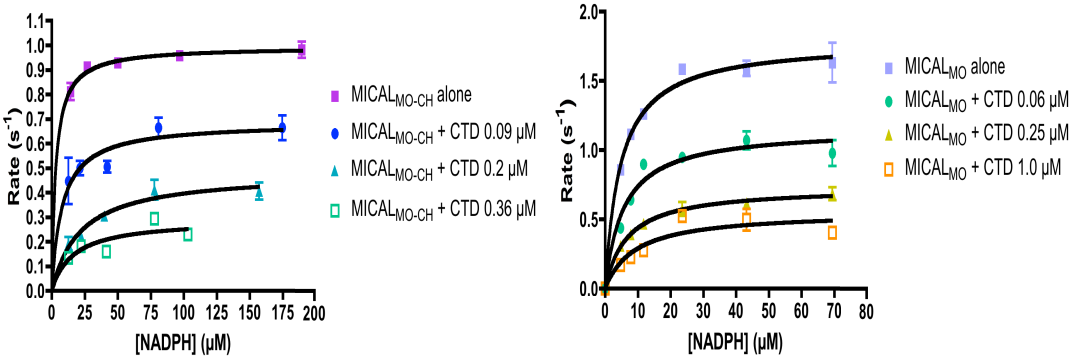

igure 4.1b. MICAL$_{CTD}$, added *in trans*, strongly inhibits NADPH oxidase activity of oth MICAL$_{MO}$ and MICAL$_{MO-CH}$ (M. Urquiza and S. Alqassim).

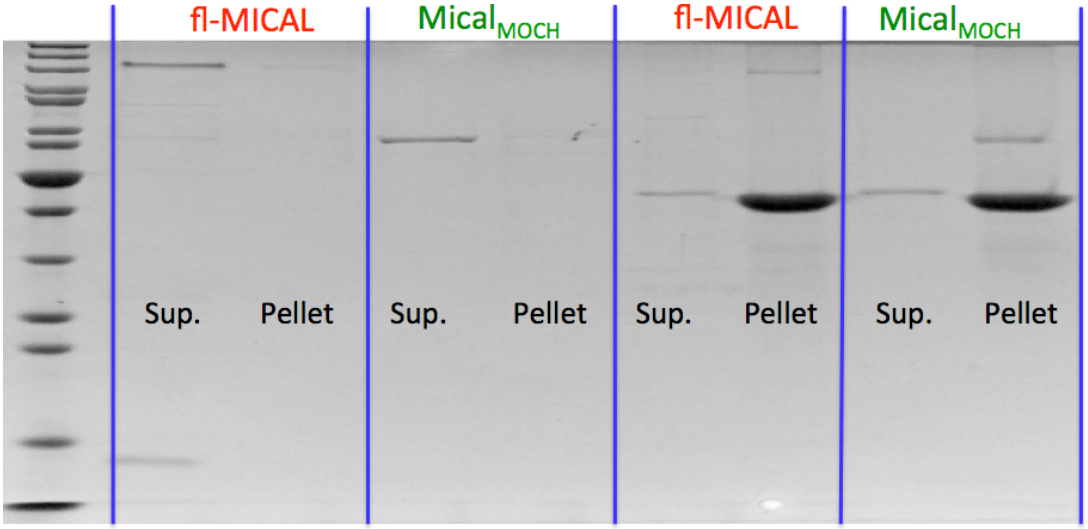

igure 4.2. Despite the presence of the auto-inhibitory C-terminal domain *in cis*, fl-ſICAL binds to F-actin similarly to constructs with the C-terminal domain removed, ıch as MICAL$_{MO-CH}$.

2b. F-actin fiber disassembly by fl-MICAL and MICAL-MO-CH.

Having observed that the CTD apparently does not preclude full-length MICAL from binding F-actin, we tested whether the CTD may work by inhibiting actin-disassembly only. It has been shown that constructs of MICAL lacking the CTD can rapidly disassemble F-actin in the presence of NADPH (59), but this behavior has not been tested with the full-length protein. By simply adding an NADPH-incubation step to the co-sedimentation protocol, it is possible to observe dramatic disassembly of F-actin by MICAL-MO-CH in the presence even of quantities of the enzyme too small to appear on the gel (Fig. 4.3). However in the case of fl-MICAL, no disassembly is observed, even when the incubation time was extended several fold. These results indicate that the presence of the CTD, while having no effect on F-actin binding, does indeed inhibit F-actin modification.

2c. Kinetics of fl-MICAL and $MICAL_{MO\text{-}CH}$ with F-actin.

Given the fact that fl-MICAL and $MICAL_{MO\text{-}CH}$ can both bind to F-actin while exhibiting strongly different behavior regarding actin disassembly, we sought mechanistic clues as to the difference between the two. As expected, $MICAL_{MO\text{-}CH}$ showed a dramatic increase in NADPH consumption upon addition of F-actin (Fig. 4.4). In contrast, in the presence of F-actin, fl-MICAL, rather than being catalytically inert, exhibited a dramatic increase in NADPH consumption as well, to a level similar to that observed with $MICAL_{MO\text{-}CH}$ (Fig. 4.4).

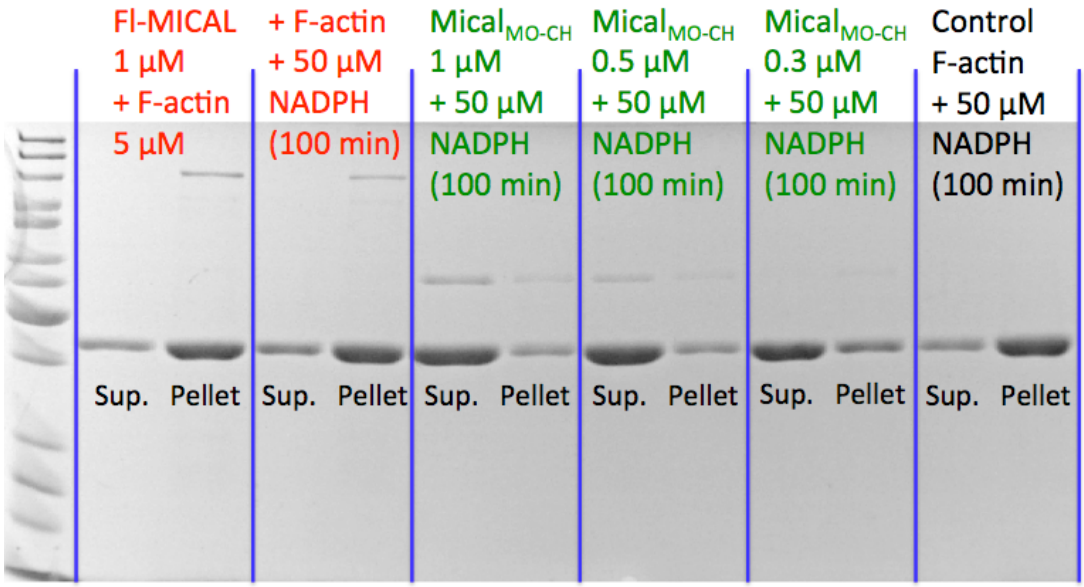

igure 4.3. Although fl-MICAL binds to F-actin, it shows none of the actin-isassembling activity of other MICAL constructs lacking the C-terminus, such as fICAL$_{MO-CH}$, which even when diluted below the detection range of the gel is still ɔle to disassemble a majority of the F-actin (5 µM).

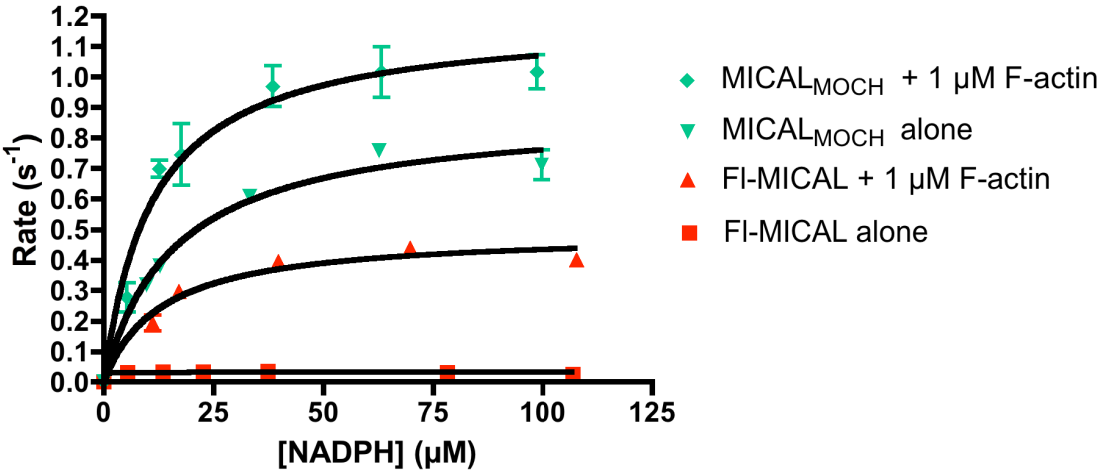

igure 4.4. Like other MICAL constructs lacking auto-inhibition, such as MICAL$_{MO-H}$, fl-MICAL shows a large increase in NADPH oxidation in the presence of F-actin.

3. Peroxide production ratios.

This combination of actin binding, high NADPH consumption, and negligible F-actin disassembly we observed for fl-MICAL in the presence of F-actin presented an obvious paradox: if fl-MICAL is consuming NADPH rapidly while bound to F-actin, but not actually disassembling actin, what are the NADPH equivalents being used for? To try to answer this question we measured hydrogen peroxide (H_2O_2) production. The Amplex Red is perhaps the most common method, but has been shown to be unreliable in many conditions (65) and, moreover, the peroxidase cross-reacts with NADPH which would confound the measurements. To overcome these problems we used a non-enzymatic assay based on the ability of peroxides to convert Fe(II) to Fe(III), which in turn reacts with Xanthine Orange to produce a blue adduct absorbing at 560 nm.

We found that in the absence of actin, despite the large difference in their overall activities, fl-MICAL and $MICAL_{MO\text{-}CH}$ produced approximately as many equivalents of H_2O_2 as they consumed of NADPH (Fig. 4.5). However, in the presence of F-actin, MICAL-MO-CH alone showed a sharp decline in relative H_2O_2 production, to about 1 H_2O_2 per 2 NADPH consumed. fl-MICAL, notably, showed no such decline. This result is consistent with the preceding findings in that it suggests fl-MICAL, though accelerated by binding to F-actin, remains in an essentially H_2O_2-producing mode; $MICAL_{MO\text{-}CH}$, on the other hand, is by itself able to couple NADPH consumption to actin modification and disassembly.

4. Kinetics of fl-MICAL with Plexin/Rnd1/GTP.

Given the extensive research linking MICALs with semaphorin signaling and

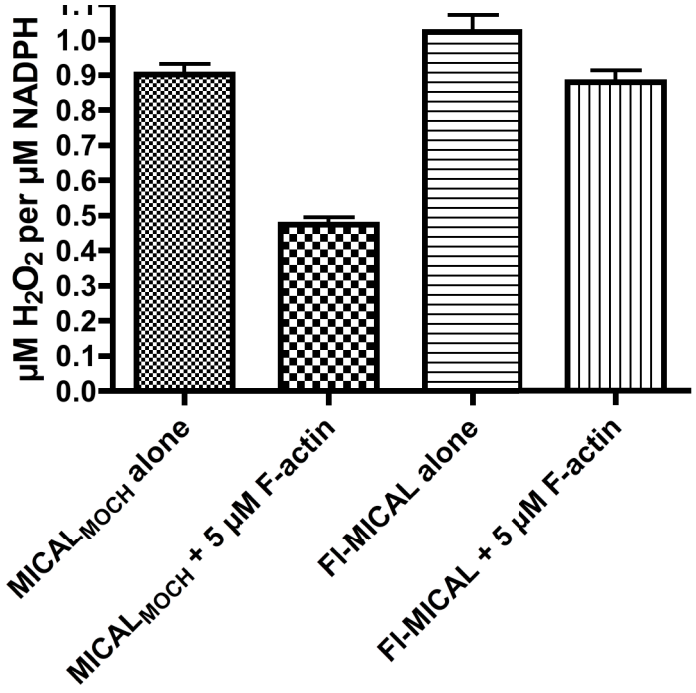

gure 4.5. Although fl-MICAL shows an increase in the rate of NADPH consumption the presence of F-actin, it shows little change in the proportion of NADPH used for $_2O_2$ production. In an actin-disassembling construct such as $MICAL_{MO\text{-}CH}$, however, is proportion decreases by at least half.

activation of plexins, it is expected that activation of plexin by dimerization of its intracellular domain and binding of an active small GTP-binding protein should convert plexin into an active state and activate MICAL as well. We tested this by expressing and purifying mouse Plexin-A1 intracellular domain ($PlexA1_{ic}$) as well as mouse Rnd1. (The latter was chosen because it binds and is activated by, but does not hydrolyze GTP.) To test whether plexin is appreciably dimerized at the concentrations planned for the experiment, we carried out size exclusion. Indeed, approximately 20% of the total plexin ran in a peak adjacent to the main one, with both closely corresponding to the expected dimer and monomer masses, respectively: 70 and 142 kDa expected, 71.5 and 157 kDa from the linear fit (Fig. 4.6a). Proceeding with kinetics, we observed a substantial rate increase in fl-MICAL's NADPH consumption when $PlexA1_{ic}$ + Rnd1•GTP were added (Fig. 4.6b). This effect was considerably greater than that produced by a lysozyme control (Fig. 4.6b)

5. Kinetics of fl-MICAL with Plexin/Rnd1•GTP and F-actin.

Having seen that $PlexA1_{ic}$ + Rnd1•GTP suffice to strongly enhance fl-MICAL activity, and that fl-MICAL by itself is unable to disassemble F-actin, we expected that these proteins might indeed be the key to activating the F-actin disassembly mechanism. However, kinetic measurements showed that addition of $PlexA1_{ic}$ + Rnd1•GTP resulted in no further increase in the rate of NADPH consumption by fl-MICAL over that already seen from F-actin alone (Fig. 4.7a). Furthermore, co-sedimentation showed no change in F-actin binding or disassembly by fl-MICAL in the presence of these factors (Fig. 4.7b). Hence, we conclude that $PlexA1_{ic}$ + Rnd1•GTP is not sufficient to activate actin

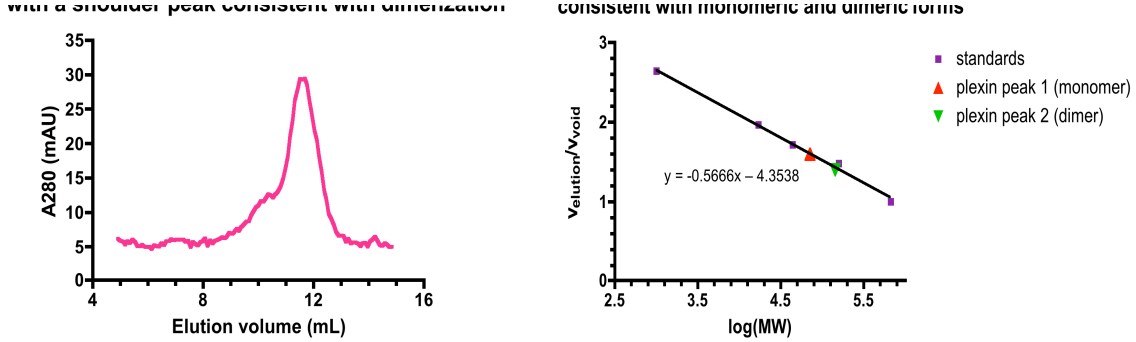

Figure 4.6a. Under conditions similar to the kinetics experiments, PlexA1$_{ic}$ shows a significant shoulder peak, which elutes from size exclusion at a volume very closely corresponding to a dimer (~150 kDa).

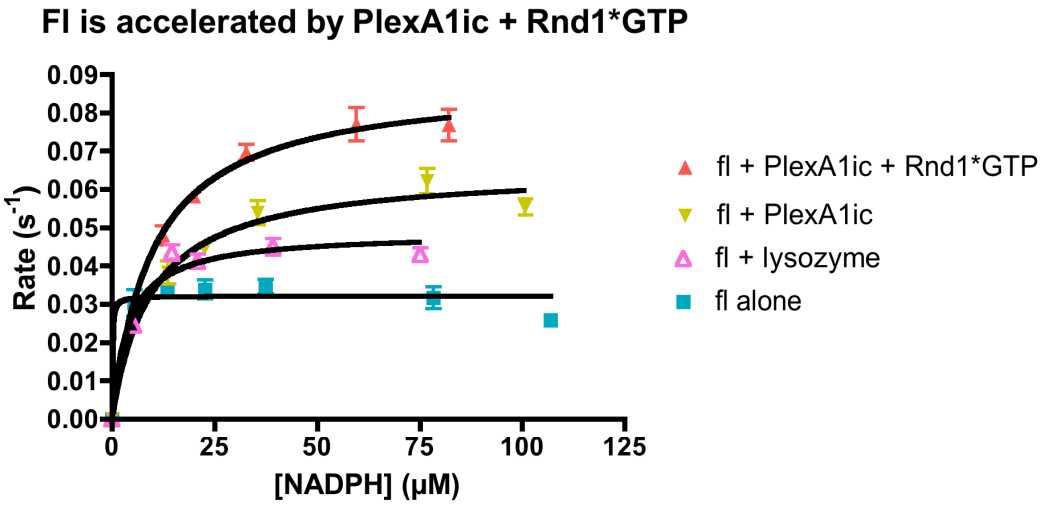

Figure 4.6b. The combination of PlexA1$_{ic}$ and Rnd1*GTP nearly triples the NADPH consumption of fl-MICAL, while PlexA1$_{ic}$ alone shows a weaker effect. Lysozyme, as control, produces only a modest increase.

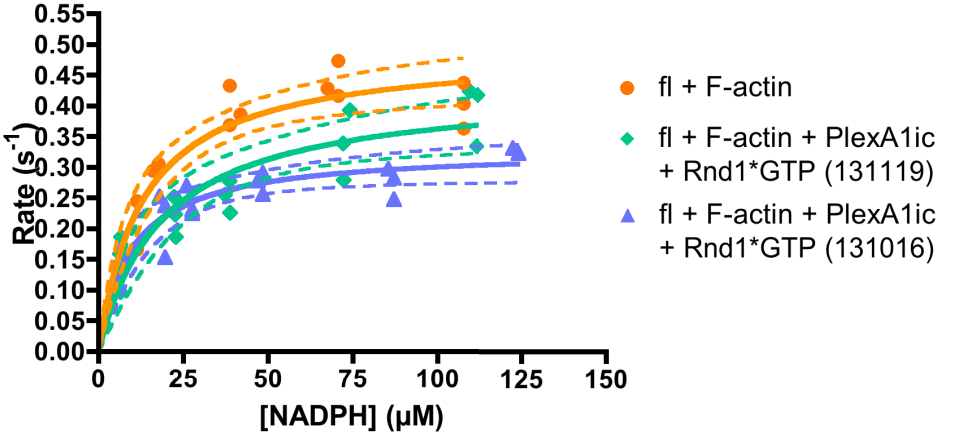

gure 4.7a. In the presence of F-actin, PlexA1$_{ic}$ and Rnd1*GTP produce no additional celeration of fl-MICAL NADPH consumption.

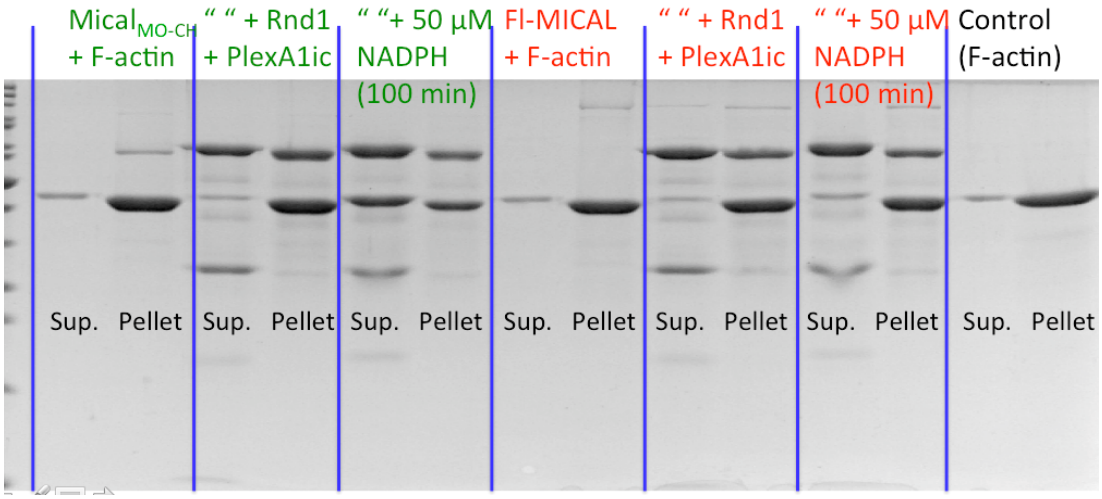

igure 4.7b. Co-sedimentation reveals that PlexA1$_{ic}$ with Rnd1*GTP also does not fect actin binding by fl-MICAL, nor does it activate F-actin disassembly. MICAL$_{MO-I}$ also shows no significant change in the presence of these factors.

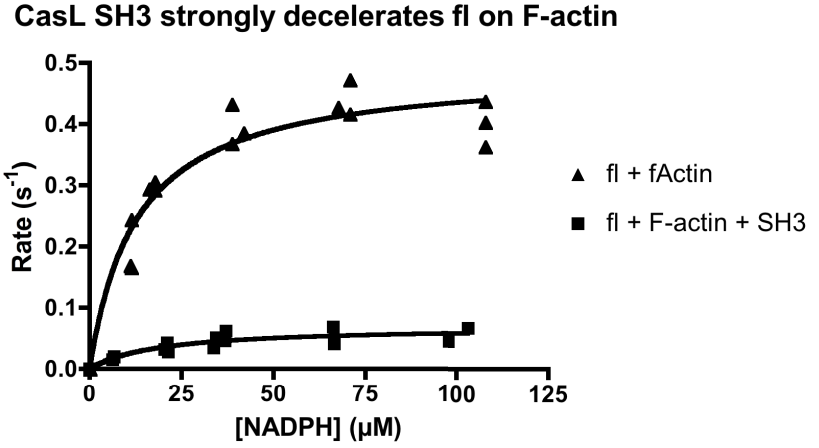

ure 4.8. The SH3 domain of CasL does not activate fl-MICAL NADPH oxidation in presence of F-actin and in fact strongly inhibits it, arguing against CasL being the siological activator of actin disassembly by fl-MICAL.

disassembly by fl-MICAL.

6. Kinetics of fl-MICAL with CasL SH3 and F-actin.

Due to the known interaction of CasL's SH3 domain with fl-MICAL, it was a plausible candidate for activating F-actin disassembly by fl-MICAL. Therefore, we tested whether adding SH3 of CasL might increase NADPH oxidation by fl-MICAL in the presence of F-actin. However, kinetics actually showed a strong inhibitory effect, (Fig. 4.8).

DISCUSSION.

Our experiments have focused on the current model of MICAL activation and control in an attempt to identify the main factors involved in MICAL activation and reconstitute the expected properties of the system. The association of MICAL's CTD with the plexin intracellular domain, and the CTD's ability to function, in turn, as a dominant negative suppressor of MICAL (5), is directly connected with the model of Plexin activation outlined, for example, in the work of Negishi & Katoh (24, 33, 20, 73). The latter studies relied on cell-based studies in COS-7 cells to show that dimerization or clustering with anti-plexin antibodies was necessary for semaphorin signal transduction. Earlier work has outlined the association of GTP-bound Rnd1 with Plexin and its role in actin disassembly (34, 35, 64). Based on structural results, such as the location of the Rho-binding domain and the known propensity of plexins to form at least crystallographic dimers, the activation of plexin has been described as an "AND-gate" (25), requiring concommitant binding of GTP-bound Rnd1 (or Rac1) and clustering.

Our results confirm some aspects of this model of MICAL activation, but in many respects diverge greatly from it. While we were able to detect a considerable increase in the NADPH oxidation kinetics of fl-MICAL in the presence of Plexin and Rnd1•GTP (greater than control), we did not detect any such enhancement for actin-bound fl-MICAL (indeed if anything there was a slight slowdown). Furthermore, these two proteins exhibited no ability to induce F-actin disassembly by fl-MICAL. Since CasL SH3 domain is another well-known interactor of MICAL (41) it seemed a plausible alternate candidate for the activator, but it actually inhibited fl-MICAL strongly in the presence of F-actin.

Transfection of the CTD has been reported to function as a dominant-negative (5) and halt MICAL H_2O_2 production (as measured by Amplex Red) and its deletion from the *MICAL* gene gives phenotypes resembling constitutive semaphorin signaling (40, 51, 53). Consistent with the expectation that the presence of the CTD results in auto-inhibition, we have observed that that full-length MICAL consumes NADPH far more slowly than a construct lacking the CTD region; also, the last ~205 residues of the CTD appears able in trans to restore this auto-inhibition, strongly inhibiting NADPH consumption of the MICAL-MO-CH variant (K_i=~300 nM). However, we found the presence of the CTD in cis to have little or no effect on the actual actin-binding property of fl-MICAL versus MICAL-MO-CH. Co-sedimentation experiments suggest that large molar excess of CTD in trans (>5x) can weakly displace MICAL-MO-CH and -MO (K_d=~5 μM) from F-actin, but it does not appear to make any major difference in the case of full-length MICAL (with a CTD to MICAL ratio of 1:1).

A more complex role for the CTD is also suggested by the enzymatic behavior of

fl-MICAL in the presence of F-actin. Whereas we expected (based on the simple need to keep potentially toxic H_2O_2 production tightly regulated) that the CTD would continue to restrain NADPH consumption to at most the level of a leak until its displacement by some specific activating factors (Plexin + Rnd1•GTP), we instead find that F-actin alone is sufficient to increase fl-MICAL NADPH consumption to something on the order of the non-autoinhibited MICAL-MO-CH. Yet, both the absence of any observable disassembly of F-actin and the lack of any stoichiometric deficit of H_2O_2 production by F-actin bound fl-MICAL suggests a distinct mechanism from that involved in actin disassembly is at work in this case.

In view of these results it appears that, in the absence of other factors, the CTD of fl-MICAL is displaced or adjusted upon actin binding in such a way as to allow increased access of O_2/NADPH to the active site, but not significant access or modification of the two proposed substrate actin residues (M44 and M47). The CTD may therefore function as a "flap" that can be variably displaced, leading to different modes of operation. Structural determination of the CTD would undoubtedly assist in resolving this question, but its extremely high solubility and tendency to misfold has impeded crystallization attempts thus far.

Overall, a key outstanding issue is to determine exactly what additional factor(s) are necessary to switch fl-MICAL into the actin-disassembling state that is so readily observed in constructs lacking the CTD, and which is evinced by numerous cell-based and in vitro studies (40, 51-53, 59, 60, 55). This factor may work in concert with plexin and Rnd1, perhaps being itself activated to carry out the MICAL actin-disassembly function. Certainly more proteins can be purified and tested in the reaction

mixture, in the manner of a screen, but the lack of compelling candidate(s) at the moment, the difficulties of expressing many of these proteins in large amounts, as well as the growing complexity of possible cross-reactions as more proteins are added limits this approach. Possibly further genetic, cell-based or interaction studies will turn up more leads which could then be tested in this system.

One possibility that is consistent with our findings, however, is that Plexin and Rnd1 do not directly control MICAL's actin disassembly function, but rather exert their effects on axon guidance by first modulating its H_2O_2-production. Prior to the discovery of its actin-modifying capability, fl-MICAL was proposed to operate as a signaling protein, using the small molecule H_2O_2, (40, 44, 42, 58, 69). There is no question at this point that H_2O_2 can act as a signaling molecule, with significant effects on actin's redox state (48-50, 69). Indeed, other observations of MICAL kinetics have suggested that it may exhibit multiple phases of activity or dual roles in actin disassembly, or even that in some cases its actin disassembly may be spontaneously reversible (43, 44, 65).

Furthermore, free-floating Plexin intracellular domain in isolation is never found in normal axon guidance; it is always connected directly to the Plexin transmembrane helix. Therefore if direct physical interaction between plexin and MICAL is necessary for MICAL activity, and at the same time direct interaction between MICAL and F-actin is required for disassembly, it should only be possible for MICAL to disassemble actin that is extremely close to the membrane, leaving the vast majority of the F-actin in the growth cone (and cell) inaccessible.

Growth-cone dynamics is thought to involve actin "treadmilling", with assembly taking place at the distal (membrane) edge, and disassembly generally occurring

proximally, deeper in the cytosol (1). Therefore, MICAL would have to modify a significant amount of actin either before or the instant it polymerized, before it diffused or treadmilled out of reach of the MICAL-plexin complex. It is unclear whether this occurs or is possible.

On the other hand, it does seem clear that large quantities of MICALs localize to the cytosol, well out of reach of plexin, yet can and do disassemble actin there. Further, in MICAL-overexpressing cells, F-actin often is depleted in the cytosol and enriched near the membrane (59, 53). This cannot be accounted for by direct activation by a membrane-bound plexin, but again suggests an additional factor is required for F-actin disassembly, possibly involving a peroxide signal.

It seems plausible, then, that H_2O_2 signaling (or some other messenger produced by activated MICAL at the membrane) activates another population of MICAL molecules located deeper within the cytosol, allowing for actin disassembly there. Our observation of distinct modes of operation for the same molecule, with very different levels of H_2O_2 production versus actin modification activity and highly differing responses depending on F-actin occupancy, suggests that the proposal of H_2O_2 signaling may remain integral to some aspects of MICAL function. An important challenge for future work will involve isolating these aspects, for example by searching for mutants or inhibitors that produce exclusively H_2O_2 or exclusively actin-disassembly.

Chapter 5: Conclusions and Future Directions.

5.1. Conclusions and ongoing questions.

The present results potentially point the way to a more nuanced understanding of MICAL activation, by hinting that the peroxide-producing and actin-disassembling reaction of the enzyme might serve distinct functions, and be carried out by spatially distinct sub-populations of the total MICAL population of the cell.

5.2. Finding the "reservoir" of inactive MICAL.

Given the relatively high H_2O_2 production of free fl-MICAL when it finds F-actin, and the likely physiological harm of such if not regulated, it is plausible that some kind of additional sequestering or inactivating principle is at work in keeping this binding in check most of the time. A natural possibility, given its strong inhibitory effect on MICAL NADPH oxidase activity, is CasL. It is already known of course that MICAL interacts with the SH3 domain of CasL, but those same experiments also found an equal if not stronger co-localization of MICAL with vimentin (41).

Further experiments should be carried out to assess the role of the intermediate filaments as a "reservoir" of cellular MICAL, with CasL, for example with peroxide-sensitive fluorophores conjugated with vimentin-binding antibodies. In general, in keeping with the model of separate functions, little peroxide should be detectable from MICAL deeper in the cell, while larger amounts should appear near the membrane; the reverse pattern should be evident if actin-disassembly is monitored, for example by pyrene-labeling of a fraction of the cellular actin.

Crucially, such peroxide production and actin disassembly must also be seen to change in a time-dependent way if it is to be deemed consistent with not just a steady-

state balancing out of MICAL effects, but with *signaling*: information transmission by external guidance stimuli, e.g., by a causal dependence on addition of semaphorin signal to the extracellular medium.

For example, although recent results (52) have shown that MsrB expression can rescue the phenotypic effects of MICAL overexpression or constitutive activity and that it produces such effects when underexpressed, the importance of MsrB in actually carrying an actin de-oxidizing "signal"--rather than, say, in merely establishing a steady-state cellular redox set-point through a kind of "oxidative tug-of-war" with MICAL, is unclear.

Indeed, given that mice null for both Msr enzymes survive to adulthood and do not show serious neurological problems (61), the shallow active sites and low substrate specificity of the Msr enzymes (74), and the fact that many of the rescues demonstrated by MsrB overexpression are actually against $MICAL_{MO\text{-}CH}$--a construct that, being constitutively active, is inherently incapable of signaling (52)—the role of Msr and even of MICAL's actin-disassembly function in a semaphorin-signaling context remain to be clarified.

5.3. Assessing causes for inability of fl-MICAL to modify F-actin.

Another question that arises from these results is that, if MICAL modifies actin by making locally high [H_2O_2], not by direct substrate modification, how could that local concentration not be enough to modify M44/47 in the case of fl-MICAL, but plenty high for MICAL-MOCH when both are sitting right on the actin? Two possible explanations that come to mind. First, that there is an enzymatic activity that disassembles F-actin but is not turned when the CTD is still present *in cis* with no other factors; or, second, that the CTD of fl-MICAL obscures M44/47 in such a way that little or no peroxide is able to

reach and modify these residues. To test these possibilities, NMR could be employed to measure deuterium exchange with the solvent, thus probing the solvent exposure of actin M44/47 when different MICAL constructs are bound and particularly in the presence or absence of CTD *in cis*.

5.4. Parsing of plexin downstream signaling.

In addition to the "AND-gate model" requiring two different and simultaneous inputs in order to be activated, plexin in turn acts upon actin polymerization through at least two essential routes: through MICAL activation by the plexin C2 domain upon receptor activation, and through down-regulation of R-Ras and M-Ras signaling mediated by the GTPase-activating protein (GAP) function of plexin (24, 25). Plexin activates Rho and Rac, these activate LIMK1, which then phosphorylates cofilin, which then becomes inactive (37).

Prior work (29) has suggested that cell collapse through plexin signaling requires the latter's GAP activity, and particularly the two conserved catalytic arginines, R1407 and 1724 (24, 25). Therefore it would be interesting to test whether MICAL--which is very unlikely to be a substrate of a GTPase-activating domain such as plexin's--nonetheless requires intact plexin GAP activity in order to bridge plexin activation and actin depolymerization.

"Inactive" mutants of plexin's GAP--particularly of the C2 arginine R1724--could be prepared and tested for effects on fl-MICAL enzymatic activity using many of the *in vitro* reconstitution methods described in the foregoing, while binding between the C2 domain and MICAL could be probed by co-immunoprecipitation and MALDI-TOF. However, possibly the most likely finding will be that Ras-GAP activity and MICAL

activation serve complementary, rather than overlapping roles. It might also be of interest to experiment on the effects of R-Ras as opposed to MICAL mutations on cell contraction, for instance in COS-7 cells.

5.5. Structural determination of MICAL-CTD.

There remains a sore need for structural study to shed light on the mechanistic side of these observations. Structures of intracellular plexin A and B domains were solved as early as 2007, and given the very high degree of sequence similarity among the plexin A intracellular regions, it is likely that not much new would be contributed by a structure of Plexin A1, say, versus Plexin A3 which has >80% identity and serves a closely similar function.

Similarly, structures have long since been reported for Rnd1 itself, as well as bound to the Plexin rho-binding domain (34), although a co-crystal of the full plexin intracellular domain bound to GTP-bound Rnd1 might provide useful insight into the intramolecular changes that underlie plexin activation. This was not attempted in any of the crystallization trials here described and would be an important challenge, especially in consideration of the kinetics results showing that plexin intracellular domain combined with GTP-bound Rnd1 are able to significantly accelerate fl-MICAL NADPH consumption and H_2O_2 production.

Probably the most directly useful structural result, which is still lacking, would be resolution of the MICAL C-terminal region. Co-crystallization attempts of this with the MICAL-MO domain may have been unsuccessful using known $MICAL_{MO}$ crystallization conditions, but this task merits further work. The structure of the C-terminus alone could also reveal a great deal about how MICAL is regulated, including its paradoxical restraint

of H_2O_2 production and simultaneous easy displacement to allow F-actin binding.

5.6. Studies of MICAL-CTD oligomerization.

There remains the matter, implied in the HPLC and size-exclusion results, of the CTD's tendency to oligomerize even before misfolding *per se*. Different solution conditions, or mutagenesis as above but with the aim of reducing intermolecular interactions, might hold the key. Also it is not understood whether such oligomerization might somehow be a feature of the CTD's normal operation, so future experiments examining this effect, too, might prove fruitful.

Appendix: Cloning, Expression, Purification and Crystallization Attempts on HIF-2α and Respiratory Syncytial Viral Proteins M2-1 and P.

A.1. Introduction to Hypoxia-Inducible Factor 2-alpha (HIF2α).

Hypoxia-inducible factors (HIF-1 and -2) are heterodimeric proteins, comprised of HIF-1β (ARNT) and either HIFα (1α or 2α), that couple cellular oxygen levels to gene expression in metazoa (75). The main mechanism for their achieving this depends on three main features: 1) constitutive expression of both HIF monomers; 2) a strongly oxygen-dependent prolyl hydroxylase activity, which marks key prolines of HIF-1α and 2α for E3 ubiquitin ligase-mediated degradation; and 3) the transcription factor activity of the HIF heterodimers, which stimulates expression of hundreds of target genes through binding to Hypoxia Response Elements in DNA (HREs) (76).

By this arrangement, decreases in oxygen levels lead to decreased degradation of the HIF-1/2α monomers and increased levels of the HIF transcription factor and of HRE-controlled genes. Such genes include VEGF, GLUT1, Semaphorin 4D, hexokinase, and histone demethylases (76, 77, 78).

Each HIF monomer contains an N-terminal basic helix-loop-helix (bHLH) domain, responsible for DNA-binding, a Per-ARNT-Sim (PAS-B) domain, which is thought to be primarily responsible for dimerization, and C-terminal sequences that recruit transcriptional coactivators (75, 79). Structural studies have found that PAS-B domains in general are capable of extraordinary conformational flexibility in response to mild perturbations, and surprisingly, the PAS-B domain of HIF-2α contains a large cavity (~290 $Å^3$) capable of holding a variety of small molecule ligands (75, 80).

One such candidate is the small molecule acriflavine (Fig. A1), which was

discovered through a cell-based library screen to block formation of the HIF-1 heterodimer. It does so by binding to the normal heterodimerization region on HIF-1α (76). Moreover, acriflavine demonstrated an ability to reduce or halt tumor progression in a mouse prostate cancer model (76). Given these observations--as well as the highly pro-proliferative, pro-angiogenic, pro-glycolytic, and anti-silencing nature of most HIF transcription target genes, the need for cancer cells to adapt to the often hypoxic tumor environment, and the fact that high expression of HIF in tumors corresponds to poorer clinical outcomes (76, 81)--blocking HIF dimerization presents a promising target for cancer therapy. We therefore sought to determine the structure of the HIF-2α PAS-B domain co-crystallized with acriflavine.

A.1.1. Experiments with HIF2α.

HIF-2α (PAS-B region, a.a. 281-410) was initially obtained already cloned into a PGEX-5X vector (courtesy of Dr. Greg Semenza, Johns Hopkins School of Medicine). This construct produces fusion protein containing a GST tag, which is removable by Factor Xa, which cleaves at I(E/D)GR sequence sites. Although it expressed readily (up to 20 mg/L of fusion in LB) in most constructs tried, and Factor Xa cleavage and GST tag removal proceeded well (>95% cleavage after 8 hr, using 1 U per μM fusion, in 20 mM Tris, 100 mM NaCl, 2 mM $CaCl_2$, pH 8 (Fig090415), followed by protease inactivation with PMSF or removal with Factor Xa beads, the PAS-B domain of HIF-2α was highly prone to precipitation after tag removal, with frequently more than two-thirds of the original sample precipitating during purification.

Other attempts to remove the GST tag, such as through a MonoS column, also resulted in dramatic losses of protein (more than 6/7 of the total), suggesting that the

presence of GST even after cleavage was necessary to some degree for stabilization. Part of the overall problem as well had to do with the tendency of HIF-2α to precipitate in the presence of calcium--which is however required for Factor Xa cleavage.

In an attempt to overcome these problems, a variety of buffer and expression conditions were tested. After initial test expression runs of 3 hours at 37 ºC, induction temperature was decreased to 25º, then 18º, for periods ranging from 6 hours to overnight (~12 hours), with IPTG amounts between 0.4 and 1.0 mM and optical densities at induction between 0.6 and 1.5. Gels from the pellet following these inductions were generally uninformative, as the yield of protein was very high in all cases and seemed to have no bearing on the instability of the molecule.

SourceQ separation was more successful at separating HIF-2α from GST, yielding up to 1.5 mg/mL (Fig. A2). However, concentrations higher than 5 mg/mL were not achieved, as the HIF-2α would jam the concentrator. Crystallization trays were attempted using the conditions reported for the HIF heterodimer in Scheuermann et al. (75): 100 mM BisTris, 15-30% PEG 3350, and pH 5.5-6.5. This and similar conditions did not produce crystals for the monomer. Hampton Cryo HT and Crystal Screen did not produce leads.

Given the success experienced previously with Plexin A1 intracellular domain, a SUMO-containing construct of HIF-2α was prepared, but this exhibited many of the same basic problems: reasonable amounts of fusion could be obtained, and concentrated, but upon removal of the SUMO tag solubility plummeted. Best solubilities were attained with PBS, pH 7.5, 10 % glycerol. Besides some signs of crystalline precipitation, addition

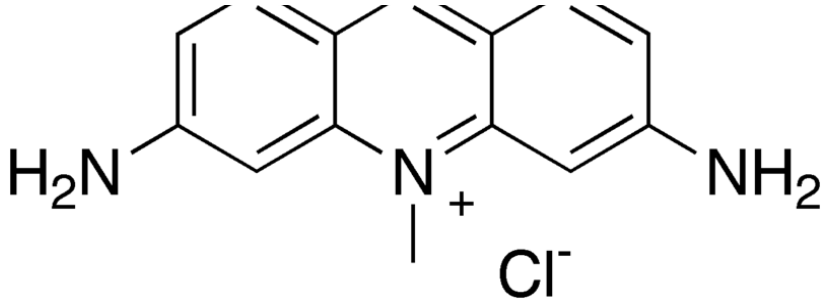

igure A1. Structure of acriflavine (acriflavinium chloride), a dye commonly used as
ı antiseptic. Acriflavine has been observed to retard tumor growth, most likely by
ıterfering with HIF dimerization.

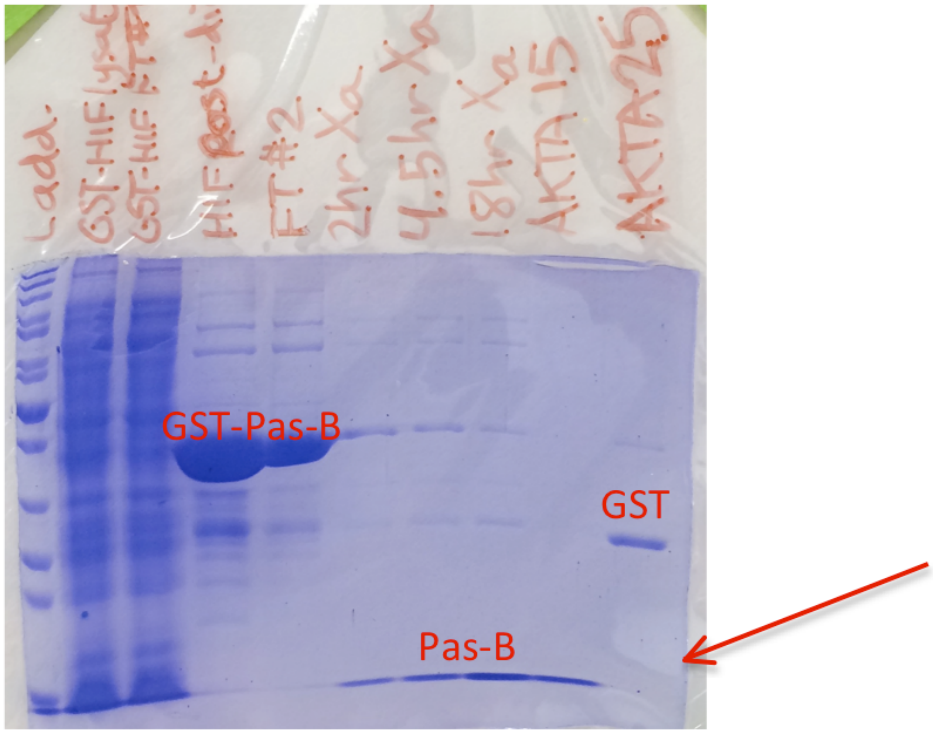

gure A2. Typical elution, cleavage and SourceQ purification of GST-HIF2α PAS-B
ion. Factor Xa cleavage of the GST tag is nearly complete by 4.5 hours, and PAS-B
ı GST are readily separated by anion exchange.

of acriflavine itself (50 μM) did not seem to improve the chances of crystallization, nor the stability of the protein in solution.

A.2 Introduction to Respiratory Syncytial Virus Proteins M2-1 and P.

Respiratory syncytial virus (RSV), of the pneumovirus family, is a common cause of bronchiolitis in infants, affecting nearly 100% within the first 2 years of life (82). Also, the bovine form of the disease, BRSV, causes widespread infections of calves, leading to major economic losses for the cattle industry (83).

M2-1 and P are two interacting components of the RSV transcriptional machinery, concentrating at cytoplasmic inclusion bodies where viral RNA is synthesized. M2-1, which forms a tetramer, functions as an RNA-binding processivity factor (82), while P is a competitive inhibitor of RNA binding to M2-1. Interestingly, NMR studies indicate M2-1 bears structural homology to the Ebola virus VP30 protein (83).

Mutants in the P-interaction region of M2-1, or in the regions responsible for tetramer formation, show reduced RNA transcription (82), indicating that such interactions are a potential target for antiviral drugs (in much the same manner that acriflavine is for HIF in cancers). We therefore sought crystal structures of both M2-1 and P separately, and potentially in dimerized form.

A.2.1 Reconstitution and crystallization of M2-1 and P.

Respiratory syncytial virus proteins M2-1 and P were expressed, purified and sent in lyophilized form from the laboratory of Dr. G. Pratt-Gay, Inst. Beloir. Upon arrival they were reconstituted with pure water with 20 mM DTT, then dialyzed overnight into a buffer of 50 mM phosphate buffer, pH 7, with 0.4 M NaCl, 1 mM DTT, and 40 μM $ZnSO_4$. Thereafter the samples were centrifuged and concentrated until M2-1 reached 3.2

mg/mL and P reached 2.10 mg/mL, then frozen at -80 ºC with 15% glycerol.

Crystal trays were then prepared, including Hampton Crystal Screen HT, Hampton Cryo, and Nextal PEGs suite and a screen designed using the Formulatrix software, based on common ingredients of promising drops found from the PEGs suite. In the case of P protein, this process led to improved conditions, and trays were set up using 20 mM HEPES, pH 7.0-8.0 and Li_2SO_4 1.2-1.7 M. These produced large amounts of crystals, and in subsequent trays the pH range was increased to 7.8-8.8 while the Li_2SO_4 was reduced to between 0.8 and 1.3 M. Crystals produced by this method appeared to be twinned however, with a distinct cruciform shape being apparent at the edges of the crystallization condition (Fig. A3). Crystals closer to the center of the conditions range were irregular in shape, possibly radiations of tiny separate crystals outward from a central point.

One such crystal produced an unmistakable protein diffraction pattern, to about 8 Å (Fig. A4). But, though more crystals were produced by these and similar conditions and mounted and shot, no further protein diffraction was observed, other than salt. Later M2-1 also produced similar irregular, probably compound "crystals"; none produced protein diffraction patterns, except rings, indicating salt or extremely high mosaicity.

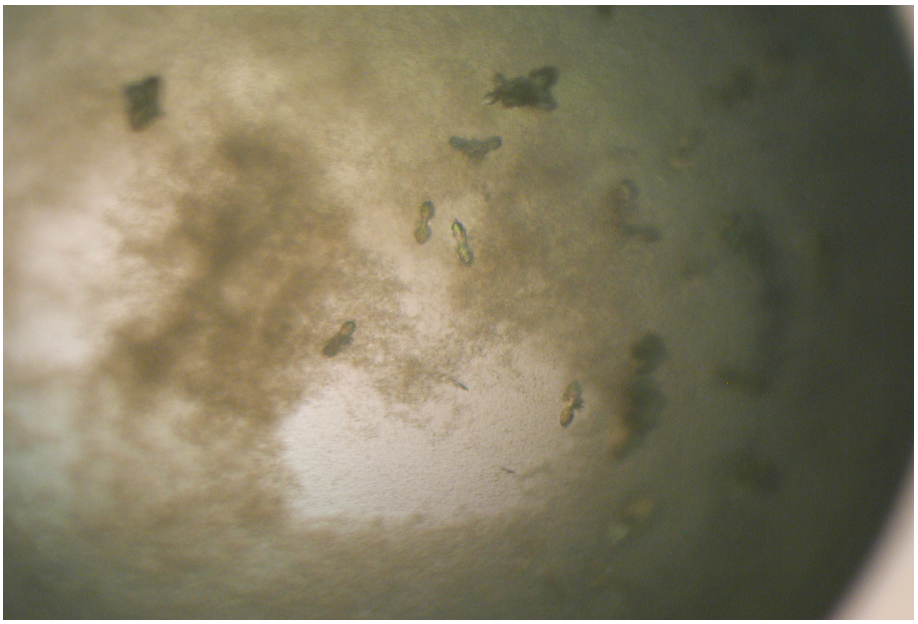

ɡure A3. Example of crystals obtained from respiratory syncytial virus protein P. ote the distinctive bi-lobed crystal habit, which with varying conditions becomes ıciform or irregular.

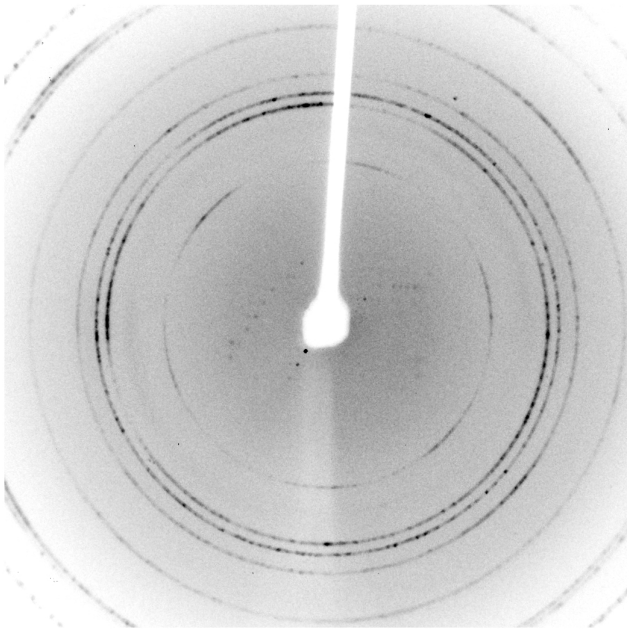

ɡure A4. Protein diffraction pattern obtained from P crystal.

Bibliography.

1. Kolodkin, A.L. and M. Tessier-Lavigne, *Mechanisms and molecules of neuronal wiring: a primer*. Cold Spring Harb Perspect Biol, 2011. **3**(6).
2. Prokop, A., et al., *Using fly genetics to dissect the cytoskeletal machinery of neurons during axonal growth and maintenance*. J Cell Sci, 2013. **126**(Pt 11): p. 2331-41.
3. Raper, J. and C. Mason, *Cellular strategies of axonal pathfinding*. Cold Spring Harb Perspect Biol, 2010. **2**(9): p. a001933.
4. Bonanomi, D. and S.L. Pfaff, *Motor axon pathfinding*. Cold Spring Harb Perspect Biol, 2010. **2**(3): p. a001735.
5. Terman, J.R., et al., *MICALs, a family of conserved flavoprotein oxidoreductases, function in plexin-mediated axonal repulsion*. Cell, 2002. **109**(7): p. 887-900.
6. Fujisawa, H., *Discovery of semaphorin receptors, neuropilin and plexin, and their functions in neural development*. J Neurobiol, 2004. **59**(1): p. 24-33.
7. Nugent, A.A., A.L. Kolpak, and E.C. Engle, *Human disorders of axon guidance*. Curr Opin Neurobiol, 2012. **22**(5): p. 837-43.
8. Lowery, L.A. and D. Van Vactor, *The trip of the tip: understanding the growth cone machinery*. Nat Rev Mol Cell Biol, 2009. **10**(5): p. 332-43.
9. Chedotal, A. and L.J. Richards, *Wiring the brain: the biology of neuronal guidance*. Cold Spring Harb Perspect Biol, 2010. **2**(6): p. a001917.
10. Pasterkamp, R.J., et al., *MICAL flavoprotein monooxygenases: expression during*

neural development and following spinal cord injuries in the rat. Mol Cell Neurosci, 2006. **31**(1): p. 52-69.

11. McCall, J., N. Weidner, and A. Blesch, *Neurotrophic factors in combinatorial approaches for spinal cord regeneration*. Cell Tissue Res, 2012. **349**(1): p. 27-37.
12. McCormick, A.M. and N.D. Leipzig, *Neural regenerative strategies incorporating biomolecular axon guidance signals*. Ann Biomed Eng, 2012. **40**(3): p. 578-97.
13. Vitriol, E.A. and J.Q. Zheng, *Growth cone travel in space and time: the cellular ensemble of cytoskeleton, adhesion, and membrane*. Neuron, 2012. **73**(6): p. 1068-81.
14. Ohashi, K., et al., *LIM kinase has a dual role in regulating lamellipodium extension by decelerating the rate of actin retrograde flow and the rate of actin polymerization*. J Biol Chem, 2011. **286**(42): p. 36340-51.
15. Barton, W.A., et al., *Structures of axon guidance molecules and their neuronal receptors*. Adv Protein Chem, 2004. **68**: p. 65-106.
16. Patel, B.N. and D.L. Van Vactor, *Axon guidance: the cytoplasmic tail*. Curr Opin Cell Biol, 2002. **14**(2): p. 221-9.
17. Winberg, M.L., et al., *Plexin A is a neuronal semaphorin receptor that controls axon guidance*. Cell, 1998. **95**(7): p. 903-16.
18. Yazdani, U. and J.R. Terman, *The semaphorins*. Genome Biol, 2006. **7**(3): p. 211.
19. Klostermann, A., et al., *The chemorepulsive activity of the axonal guidance signal semaphorin D requires dimerization*. J Biol Chem, 1998. **273**(13): p. 7326-31.
20. Negishi, M., I. Oinuma, and H. Katoh, *Plexins: axon guidance and signal*

transduction. Cell Mol Life Sci, 2005. **62**(12): p. 1363-71.

21. Nogi, T., et al., *Structural basis for semaphorin signalling through the plexin receptor*. Nature, 2010. **467**(7319): p. 1123-7.
22. Takahashi, T., et al., *Plexin-neuropilin-1 complexes form functional semaphorin-3A receptors*. Cell, 1999. **99**(1): p. 59-69.
23. Janssen, B.J., et al., *Neuropilins lock secreted semaphorins onto plexins in a ternary signaling complex*. Nat Struct Mol Biol, 2012. **19**(12): p. 1293-9.
24. Oinuma, I., et al., *The Semaphorin 4D receptor Plexin-B1 is a GTPase activating protein for R-Ras*. Science, 2004. **305**(5685): p. 862-5.
25. He, H., et al., *Crystal structure of the plexin A3 intracellular region reveals an autoinhibited conformation through active site sequestration*. Proc Natl Acad Sci U S A, 2009. **106**(37): p. 15610-5.
26. Tong, Y., et al., *Structure and function of the intracellular region of the plexin-b1 transmembrane receptor*. J Biol Chem, 2009. **284**(51): p. 35962-72.
27. Hota, P.K. and M. Buck, *Plexin structures are coming: opportunities for multilevel investigations of semaphorin guidance receptors, their cell signaling mechanisms, and functions*. Cell Mol Life Sci, 2012. **69**(22): p. 3765-805.
28. Rohm, B., et al., *The semaphorin 3A receptor may directly regulate the activity of small GTPases*. FEBS Lett, 2000. **486**(1): p. 68-72.
29. Zanata, S.M., et al., *Antagonistic effects of Rnd1 and RhoD GTPases regulate receptor activity in Semaphorin 3A-induced cytoskeletal collapse*. J Neurosci, 2002. **22**(2): p. 471-7.
30. Oinuma, I., et al., *Direct interaction of Rnd1 with Plexin-B1 regulates PDZ-*

RhoGEF-mediated Rho activation by Plexin-B1 and induces cell contraction in COS-7 cells. J Biol Chem, 2003. **278**(28): p. 25671-7.

31. Turner, L.J., S. Nicholls, and A. Hall, *The activity of the plexin-A1 receptor is regulated by Rac*. J Biol Chem, 2004. **279**(32): p. 33199-205.
32. Takahashi, T. and S.M. Strittmatter, *Plexina1 autoinhibition by the plexin sema domain*. Neuron, 2001. **29**(2): p. 429-39.
33. Oinuma, I., H. Katoh, and M. Negishi, *Molecular dissection of the semaphorin 4D receptor plexin-B1-stimulated R-Ras GTPase-activating protein activity and neurite remodeling in hippocampal neurons*. J Neurosci, 2004. **24**(50): p. 11473-80.
34. Tong, Y., et al., *Binding of Rac1, Rnd1, and RhoD to a novel Rho GTPase interaction motif destabilizes dimerization of the plexin-B1 effector domain*. J Biol Chem, 2007. **282**(51): p. 37215-24.
35. Wang, H., et al., *Structural basis of Rnd1 binding to plexin Rho GTPase binding domains (RBDs)*. J Biol Chem, 2011. **286**(29): p. 26093-106.
36. Chadborn, N.H., et al., *PTEN couples Sema3A signalling to growth cone collapse*. J Cell Sci, 2006. **119**(Pt 5): p. 951-7.
37. Yang, N., et al., *Cofilin phosphorylation by LIM-kinase 1 and its role in Rac-mediated actin reorganization*. Nature, 1998. **393**(6687): p. 809-12.
38. Eickholt, B.J., F.S. Walsh, and P. Doherty, *An inactive pool of GSK-3 at the leading edge of growth cones is implicated in Semaphorin 3A signaling*. J Cell Biol, 2002. **157**(2): p. 211-7.
39. Deo, R.C., et al., *Structural bases for CRMP function in plexin-dependent*

semaphorin3A signaling. EMBO J, 2004. **23**(1): p. 9-22.

40. Schmidt, E.F., S.O. Shim, and S.M. Strittmatter, *Release of MICAL autoinhibition by semaphorin-plexin signaling promotes interaction with collapsin response mediator protein*. J Neurosci, 2008. **28**(9): p. 2287-97.
41. Suzuki, T., et al., *MICAL, a novel CasL interacting molecule, associates with vimentin*. J Biol Chem, 2002. **277**(17): p. 14933-41.
42. Nadella, M., et al., *Structure and activity of the axon guidance protein MICAL.* Proc Natl Acad Sci U S A, 2005. **102**(46): p. 16830-5.
43. Zucchini, D., et al., *Kinetic and spectroscopic characterization of the putative monooxygenase domain of human MICAL-1*. Arch Biochem Biophys, 2011. **515**(1-2): p. 1-13.
44. Vanoni, M.A., T. Vitali, and D. Zucchini, *MICAL, the Flavoenzyme Participating in Cytoskeleton Dynamics*. Int J Mol Sci, 2013. **14**(4): p. 6920-59.
45. Sun, H., et al., *Solution structure of calponin homology domain of Human MICAL-1*. J Biomol NMR, 2006. **36**(4): p. 295-300.
46. Siebold, C., et al., *High-resolution structure of the catalytic region of MICAL (molecule interacting with CasL), a multidomain flavoenzyme-signaling molecule*. Proc Natl Acad Sci U S A, 2005. **102**(46): p. 16836-41.
47. Chaiyen, P., M.W. Fraaije, and A. Mattevi, *The enigmatic reaction of flavins with oxygen*. Trends Biochem Sci, 2012. **37**(9): p. 373-80.
48. Stone, J.R. and S. Yang, *Hydrogen peroxide: a signaling messenger*. Antioxid Redox Signal, 2006. **8**(3-4): p. 243-70.
49. Gough, D.R. and T.G. Cotter, *Hydrogen peroxide: a Jekyll and Hyde signalling*

molecule. Cell Death Dis, 2011. **2**: p. e213.

50. Burgoyne, J.R., et al., *Hydrogen peroxide sensing and signaling by protein kinases in the cardiovascular system*. Antioxid Redox Signal, 2013. **18**(9): p. 1042-52.
51. Hung, R.J., et al., *Mical links semaphorins to F-actin disassembly*. Nature, 2010. **463**(7282): p. 823-7.
52. Hung, R.J., et al., *SelR reverses Mical-mediated oxidation of actin to regulate F-actin dynamics*. Nat Cell Biol, 2013. **15**(12): p. 1445-54.
53. Giridharan, S.S., et al., *Differential regulation of actin microfilaments by human MICAL proteins*. J Cell Sci, 2012. **125**(Pt 3): p. 614-24.
54. Simon, O., et al., *Plexin-A1 Intracellular Domain and Rnd1 Together Suffice to Lift Autoinhibition of MICAL-1's Monooxygenase, but not its Actin-Disassembling Activities*. Manuscript in preparation. 2014.
55. Lundquist, M.R., et al., *Redox Modification of Nuclear Actin by MICAL-2 Regulates SRF Signaling*. Cell, 2014. **156**(3): p. 563-76.
56. Aberle, H., *Redox switch for actin*. Nat Cell Biol, 2013. **15**(12): p. 1403-4.
57. (Kolk, S.M. and R.J. Pasterkamp, *MICAL flavoprotein monooxygenases: structure, function and role in semaphorin signaling*. Adv Exp Med Biol, 2007. **600**: p. 38-51.
58. Morinaka, A., et al., *Thioredoxin mediates oxidation-dependent phosphorylation of CRMP2 and growth cone collapse*. Sci Signal, 2011. **4**(170): p. ra26.
59. Hung, R.J., C.W. Pak, and J.R. Terman, *Direct redox regulation of F-actin assembly and disassembly by Mical*. Science, 2011. **334**(6063): p. 1710-3.

60. Lee, B.C., et al., *MsrB1 and MICALs regulate actin assembly and macrophage function via reversible stereoselective methionine oxidation*. Mol Cell, 2013. **51**(3): p. 397-404.

61. Drazic, A. and J. Winter, *The physiological role of reversible methionine oxidation*. Biochim Biophys Acta, 2014.

62. Oien, D.B. and J. Moskovitz, *Substrates of the methionine sulfoxide reductase system and their physiological relevance*. Curr Top Dev Biol, 2008. **80**: p. 93-133.

63. Garavini, H., et al., *Crystal structure of the core domain of RhoE/Rnd3: a constitutively activated small G protein*. Biochemistry, 2002. **41**(20): p. 6303-10.

64. Hota, P.K. and M. Buck, *Thermodynamic characterization of two homologous protein complexes: associations of the semaphorin receptor plexin-B1 RhoGTPase binding domain with Rnd1 and active Rac1*. Protein Sci, 2009. **18**(5): p. 1060-71.

65. McDonald, C.A., Y.Y. Liu, and B.A. Palfey, *Actin stimulates reduction of the MICAL-2 monooxygenase domain*. Biochemistry, 2013. **52**(35): p. 6076-84.

66. Putnam, C.D., et al., *X-ray solution scattering (SAXS) combined with crystallography and computation: defining accurate macromolecular structures, conformations and assemblies in solution*. Q Rev Biophys, 2007. **40**(3): p. 191-285.

67. Zhou, Y., et al., *MICALs in control of the cytoskeleton, exocytosis, and cell death*. Cell Mol Life Sci, 2011. **68**(24): p. 4033-44.

68. Kigel, B., et al., *Successful inhibition of tumor development by specific class-3 semaphorins is associated with expression of appropriate semaphorin receptors*

by tumor cells. PLoS One, 2008. **3**(9): p. e3287.

69. Veal, E.A., A.M. Day, and B.A. Morgan, *Hydrogen peroxide sensing and signaling*. Mol Cell, 2007. **26**(1): p. 1-14.
70. Milzani, A., et al., *The oxidation produced by hydrogen peroxide on Ca-ATP-G-actin*. Protein Sci, 2000. **9**(9): p. 1774-82.
71. Dalle-Donne, I., et al., *Methionine oxidation as a major cause of the functional impairment of oxidized actin*. Free Radic Biol Med, 2002. **32**(9): p. 927-37.
72. Fedorova, M., N. Kuleva, and R. Hoffmann, *Identification of cysteine, methionine and tryptophan residues of actin oxidized in vivo during oxidative stress*. J Proteome Res, 2010. **9**(3): p. 1598-609.
73. Oinuma, I., et al., *Semaphorin 4D/Plexin-B1 stimulates PTEN activity through R-Ras GTPase-activating protein activity, inducing growth cone collapse in hippocampal neurons*. J Biol Chem, 2010. **285**(36): p. 28200-9.
74. Boschi-Muller, S., A. Gand, and G. Branlant, *The methionine sulfoxide reductases: Catalysis and substrate specificities*. Arch Biochem Biophys, 2008. **474**(2): p. 266-73.
75. Scheuermann, T.H., et al., *Artificial ligand binding within the HIF2alpha PAS-B domain of the HIF2 transcription factor*. Proc Natl Acad Sci U S A, 2009. **106**(2): p. 450-5.
76. Lee, K., et al., *Acriflavine inhibits HIF-1 dimerization, tumor growth, and vascularization*. Proc Natl Acad Sci U S A, 2009. **106**(42): p. 17910-5.
77. Sun, Q., et al., *Hypoxia-inducible factor-1-mediated regulation of semaphorin 4D affects tumor growth and vascularity*. J Biol Chem, 2009. **284**(46): p. 32066-74.

78. Xia, X., et al., *Integrative analysis of HIF binding and transactivation reveals its role in maintaining histone methylation homeostasis*. Proc Natl Acad Sci U S A, 2009. **106**(11): p. 4260-5.

79. Erbel, P.J., et al., *Structural basis for PAS domain heterodimerization in the basic helix--loop--helix-PAS transcription factor hypoxia-inducible factor*. Proc Natl Acad Sci U S A, 2003. **100**(26): p. 15504-9.

80. Evans, M.R., P.B. Card, and K.H. Gardner, *ARNT PAS-B has a fragile native state structure with an alternative beta-sheet register nearby in sequence space*. Proc Natl Acad Sci U S A, 2009. **106**(8): p. 2617-22.

81. Hanahan, D. and R.A. Weinberg, *Hallmarks of cancer: the next generation*. Cell, 2011. **144**(5): p. 646-74.

82. Tran, T.L., et al., *The respiratory syncytial virus M2-1 protein forms tetramers and interacts with RNA and P in a competitive manner*. J Virol, 2009. **83**(13): p. 6363-74.

83. Blondot, M.L., et al., *Structure and functional analysis of the RNA- and viral phosphoprotein-binding domain of respiratory syncytial virus M2-1 protein*. PLoS Pathog, 2012. **8**(5): p. e1002734.

Olivier Simon

Email: Osimon2@jh.edu
Department of Biophysics & Biophysical Chemistry
Johns Hopkins University, School of Medicine
725 N. Wolfe St., Wood Basic Science Building 605
Baltimore, MD 21205

Education

Ph.D. expected 2014 BCMB – Biophysics Johns Hopkins School of Medicine

• Dissertation: cloning, expression, purification, and biochemical characterization of the interactions of Plexin-A1, Rnd1, and F- actin with various constructs of MICAL-1. Mentors: Mario Amzel, Ph.D. and Mario Bianchet, Ph.D.

B.S., summa cum laude 2007 Biochemistry University of New Mexico, Albuquerque

Professional Experience

Graduate Research Assistant 2008-2014 Laboratory of Dr. Mario Amzel
Johns Hopkins School of Medicine

Research Rotation 2008 Laboratory of Dr. Zaver Bhujwalla
Johns Hopkins School of Medicine

• Studied hyaluronan distribution in COX-2 knockout cells by fluorescence microscopy.

Research Rotation 2007-08 Laboratory of Dr. Nancy Davidson
Johns Hopkins School of Medicine

• With Dr. Qun Zhou, studied effects of sulphoraphane and HDAC inhibitors on DNMT1 and Nrf-2 expression in MD-MBA-231 cells, using Western blotting and SILAC labeling.

Research Rotation 2007 Laboratory of Dr. William Bishai
Johns Hopkins School of Medicine

• Grew, induced and imaged conditionally complemented WhmD deletion strains of *M. smegmatis*

Awards and Honors

October 2012 Poster prize, 2nd place, BCMB annual retreat BCMB program

Spring 2006 Inducted to Phi Beta Kappa

Publications

Simon, O., Alqassim S. S., Urquiza M., Bianchet M. A., and Amzel L. M. The Plexin-A1 Intracellular Domain and Rnd1 Together Suffice to Lift Autoinhibition of MICAL-1's Monooxygenase, but not its Actin-Disassembling Activities. *Manuscript in preparation.*

Posters and Abstracts

Simon O., Alqassim S. S., Urquiza M., Bianchet M. A., Amzel L. M. Regulation of the Redox Activity of MICAL. BCMB Annual Retreat, Baltimore MD, October 2012.

• Created MICAL C-terminal construct used for kinetics experiments. Contributed co-sedimentation result indicating abolished F-actin binding in MICAL constructs treated with C-terminal protein.

Simon O., Heynekamp J. J., Hunsaker L. A., Deck L. M. and Vander Jagt D. L. Synthesis and Biological Studies of Resveratrol Analogues. UNM Biochemistry Retreat at Sevilleta, April 2006.

• Based on resveratrol analogue organic synthesis (Wittig reactions) in the laboratory of Lorraine M. Deck.

Oral Presentations

Simon O., Sillerud, L. NMR Evidence of Ordered Structure in Intracellular Loop 2 of Estrogen Receptor GPR30. UNM Biochemistry Retreat at Sevilleta, April 2007.

• Honors research: NOESY and TOCSY data acquisition, processing, peak assignment and simulated annealing on Bcl-2 and GPR30 with Laurel O. Sillerud.

Professional Affiliations

Biophysical Society 2011, 2014